ON THE INTERPRETATION OF STABLE ISOTOPES IN ANTARCTIC PRECIPITATION

DE INTERPRETATIE VAN STABIELE ISOTOPEN
IN ANTARCTISCHE NEERSLAG
(met een samenvatting in het Nederlands)

Proefschrift ter verkrijging van de graad van doctor aan de Universiteit Utrecht
op gezag van de Rector Magnificus, Prof. dr. W.H. Gispen,
ingevolge het besluit van het College voor Promoties
in het openbaar te verdedigen op woensdag 8 februari 2006 des middags te 12.45 uur

door

Michiel Martijn Helsen

geboren op 30 april 1977, te Enschede

promotor: Prof. Dr. Johannes Oerlemans

co-promotoren: Dr. Roderik S.W. van de Wal
Dr. Michiel R. van den Broeke

Institute for Marine and Atmospheric research Utrecht (IMAU)
Faculty of Science
Department of Physics and Astronomy
Utrecht University

Financial support was provided by the Netherlands Organisation for Scientific Research (NWO) within the framework op the European Project for Ice Coring in Antarctica (EPICA).

Contents

1 Introduction **1**
- 1.1 Antarctica . . . 1
- 1.2 Stable water isotopes . . . 4
- 1.3 Isotopic modelling . . . 7
- 1.4 Antarctic meteorology and precipitation . . . 11
- 1.5 This thesis . . . 13
  - 1.5.1 Goal . . . 13
  - 1.5.2 Research approach . . . 14
  - 1.5.3 Outline . . . 15

2 Oxygen isotope variability in snow from western Dronning Maud Land and its relation to temperature **19**
- 2.1 Introduction . . . 20
- 2.2 Isotope records . . . 22
- 2.3 Reconstruction of the seasonal isotopic variability . . . 25
- 2.4 Accumulation record . . . 27
- 2.5 Temperature during accumulation . . . 30
- 2.6 Implications for the $\delta^{18}O$-T relationship . . . 35
- 2.7 Summary and conclusions . . . 38

3 Modelling the isotopic composition of snow for a particular precipitation event in Dronning Maud Land **41**
- 3.1 Introduction . . . 42
- 3.2 Observations . . . 43
- 3.3 Isotope modelling along trajectories . . . 45
- 3.4 Trajectory model . . . 46
- 3.5 Results . . . 47
  - 3.5.1 The snowfall event of 10-11 January 2002 . . . 47
  - 3.5.2 Trajectories . . . 48
  - 3.5.3 Isotope modelling results . . . 51
- 3.6 Discussion and Conclusion . . . 52

4 A Rayleigh-type isotope distillation model along backward trajectories 55
4.1 Introduction . . . 55
4.2 The original MCIM . . . 56
4.2.1 Supersaturation function . . . 57
4.2.2 Mixing ratios . . . 57
4.2.3 Simulated isotopic composition . . . 58
4.2.4 Isotope distillation excluding the mixed cloud effect . . . 59
4.3 Initial isotopic composition . . . 62
4.4 Fractionation threshold . . . 63
4.5 Isotopic recharge . . . 67
4.6 Summary . . . 69

5 Simulation of snow pit records in Dronning Maud Land for the period 1998-2002 73
5.1 Introduction . . . 74
5.2 Study area and accumulation history . . . 76
5.3 Trajectories . . . 78
5.4 Isotopic distillation . . . 85
5.5 Firn diffusion . . . 90
5.6 Simulated snow pit records . . . 91
5.6.1 $\delta^{18}O$ . . . 91
5.6.2 Deuterium excess . . . 94
5.7 Discussion . . . 94
5.8 Conclusions . . . 98

6 A 22 year simulation of isotopic composition of snowfall over the Antarctic continent 101
6.1 Introduction . . . 102
6.2 Methods . . . 103
6.2.1 Trajectory starting points . . . 103
6.2.2 Isotopic modelling along trajectories . . . 104
6.3 Results . . . 105
6.3.1 Antarctic climate in ERA-40 . . . 105
6.3.2 Spatial distribution of $\delta^{18}O$ . . . 109
6.3.3 Spatial δ-T relations . . . 112
6.3.4 Spatial pattern of d-excess . . . 115
6.3.5 The seasonal cycle . . . 118
6.4 Discussion . . . 121
6.5 Conclusions . . . 123

Bibliography 125

Summary 137

Samenvatting 141

Scientific publications **147**

Curriculum vitae **149**

Dank je! **151**

Chapter 1

Introduction

1.1 Antarctica

In many respects, Antarctica is an extraordinary continent. Not only is it the coldest place on Earth (a record minimum near-surface temperature of -89.2 °C has been measured at Vostok), it is also the driest continent, with an average accumulation of only 161 ± 6 mm yr^{-1} (IPCC, 2001), only 20 % of the annual precipitation in the Netherlands. And yet, the Antarctic continent stores 70 % of the world's fresh water, mostly in the East Antarctic ice sheet (Figure 1.1). The Antarctic ice sheet covers almost the entire continent; only mountain ranges (e.g. Antarctic Peninsula, Transantarctic Mountains) and a few coastal oases emerge from beneath it. Complete melting of the Antarctic ice sheet would cause global sea level to rise by 61.1 m (IPCC, 2001). Due to its enormous ice sheet, Antarctica is also the highest continent on earth, with a mean elevation of ∼2000 m above sea level (a.s.l.). The East Antarctic ice sheet consists of several domes, of which Dome A is the highest with an estimated elevation of 4091 m a.s.l.

Due to its remote environment and location, human activity on Antarctica has been limited. Less than two centuries ago, in 1820, the Russian explorer Fabian Bellingshausen claimed to have first sighted the Antarctic mainland. Shortly after this, the American seal hunter John Davis first set foot on the continent in 1821. In 1911, at the peak of the era of heroic exploration in Antarctica, Roald Amundsen (Norway) beat Robert F. Scott (UK) in the race to the geographic South Pole. Scott's party died in the return from the pole, cementing the popular image of Antarctica as unapproachable and inhospitable. In the following decades, Antarctica was seldom visited by explorers, and scientific activities were scarce. An exception to this are the expeditions of Admiral Richard E. Byrd (US), who introduced modern technology in polar exploration, such as the use of air planes and radio communication. Antarctic scientific activities abruptly increased with the International Geophysical Year (IGY) in 1957-58, when many countries set up large scientific expeditions to Antarctica. During the IGY, numerous bases were established, including the US Amundsen-Scott station at South Pole and the Russian station Vostok, which are currently the only

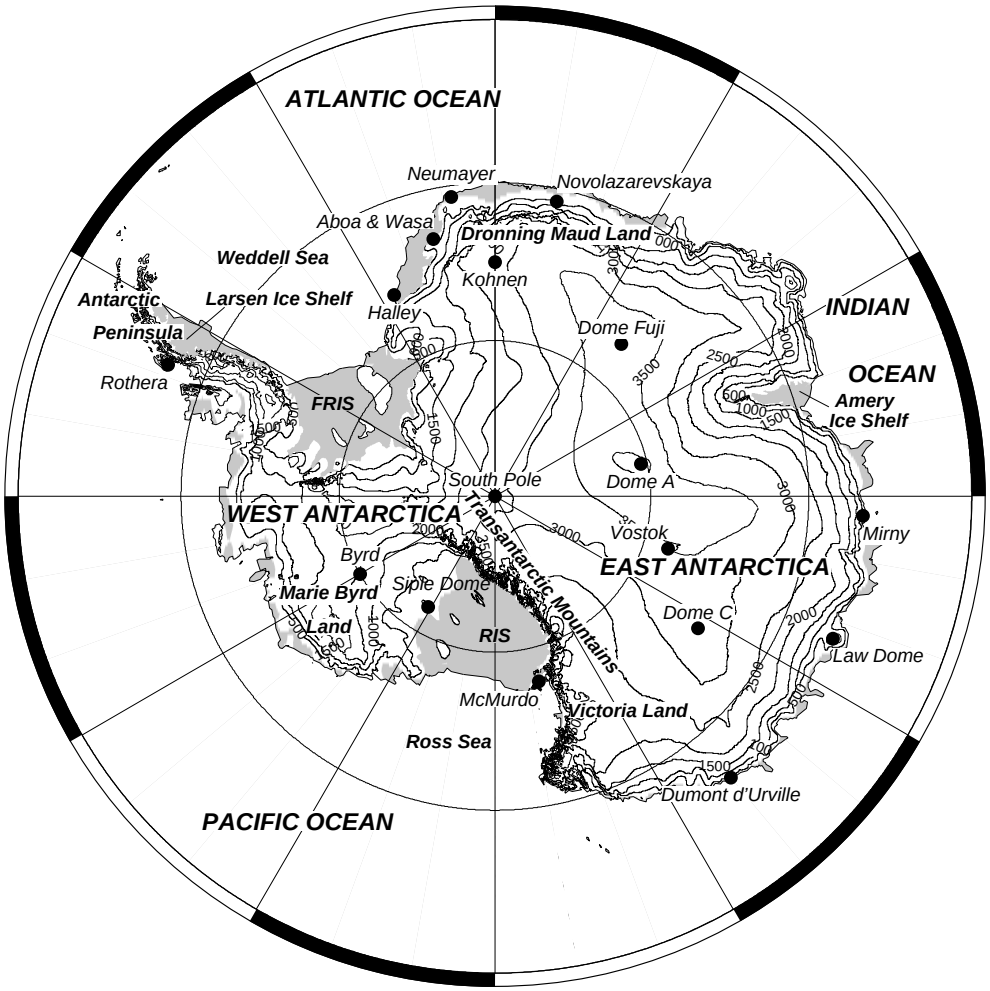

Figure 1.1: *Antarctica. Gray areas indicate ice shelves; FRIS refers to the Filchner-Ronne Ice Shelf and RIS to the Ross Ice Shelf. Elevation data are from the Radarsat Antarctic Mapping Project digital elevation model version 2 (Liu* et al.*, 2001).*

two inland stations that are occupied year-round.

In recent years, Antarctic scientific activity has increasingly concentrated on climate research, which is partly due to concern about the potential impact of global warming. Since we are facing an uncertain climatic future due to increasing levels of greenhouse gasses, there is a strong need for climate predictions. To be able to make sound predictions of future climate, it is essential to understand climate behaviour in the past.

Antarctic research has contributed significantly to our understanding of the climate system, especially due to the wealth of paleoclimatic information stored in the Antarctic ice sheet. To access these climate records, ice cores have been drilled through the ice sheet. These km-long cylinders of ice provide a detailed climate record, because each layer of ice once accumulated as snow (with its inclusions) at the surface of the ice sheet, including wind-blown dust, ash and atmospheric gases. One of the best-known climate proxies is the isotopic composition of water molecules, which contains information on atmospheric temperature. Especially on a glacial-interglacial time-scale, this parameter provides compelling evidence of the variable nature of the global climate system. Additionally, a large advantage of ice cores is that they also contain atmospheric gasses trapped in air bubbles. This allows to study the relationship between atmospheric temperature and greenhouse gasses like carbon dioxide (CO_2) and methane (CH_4).

The Antarctic ice sheet contains the longest ice chronology on Earth, likely longer than one million years. Drilling at Vostok station revealed an ice core record of 420 kyr, showing that the Antarctic climate during this time was characterized by ∼100 kyr cycles, during which atmospheric CO_2 and CH_4 were in phase with stable isotope concentrations in the ice, with high concentrations of greenhouse gasses during interglacial periods (Petit *et al.*, 1999). Marine isotope records provide a global climate signal, and show that over 1 myr ago, these cycles had a periodicity of ∼41 ky and had lower amplitudes (Figure 1.2). However, interpretation of marine isotope records based on benthic foraminifera is not straightforward, since they contain not only a temperature signal, but also a global ice volume component (e.g. Shackleton, 2000; Bintanja *et al.*, 2005). Furthermore, unlike ice cores, marine records do not contain atmospheric gas inclusions.

One of the major ice core drilling programs is the European Project for Ice Coring in Antarctica (EPICA), which aims to obtain a full record of the climatic and atmospheric changes over the past 900 kyr. This, to investigate whether the differences in glacial cycles as seen in marine records are also archived in the ice and to extend this information with a record of atmospheric CO_2 and CH_4. EPICA's objective was to drill two deep ice cores. The first core was drilled at Dome C which yielded a climate record over the past 740 kyr. This record from Dome C indicates that interglacials before ∼400 kyr were somewhat longer but cooler than more recent interglacial periods (Figure 1.2, EPICA community members, 2004). Latest results from the Dome C ice core extend the atmospheric greenhouse gas records back to 650 kyr (Spahni *et al.*, 2005; Siegenthaler *et al.*, 2005), showing a consistent covariant pattern of greenhouse gasses in relation to the isotope record. The second core was drilled at Kohnen station, in the Atlantic sector of Antarctica. This core allows a comparison with the

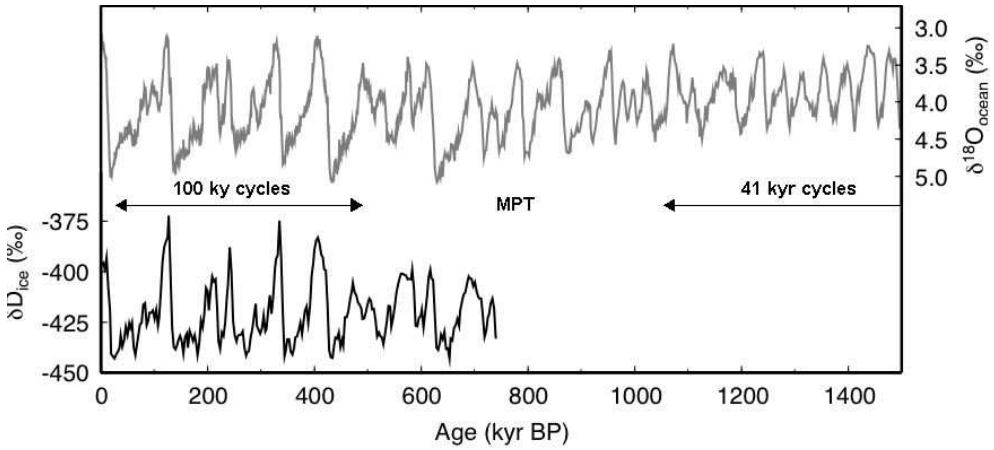

Figure 1.2: *Stacked marine $\delta^{18}O$ record (gray line; Lisiecki and Raymo, 2005) along with the EPICA Dome C δD record (3000-yr averages) (black line; EPICA community members, 2004), showing the occurrence of glacial-interglacial cycles during the last 1.5 million years. Periodicity shifts during the Mid-Pleistocene Transition (MPT) from climate cycles of 41 kyr to 100 kyr.*

ice core records from Greenland, to investigate in detail the coupling between the northern and southern hemisphere.

Climate research in the framework of EPICA addresses a multitude of time-scales. Deep ice cores focus on climate shifts of 10^4 to 10^6 yr, but shallow ice cores and snow pits contain climatic information of 10^0 tot 10^3 yr. On the other hand, meteorological experiments concentrate on processes within days. The work in this thesis addresses the imprint of meteorology in Antarctic snow, focussing on present-day Antarctic snowfall events.

1.2 Stable water isotopes

An important ice core climate proxy relies on stable isotopes, which are present in ice in a proportion that is indirectly related to the temperature of the atmosphere at the time those particles accumulated as snow. Isotopes are atoms of the same chemical element with different atomic mass, due to a different number of neutrons in its nucleus. Three stable isotopes exist of oxygen (O) and two of hydrogen (H)

Table 1.1: *Natural abundances of oxygen and hydrogen isotopes (from: Gat* et al.*, 2001).*

	^{16}O	^{17}O	^{18}O	H	D
abundance (%)	99.759	0.037	0.204	99.9845	0.0155

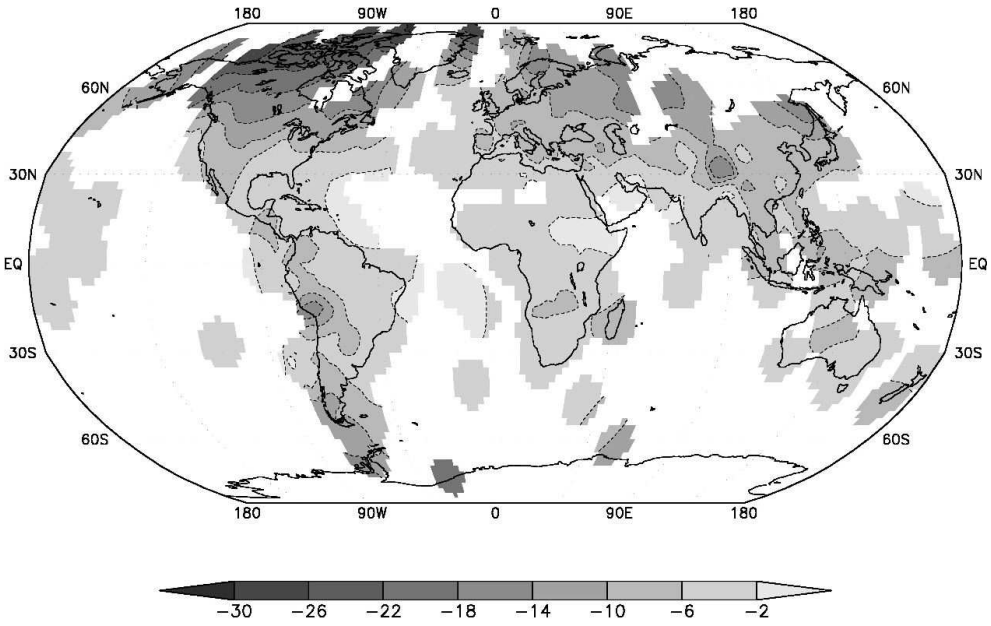

Figure 1.3: *Global distribution of amount-weighted mean annual $\delta^{18}O$ in precipitation from the Global Network of Isotopes in Precipitation (GNIP) database (Birks* et al.*, 2002). Antarctica is largely unresolved by this data set, since hardly any systematic sampling of isotopes in precipitation occurs, apart from some coastal stations.*

(Table 1.1). Hereafter, the heavy isotope ^2H is called deuterium (D). An even heavier H isotope of mass 3 exists (tritium, ^3H) but this isotopic species is unstable with a half-life of 12.32 yr and therefore not used as a temperature proxy. The light isotopic species ^{16}O and H are most abundant, heavier isotopes of these elements are rare.

Water molecules are composed of different combinations of these isotopes, such as $H_2{}^{16}O$, $H_2{}^{18}O$ and $HD^{16}O$. The abundances of these different isotopic species in water may be given by their isotopic ratios, for instance D/H or $^{18}O/^{16}O$. For practical reasons, instead of using the isotope ratio R, isotopic composition is generally given as the relative deviation δ of a sample with respect to a standard value, as defined by:

$$\delta = \frac{R_{sample}}{R_{standard}} - 1 \tag{1.1}$$

Since δ is usually a small number, values are given in ‰ (parts per thousand). The accepted standard for water samples is Vienna Standard Mean Ocean Water (VSMOW), and applied to the D/H and $^{18}O/^{16}O$ ratios for which we use the commonly adopted δD and $\delta^{18}O$ notations, respectively.

Figure 1.3 shows the observed global distribution of mean annual $\delta^{18}O$ values in precipitation. A distinct pattern exists of isotopically heavier precipitation at low

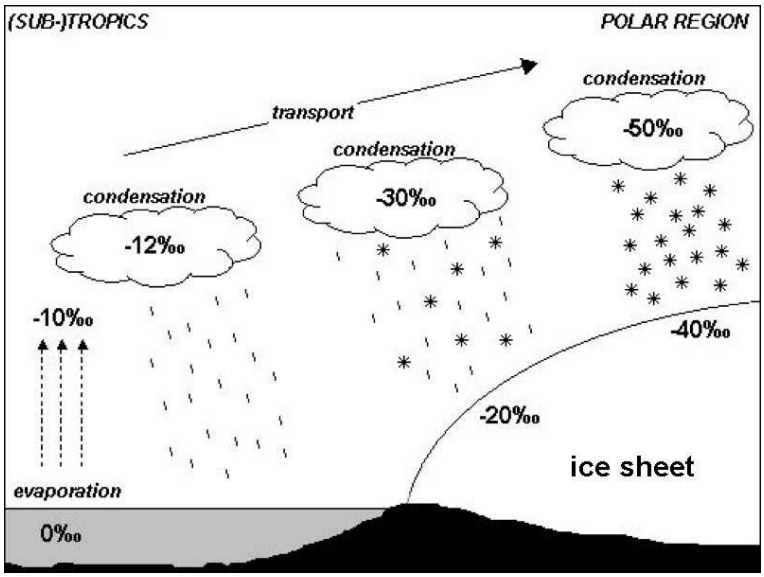

Figure 1.4: *Schematic picture of the hydrological cycle and associated isotopic distillation for* $\delta^{18}O$.

latitudes to isotopically lighter precipitation towards the polar regions. This global pattern of $\delta^{18}O$ in precipitation is related to the process of isotopic fractionation. Isotopic fractionation occurs, because the saturation vapour pressure (e_s) is less for heavy water molecules than for light water molecules at a given temperature (T), as molecular velocities are determined by T and molecular mass. Consequently, in a two-phase system of liquid and vapour, isotopic equilibration will result in a higher concentration of heavy isotopes in the liquid phase compared to the vapour phase.

A schematic representation of the effect of this process on the isotopic composition of precipitation in the high and mid-latitudes is shown in Figure 1.4. Evaporation occurs in the (sub-)tropical oceans, depleting heavy isotopes in the vapour with respect to the remaining ocean water by about 10 ‰. Cooling and associated condensation will produce precipitation with a higher contribution of heavy isotopes, and the remaining vapour will be more depleted in heavy isotopes. When air masses cool further on their way to the polar regions, rain-out of moisture and associated isotopic depletion of the vapour occurs. Hence, precipitation occurring at high latitudes (i.e. at low T) will be more depleted than precipitation at lower latitudes, resulting in the lowest concentrations of heavy isotopes in central Antarctic snow.

As a result, the resulting spatial isotope distribution shows a significant correlation with temperature in the mid- and high latitudes (Dansgaard, 1964). This spatial $\delta^{18}O - T$ relation has often been used in climate reconstructions, translating isotope signals from ice cores directly to past temperature changes (e.g. Jouzel *et al.*, 1987b; Grootes *et al.*, 1993). By doing so, it was assumed that the spatial $\delta^{18}O - T$ relation

can also be applied in time, and stays constant. However, independent temperature reconstructions have revealed that this assumption does not hold for all regions and time-scales. For the Greenland ice sheet, for instance, borehole thermometry has revealed temperature shifts on a glacial - interglacial time scale that are twice as large as would be expected from the local $\delta^{18}O - T$ relation (e.g. Cuffey *et al.*, 1995). Also on the shorter time-scale of Dansgaard-Oeschger events, the temporal $\delta^{18}O - T$ relationship can vary rapidly (Landais *et al.*, 2004). Moreover, the $\delta^{18}O - T$ relation becomes further obscured by changes in the water vapour source area (Boyle, 1997), by the seasonal distribution of precipitation (Werner *et al.*, 2000), and by changes in the strength of the temperature inversion (Van Lipzig *et al.*, 2002a). Due to these complicating factors, isotope records from ice cores should not be quantitatively translated into temperature changes without calibration using independent temperature records or proxies, in particular not on short time scales.

The above-mentioned description of isotopic depletion focusses on $\delta^{18}O$, but the same process leads to a depleted values of δD in polar precipitation. The changes in $\delta^{18}O$ and δD in atmospheric water are fairly well correlated (e.g. Dansgaard, 1964), so that in a $\delta^{18}O - \delta D$ graph the isotopic compositions of precipitation are aligned along a line for which a global average is (Global Meteoric Water Line; Craig, 1961):

$$\delta D = 8\delta^{18}O + 10‰ \tag{1.2}$$

Any deviation from this line is expressed in the second-order parameter deuterium-excess (hereafter called d-excess), defined as follows (Dansgaard, 1964):

$$d{-}excess = \delta D - 8\delta^{18}O \tag{1.3}$$

The d-excess parameter reflects different behaviour of the two isotopic species ($H_2{}^{18}O$ and $HD^{16}O$), and is assumed to be especially sensitive to conditions during evaporation in the oceanic source area, and conditions prevailing during snow formation. Therefore, d-excess is often used as an indicator for (changes in) moisture source conditions (e.g. Merlivat and Jouzel, 1979; Jouzel *et al.*, 1982; Vimeux *et al.*, 1999).

1.3 Isotopic modelling

To provide the climatic interpretation of isotope records in ice cores with a better physical basis, much effort has gone into modelling of the isotopic composition of precipitation. Pioneering work was done by Dansgaard (1964), who presented the concept of Rayleigh fractionation. This is based on the assumption that isotopic fractionation during condensation occurs in isotopic equilibrium and that the newly formed condensate is immediately removed from the air mass. The resulting isotopic composition of precipitation (δ_p) in such a model depends on the fraction (F) of the moisture in the air mass compared to its initial moisture content in the source region, and of the equilibrium fractionation coefficient (α_{eq}) between water vapour and liquid or ice:

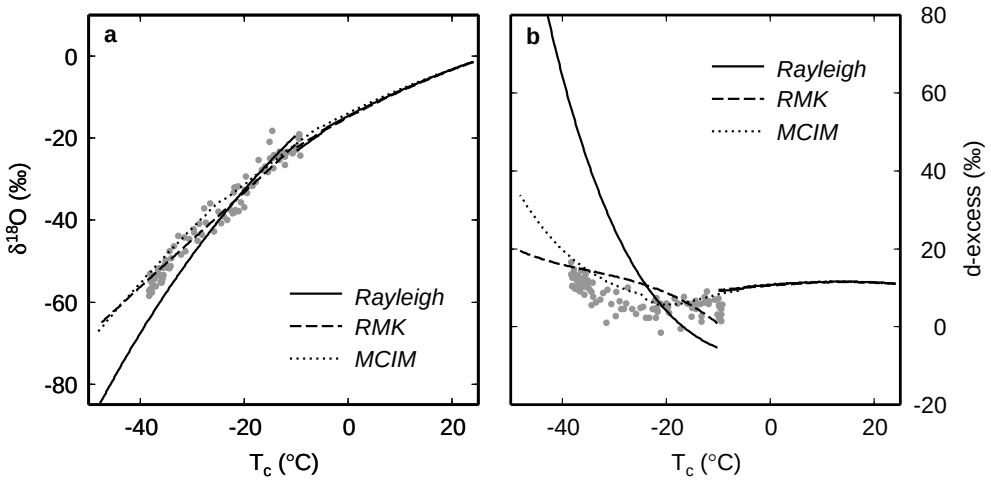

Figure 1.5: *Modelled $\delta^{18}O$ (a) and d-excess (b) as a function of T_c as predicted by different simple isotope distillation models: the Rayleigh model from Dansgaard (1964) (solid line), the Rayleigh Model including the Kinetic isotopic effect (dashed line, RMK: Jouzel and Merlivat, 1984) and the Mixed Cloud Isotopic Model (dotted line, MCIM: Ciais and Jouzel, 1994). Antarctic observations (gray dots) are from Dahe* et al. *(1994), for which values of T_c are calculated from surface temperatures (T_s) using: $T_c = 0.67T_s - 1.2$ (Jouzel and Merlivat, 1984).*

$$\delta_p = \frac{\alpha_{eq}}{\alpha_0} F^{\alpha_m - 1} - 1 \tag{1.4}$$

Since α_{eq} is a function of condensation temperature (T_c) (Majoube, 1971a,b; Merlivat and Nief, 1967), a distinction is made between α_{eq}, α_0 and α_m referring to fractionation factors at momentary T_c, initial T_c and mean T_c, respectively.

The solid lines in Figure 1.5a and b show the dependency of $\delta^{18}O$ and d-excess in precipitation on T_c for pure Rayleigh distillation. This model explains the observed isotope distribution in the mid-latitudes (not shown here). However, the Rayleigh model is not capable of explaining the observed pattern in high latitudes, as illustrated by Antarctic observations (gray dots) in Figure 1.5, where unrealistically high d-excess values are modelled. In comparison with observations, Rayleigh fractionation leads to too much depletion at low temperatures. Finally, there is an unwanted discontinuity between the condensation curves of liquid and solid precipitation, which is due to differences in α_{eq} for solid and liquid condensation, and to differences in e_s over liquid water and ice.

Jouzel and Merlivat (1984) improved modelled d-excess values by introducing a kinetic fractionation effect (α_k) to simulate differences in diffusivity of heavy and light water molecules. This effect occurs during snow formation as a result of vapour deposition on ice crystals in an environment that is supersaturated with respect to ice. The effective fractionation coefficient thus becomes:

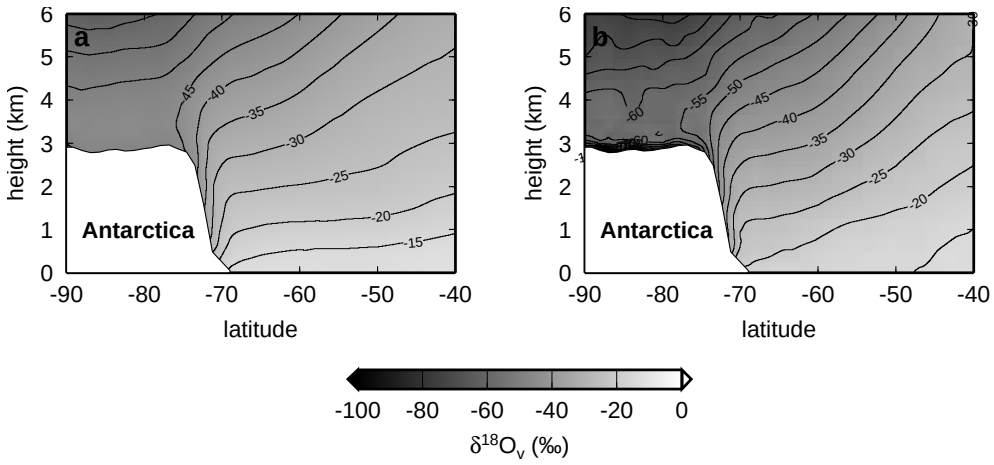

Figure 1.6: *A vertical cross-section of mean monthly $\delta^{18}O$ values of atmospheric vapour in the ECHAM4 model, along the 0° E/W meridian, for January (a) and July (b). The white area in the lower left corner represents the Antarctic continent.*

$$\alpha_{eff} = \alpha_{eq}\alpha_k = \frac{\alpha_{eq}S_i}{\alpha_{eq}D/D'(S_i - 1) + 1} \tag{1.5}$$

where D' and D are diffusion coefficients for heavy and light molecules, respectively, and S_i is supersaturation of vapour with respect to ice. The modelled d-excess values are highly sensitive to S_i. Jouzel and Merlivat (1984) parameterized S_i as a function of T_c in their RMK model (Rayleigh Model including the Kinetic isotope effect). The RMK succeeds much better in reproducing the observed isotope distribution in the polar regions (Figure 1.5, dashed line): the incorporation of α_k during snow formation results in a slightly smaller $\delta^{18}O - T_c$ gradient, and strongly lowers d-excess. Jouzel and Merlivat (1984) proposed several formulations for S_i, all resulting in different d-excess curves (of which only one is shown in Figure 1.5), but all leading to lower d-excess values than obtained by the Rayleigh model.

The discontinuity between solid and liquid precipitation still exists in the RMK model. Ciais and Jouzel (1994) solved this by adding isotopic changes occurring in mixed clouds, i.e. when vapour, liquid and ice coexist for a given range of T_c. Their so-called Mixed Cloud Isotopic Model (MCIM) allows a certain fraction of newly formed liquid and snow to remain in the cloud, enabling a simulation of isotopic changes associated with the Bergeron-Findeisen process (Bergeron, 1935; Findeisen, 1938). This is the process occurring in clouds where air is subsaturated with respect to liquid and supersaturated with respect to ice. Under these conditions, liquid droplets evaporate while snow formation occurs both by direct freezing of liquid droplets and by direct deposition of vapour onto ice crystals. Since in the MCIM the condensate is not immediately removed from the cloud, modelled isotopic distillation is slightly reduced. The behaviour of d-excess in the MCIM remains highly sensitive to the

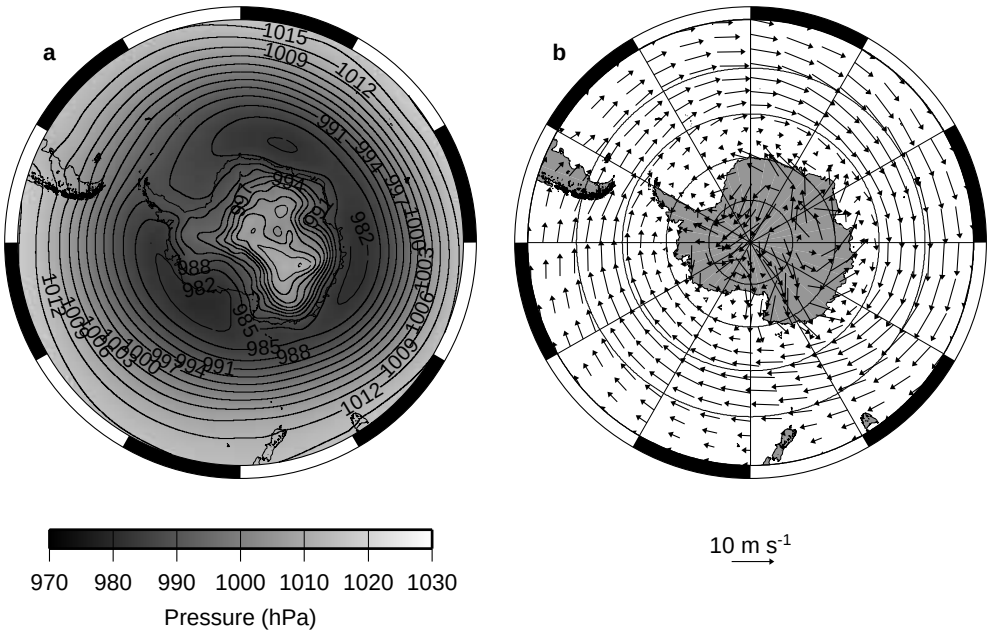

Figure 1.7: *Mean sea level pressure (a) and 10-m wind speed (b) from ERA-40.*

value of S_i. Apart from the discontinuity, differences in the shape of the d-excess curves between RMK and MCIM in Figure 1.5 can be largely attributed to different formulations of S_i.

The above mentioned models are conceptual isotope distillation models, which treat the isotopic evolution of moisture along a theoretical temperature and pressure path, not constrained by meteorological data. For a more realistic simulation of isotopic composition in precipitation, the water cycle must be realistically incorporated in the models. Therefore, general circulation models (GCMs) have been equipped with isotope tracers (Joussaume *et al.*, 1984; Jouzel *et al.*, 1987a; Hoffmann *et al.*, 1998), which are well able to reproduce the main characteristics of the present-day isotope distribution (Jouzel *et al.*, 2000), but generally suffer from an underestimation of the isotopic distillation over the large polar ice sheets (Werner *et al.*, 2001; Mathieu *et al.*, 2002; Noone and Simmonds, 2002b). Isotope fields from GCMs give a good insight in the isotopic composition of water vapour in the atmosphere. Figure 1.6 shows $\delta^{18}O$ of vapour in a cross-section of the Antarctic atmosphere along the 0° E/W meridian, as simulated by the ECHAM4 GCM (Hoffmann *et al.*, 1998; Werner and Heimann, 2002). Large-scale isotopic gradients are visible, both in latitudinal direction and in height. Such simulations of isotopic composition of atmospheric moisture are valuable, since measurements of airborne moisture are scarce (Ehhalt *et al.*, 2005). Due to the complexity of GCMs, however, it is difficult to isolate different processes and their effect on the isotopic composition of the moisture. Moreover, results from GCMs

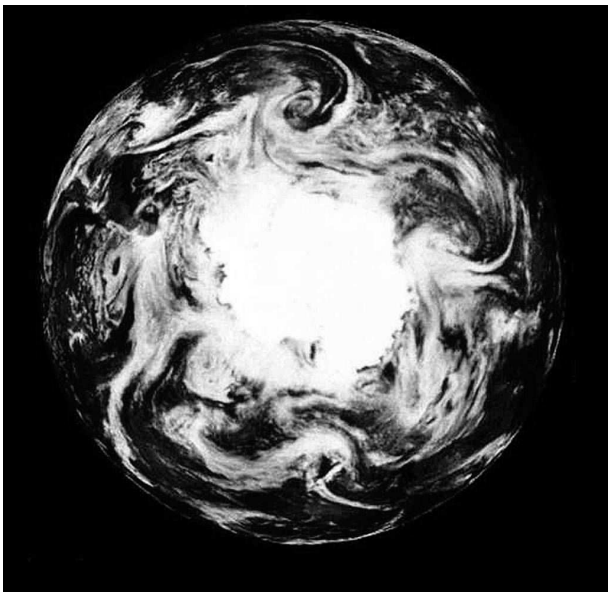

Figure 1.8: *Satellite picture, showing a multitude of cyclonic systems around Antarctica. Image courtesy NASA, JPL; source: Earth Science World ImageBank http://www.earthscienceworld.org/imagebank.*

(in climate mode) cannot be compared to specific snowfall events.

The interpretation of the isotopic composition of precipitation can benefit further from a study combining atmospheric dynamics and isotopic fractionation of moisture, which is the topic of this thesis.

1.4 Antarctic meteorology and precipitation

The present-day average atmospheric circulation in the southern hemisphere is outlined in Figure 1.7. Mean sea level pressure in the Antarctic region is shown in Figure 1.7a. A climatological low pressure zone is found around Antarctica, known as the circumpolar pressure trough. This large-scale pressure distribution forces strong westerly winds over the oceans north of it (commonly known as the 'roaring forties', 'furious fifties' and 'screaming sixties', Figure 1.7b), driving the oceanic circumpolar current. Furthermore, this pressure minimum marks an area with frequent cyclonic activity (Figure 1.8).

The pressure gradient south of the circumpolar trough enforces an anticyclonic circulation resulting in easterly flow at the continental margin (Figure 1.7). Additionally, the cold near-surface air over the ice sheet is forced downward by gravity, resulting in a katabatic wind. The strength and direction of this near-surface wind is strongly dependent of surface slope and it interacts with the large-scale wind (Van

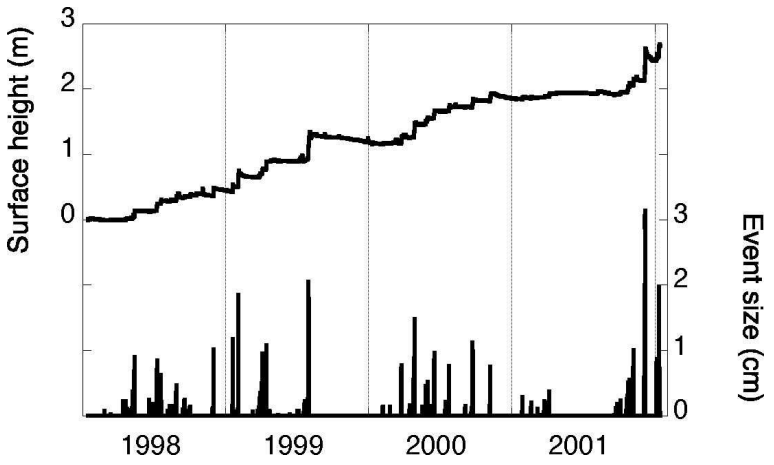

Figure 1.9: *Surface height change and magnitude of snowfall events at AWS 6 (Figure 1.10 and 1.11) in Dronning Maud Land (DML) for the period 1998-2001.*

den Broeke and Van Lipzig, 2003), which results in the complex wind pattern over the Antarctic continent (Figure 1.7b).

This low-level net outflow of air from the continent forces large-scale subsidence over central Antarctica, and air is transported southward on a higher atmospheric level. The pattern of low-level outflow of air is regularly disturbed by synoptic-scale cyclones (Figure 1.8). Such cyclones are associated with advection of relatively warm and moist air towards the ice sheet. These depressions originate mainly at the polar front (usually between 40° S and 50° S, separating temperate mid-latitude air and the cold polar air), and then spiral southward in the direction of the continent (King and Turner, 1997). The circumpolar pressure trough in Figure 1.7 shows three minima, which are preferred areas for the dissipation of cyclones. East of these regions, onshore flow is most common.

Synoptic-scale eddies are responsible for much of the poleward heat and moisture flux (Radok *et al.*, 1975; Physick, 1981), and they are extremely important in determining the distribution and amount of precipitation in Antarctica (Noone *et al.*, 1999). When warm and moist air reaches the continent, orographic lifting then induces precipitation in coastal Antarctica. Occasionally, such disturbances and their fronts reach the Antarctic interior (Sinclair, 1981; Massom *et al.*, 2004), although the steep topographic gradient at the edge of the plateau effectively functions as a barrier, making the interior very dry. Therefore, accumulation decreases rapidly from the coast to the interior. This precipitation climate is characterised by a highly intermittent accumulation record (Reijmer and Van den Broeke, 2003), as illustrated in Figure 1.9, obtained using a sonic height ranger mounted on an automatic weather station (AWS, Figure 1.10). The intermittent character of the accumulation is clearly visible: prolonged dry periods of up to six months occur between snowfall events.

On the high Antarctic plateau, clear-sky precipitation (also known as 'diamond

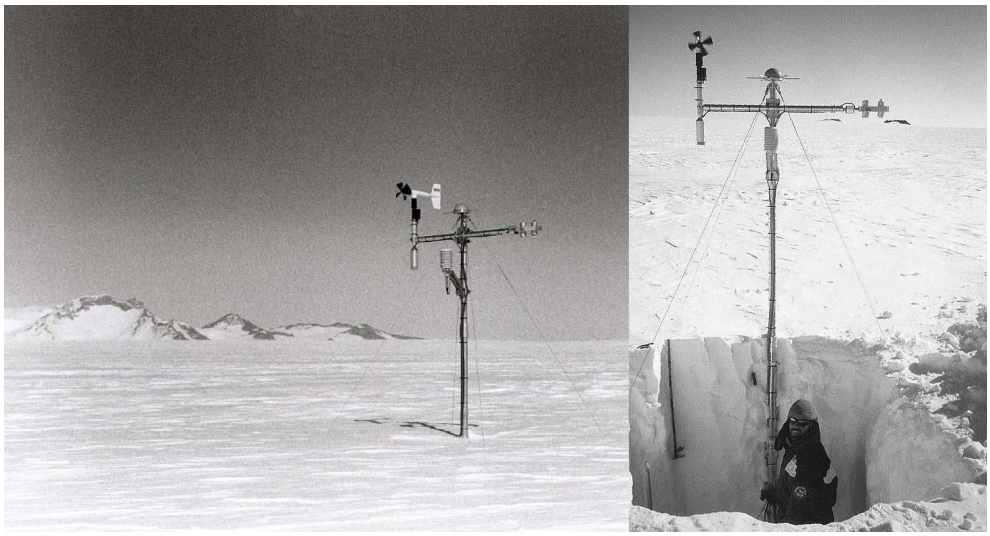

Figure 1.10: *Automatic weather station (AWS) in DML. The sonic height ranger is visible on the left side of the AWS, mounted under the anemometer. Right picture shows a snow pit where snow samples were taken for isotope analysis.*

dust') can be of major importance for the local mass balance (Bromwich, 1988). This type of precipitation is associated with radiative cooling of saturated air at very low temperatures, causing fine ice crystals to precipitate from a clear sky. There is no consensus about the dominant circulation type associated with this precipitation: Bromwich (1988) argues that baroclinic eddies are responsible for moisture advection for clear sky precipitation at South Pole, whereas clear sky precipitation is observed nearly every day at Vostok, which suggests that it is associated with the common anticyclone circulation pattern (Ekaykin, 2003). Clear sky precipitation is likely to disturb the local $\delta^{18}O$-T relation, as is probably forms in the cold Antarctic atmospheric boundary layer.

1.5 This thesis

1.5.1 Goal

The previous sections pointed out that, although stable isotopes in snow are a valuable climate proxy, their interpretation in terms of temperature can be difficult, due to uncertainties in the stability of the δ-T relation in space and time. Isotopic models reproduce the observed isotope variability in Antarctica reasonably well, but suffer from a lack of meteorological constraints, e.g. they assume a continuous cooling, whereas in reality air masses experience a more complex distillation history. The goal of this thesis is to improve the interpretation of stable isotopes in snow, by addressing

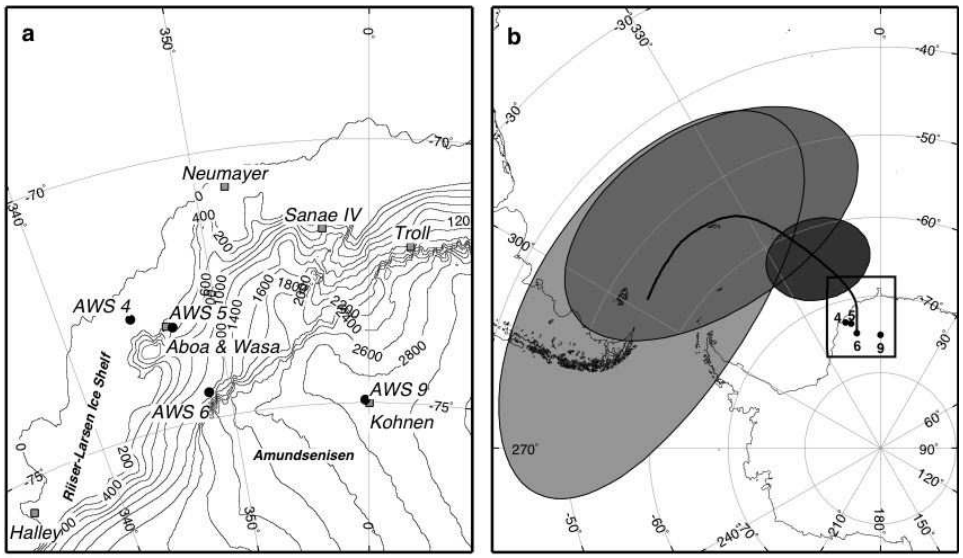

Figure 1.11: *(a) Map of western DML showing the locations of the AWSs (black dots); (b) Mean five-days backward trajectory for snowfall conditions at AWS 6. The ellipses indicate the variability of the air parcel locations at five days (light gray), three days (medium gray) and one day (dark gray) before arrival. The square in (b) indicates the area of western DML, displayed in (a).*

the influence of prevailing meteorological conditions on the isotopic composition of Antarctic precipitation.

1.5.2 Research approach

The experimental basis of this work includes observations from four AWSs in Dronning Maud Land (DML) (Figure 1.10 and 1.11a). The timing of snowfall events was recovered from sonic height rangers, mounted on these AWSs (Figure 1.9). The accumulated snow under this instrument was sampled the austral summer of 2001−2002 (Figure 1.10). Isotopic measurements on these snow samples were carried out by the Centre for Isotope Research (CIO), Groningen, the Netherlands. A host of models is used to interpret the data.

Atmospheric transport paths of moisture bringing snowfall to Antarctica were obtained using backward trajectory calculations. This technique has been used previously to infer moisture source regions for Antarctic snowfall (Reijmer *et al.*, 2002). The trajectory model used in this thesis was developed by the Royal Netherlands Meteorological Institute (Scheele *et al.*, 1996). This model calculates three-dimensional displacements of air parcels, and provides meteorological information along transport paths that serve as input for an isotopic distillation model. The meteorological input data for the trajectory calculations are taken from the European Centre

for Medium-Range Weather Forecasts (ECMWF, Reading, UK) 40-year reanalysis project (ERA-40). As an example, the mean five-day backward trajectory (weighted with accumulation amounts) is shown in Figure 1.11b, for snowfall events at AWS 6 in DML. To indicate the variability of the air parcels' position, covariance ellipses are plotted around the mean location at one, three and five days before arrival. The cyclonic character of atmospheric transport is evident from the clockwise transport pattern.

To study the influence of transport history on isotopic composition of moisture, trajectory data are combined with a Rayleigh-type isotope distillation model (MCIM: Ciais and Jouzel, 1994). This approach offers the opportunity to study isotopic changes in atmospheric moisture along transport and hopefully gives insight in the mechanisms behind observed isotopic patterns. After deposition, small scale isotopic variations quickly disappear due to firn diffusion. For a sound comparison of modelled isotopic composition of snow with observed isotope profiles in snow pits, post-depositional diffusion is calculated using a firn diffusion model (Johnsen *et al.*, 2000). Eventually, this approach was used to model the annual mean isotope pattern over the entire Antarctic ice sheet.

1.5.3 Outline

Isotopic measurements on the snow samples from DML over the period 1998−2002 are presented in Chapter 2. AWS data are used to describe the accumulation history and near-surface temperature during accumulation. The influence of the local vertical temperature profile on the isotopic record is analysed, using results from a regional climate model, to infer temperatures at the level of condensation.

Chapter 3 focusses on a particularly heavy snowfall event during the field season in 2002. Backward trajectory calculations for this event are combined with isotopic modelling, and results are compared to the observed isotopic composition of the snow. Some major difficulties in the approach are revealed, related to the combination of a highly idealised isotope distillation model with specific moisture transport information. Several model assumptions appear not to be in agreement with observed meteorology, which called for a reformulation of the calculation of the initial isotopic signature. Furthermore, conditions during transport are not always favourable for condensation (and associated isotopic fractionation), which necessitated modifications to the isotope model as well. To deal with these problems, several adjustments to the MCIM are described in Chapter 4.

In Chapter 5, the modified MCIM is used in combination with backward trajectory calculations for a simulation of the isotope records described in Chapter 2. For a sound validation of model results with observations, post-depositional isotope diffusion in firn is also taken into account.

Finally, in Chapter 6 the combined approach of isotopic modelling with backward trajectory calculations is applied to the entire Antarctic continent for the period 1980−2002. Results are compared with available observations and with isotope results from a GCM simulation.

Two chapters in this thesis have been published (Chapter 2 and 3) and two chap-

ters are currently undergoing the review process (Chapter 5 and 6). They are presented here in almost the exact form in which they are (to be) published, and therefore they can be read independently of each other. Consequently, some overlap is present between the different chapters.

Chapter 2

Oxygen isotope variability in snow from western Dronning Maud Land and its relation to temperature

Abstract

This chapter presents $\delta^{18}O$ records from snow pits from four locations in Dronning Maud Land, Antarctica that contain at least four annual cycles. The aim of the study was to analyse these records as well as the prevailing temperatures during accumulation in detail, to infer to what extent isotopic composition in this area can be interpreted as temperature information. The original seasonal amplitudes of the isotope records were reconstructed by use of a simple back-diffusion model. Automatic weather station data were used to describe the accumulation history and the near-surface temperatures; the temperatures at the atmospheric level of snow formation were inferred from a regional climate model. The results show that the strongly intermittent nature of the accumulation in this area can result in the exclusion of entire seasons from the isotope records. The temperature records also reveal that the oxygen isotope records in these snow pits are biased towards higher temperatures, since snowfall conditions are associated with higher temperatures. This effect is greatest at low temperatures. A comparison between the seasonal extreme isotopic and temperature values points out that on timescales of seasons to several years, isotopic variability cannot be interpreted with confidence as temperature changes at the accumulation sites.

This chapter has been published as: Helsen, M.M., R.S.W. van de Wal, M.R. van den Broeke, D. van As, H.A.J. Meijer, and C. Reijmer. Oxygen isotope variability in snow from western Dronning Maud Land, Antarctica and its relation to temperature. 2005. *Tellus* **57B** (5), 423-435

2.1 Introduction

Since decades, the isotopic composition in polar snow has been regarded as a valuable temperature proxy and used as such in e.g. the Vostok ice core (Petit *et al.*, 1999), the Greenland Ice Core Project (GRIP Members, 1993), and the recently obtained ice core from Dome C by the European Project for Ice Coring in Antarctica (EPICA community members, 2004). The basis of the use of oxygen isotopes in ice cores as a paleothermometer is the strong spatial relationship between average local temperature (T) and the isotope composition of local precipitation at high and mid-latitudes. The isotopic composition is usually expressed in ‰ as the deviation of a sample from the standard Vienna Standard Ocean Mean Water (VSMOW):

$$\delta^{18}O = \frac{{}^{18}O/{}^{16}O_{sample}}{{}^{18}O/{}^{16}O_{VSMOW}} - 1 \tag{2.1}$$

The spatial $\delta^{18}O$-T relationship (the so-called spatial slope) was first synthesised by Dansgaard (1964) and has often been used to interpret changes in $\delta^{18}O$ in ice cores in terms of temperature changes. However, the use of the spatial slope might not always be justified in the interpretation of isotopic changes in time (Cuffey *et al.*, 1995; Johnsen *et al.*, 1995). Numerous other factors influence the $\delta^{18}O$-T relationship, such as changing conditions in the water vapour source area (Merlivat and Jouzel, 1979), microphysical processes in clouds during snow formation (Fisher, 1991), changes in magnitude of the ratio between advective and diffusive transport (Kavanaugh and Cuffey, 2003), changes in strength of the inversion layer (Van Lipzig *et al.*, 2002a), and seasonality in precipitation (Werner *et al.*, 2000). Another phenomenon that can possibly influence the $\delta^{18}O$-T relationship is the strong short-term relationship between precipitation and temperature: precipitation events in the polar region are often accompanied with higher temperatures than average (e.g., Loewe, 1936; Robin, 1983; Peel *et al.*, 1988; Noone *et al.*, 1999).

For central Antarctica, Jouzel *et al.* (2003) argued that the present-day spatial slope can serve as a surrogate for the temporal slope on glacial-interglacial timescales. On shorter timescales, however, the present-day spatial slope might not be equal to the temporal slope. Nevertheless, in some regions, it appears possible to infer climate changes from isotope records in ice cores, at least on timescales of several decades (e.g., Arastarain *et al.*, 1986; Masson-Delmotte *et al.*, 2003). For short timescales, it may be possible to calibrate the $\delta^{18}O$-T relationship with the seasonal temperature cycle (Shuman *et al.*, 1995; Van Ommen and Morgan, 1997).

Within the framework of EPICA, a deep ice core is being drilled at Kohnen Station, Dronning Maud land, Antarctica (DML, 75° S, 0° W), which is expected to provide a high resolution climate record that covers more than a complete glacial cycle. To support the interpretation of the oxygen isotope signal from this core, numerous mass balance studies have been carried out with shallow and medium-length firn cores from DML (Isaksson *et al.*, 1999; Karlöf *et al.*, 2000; Oerter *et al.*, 1999). In addition, atmospheric modelling experiments have been performed (Van Lipzig *et al.*, 2002b; Van den Broeke *et al.*, 2002). Reijmer and Van den Broeke (2003) studied the mass balance of this area using automatic weather stations (AWSs). Their study shows that

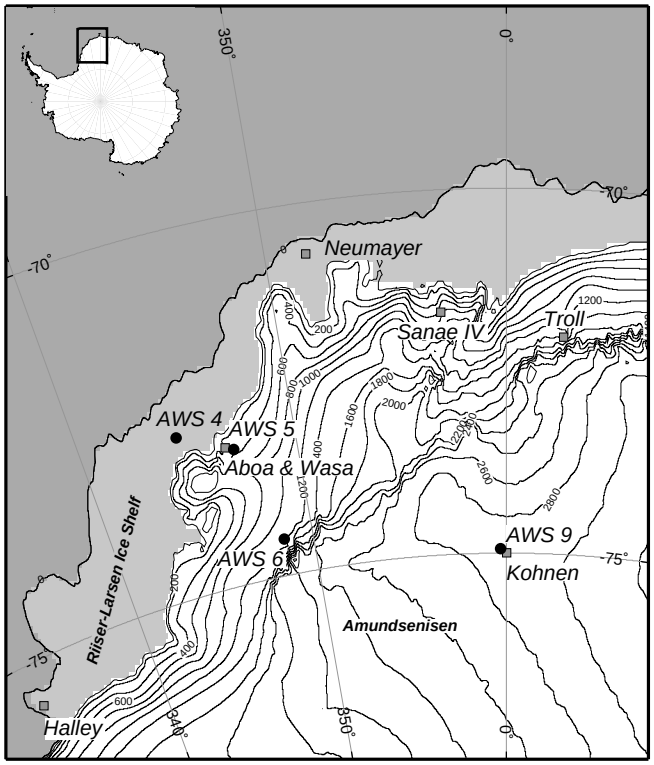

Figure 2.1: *Map of Western Dronning Maud Land, with the four locations of the snow pits near the automatic weather stations. The locations of pit KOH 1 and pit KOH 2 (in the vicinity of Kohnen Station) are not shown as a result of the scale of this map.*

the interannual variability of precipitation is large in DML and that this potentially has a large effect on the oxygen isotope signal in this area.

Although comparisons of isotopic snow composition with the climate of DML are available (e.g., Oerter *et al.*, 1999; Graf *et al.*, 2002), direct comparisons between observed isotopic composition of snow and prevailing meteorological conditions during snowfall events are sparse. McMorrow *et al.* (2001) carried out a detailed comparison between AWS data and isotope records for a different region in Antarctica, Law Dome, which is a high-accumulation area. Helsen *et al.* (2004) combined meteorological data with isotopic modelling to describe depletion of $\delta^{18}O$ of moisture over DML for one accumulation event. The present study aims to contribute to this topic by combining isotope records with meteorological observations from AWSs and to infer to what extent isotopic variability represents prevailing temperatures, with a focus on seasonal variability. Although the deep ice core at Kohnen Station is not expected to show a clear seasonal cycle (due to the low accumulation), the interpretation of isotope records from this ice core can benefit from knowledge of the nature of the

Table 2.1: *AWS topographic and climate characteristics, 1998-2001*[a]

	AWS 4	AWS 5	AWS 6	AWS 9
Start of observation	22 Dec 97	3 Feb 98	15 Jan 98	1 Jan 98
End of observation	21 Dec 01	2 Feb 01	14 Jan 02	31 Dec 01
Location	72°45.2' S, 15°29.9' W	73°06.3' S, 13°09.9' W	74°28.9' S, 11°31.0' W	75°00.2' S, 0°00.4' E
Elevation (m a.s.l.)	34	363	1160	2892
Surface slope (m km^{-1})	0.1	13.5	15.0	1.3
SSMB[b] (kg m^{-2} yr^{-1})	393	179	267	74
Snow density (kg m^{-3})	406	383	396	307
Temperature (K)	253.4	256.8	252.6	230.0
Relative humidity(%)	93	83	78	93
Specific humidity (g kg^{-1})	1.03	1.01	0.72	0.17
10 m wind speed (m s^{-1})	5.7	7.9	7.7	4.8

[a]Source: Van den Broeke *et al.* (2004). [b]SSMB, specific surface mass balance.

local accumulation history.

Section 2.2 presents isotope records from shallow snow pits from four locations in western DML (Figure 2.1). These snow pits were sampled in the vicinity of the AWSs in the field season 2001-2002; the isotope records cover the operational period of the AWSs (1998-2001). To correct for the influence of post-depositional diffusion in the snow pits, the original seasonal isotopic extremes should be reconstructed. This can be done with a simple back-diffusion model, as described in Section 2.3. Section 2.4 contains the accumulation history, derived from data from sonic height rangers (SHRs), which monitor (the change in) surface height in the vicinity of the sampling locations (Reijmer and Van den Broeke, 2003). With the temperature and accumulation data from the AWSs, we constructed profiles of condensation temperature for the snow as a function of current depth. These profiles are compared with the observed isotopic variability in samples from snow pits in order to understand the controls on the observed isotope variability. Temperature during accumulation and the variability of precipitation through the year are evaluated in Section 2.5. The implications for the $\delta^{18}O$-T relationship is discussed in Section 2.6. Section 2.7 summarises the results.

2.2 Isotope records

The snow pits from which we collected samples in the austral summer of 2001-02 are located near four AWSs along a transect connecting the coastal ice shelf (AWS 4) with the high Antarctic plateau (AWS 9) (Figure 2.1). The escarpment region (AWS 5 and 6) forms the transition between these two areas. The AWSs are all equipped with SHRs, which monitor surface height. Table 2.1 lists topographic and meteorological characteristics of these four sites.

We collected samples of snow that accumulated while the AWSs were operational (Table 2.2). To avoid errors due to spatial accumulation variability (e.g., sastrugi),

Table 2.2: *Characteristics of samples taken from snow pits in the field season 2001-02*

	AWS 4	AWS 5	AWS 6	AWS 9	KOH 1	KOH 2
Location	15 m from AWS 4	2 m from AWS 5	under SHR	under SHR	100 m NW of AWS 9	1 km N of Kohnen
sample date	25 Dec	17 Dec	14 Jan	17 Jan	13 Jan	25 Jan
depth pit	4.50 m	2.00 m	3.00 m	0.92 m	1.20 m	1.20 m
δ samples	2.0 cm	2.0 cm	2.0 cm	1.5 cm	1.5 cm	1.0 cm
ρ samples	5.0 cm	5.0 cm	5.0 cm	2.5 cm	2.5 cm	2.5 cm

the ideal snow sampling location would be right underneath the SHR, which would facilitate estimating the deposition time of the snow layers. This was done at AWSs 6 and 9. However, since the stations periodically need rebuilding to prevent them from being covered by snow, the surface around an AWS can become disturbed at the rebuilding horizon. For this reason, the snow pits at AWSs 4 and 5 were dug at a safe distance from the stations. Pit AWS 9 is located ∼2 km west of Kohnen station; radar reflectors were placed directly downwind from the AWS, which caused a disturbance in the wind field. Surface characteristics at this site showed a possible higher contribution of windblown snow to the local accumulation, relative to the surroundings. Near Kohnen Station, pit KOH 1 near a temporary satellite station and pit KOH 2 were dug and sampled at a resolution of 1 cm. The other pits were sampled at a resolution of 1.5 or 2.0 cm (Table 2.2). As pit KOH 2 was situated 2 km to the north of Kohnen station, the accumulation at this site was not disturbed by the presence of the radar reflectors or other obstacles.

We carried out snow density measurements within 50 cm of the snow sampling profile, at a vertical resolution between 2.5 and 5.0 cm (Table 2.2). The snow samples taken for isotope analysis were kept frozen during transport, to avoid isotopic fractionation after sampling.

The $\delta^{18}O$ measurements were carried out at the Centre for Isotope Research in Groningen, The Netherlands, on a SIRA 10 Isotope Ratio Mass Spectrometer with an adjacent CO_2-H_2O equilibration system. The resulting accuracy of the measurements is 0.10 ‰.

Figure 2.2 shows the results of the $\delta^{18}O$ measurements. Clearly, the isotope records cover more than the operational period of the AWSs (1998-2001), since for all AWS locations, at least four summer maxima can be distinguished in the isotope records. The timescale plotted along the horizontal axis was established by starting a new year at each summer maximum. The SHR record was used to distinguish between seasonal and sub-seasonal isotopic maxima. The difference between isotope profiles from a high-accumulation area (AWS 4: ∼393 mm w.e. yr^{-1}) and a low-accumulation area (AWS 9: ∼74 mm w.e. yr^{-1}) is apparent: in the isotope profile from AWS 4, much more intra-seasonal detail has been preserved, compared to the more sinusoidal records from around Kohnen Station (AWS 9, KOH 1 and KOH 2). Note that the horizontal scale of Figure 2.2 is different for each pit, indicating the variation in thickness of the seasonal layers (see Section 2.5). Note also that the Kohnen Station pits tend to show sharp, narrow summer maxima and less pronounced, but more

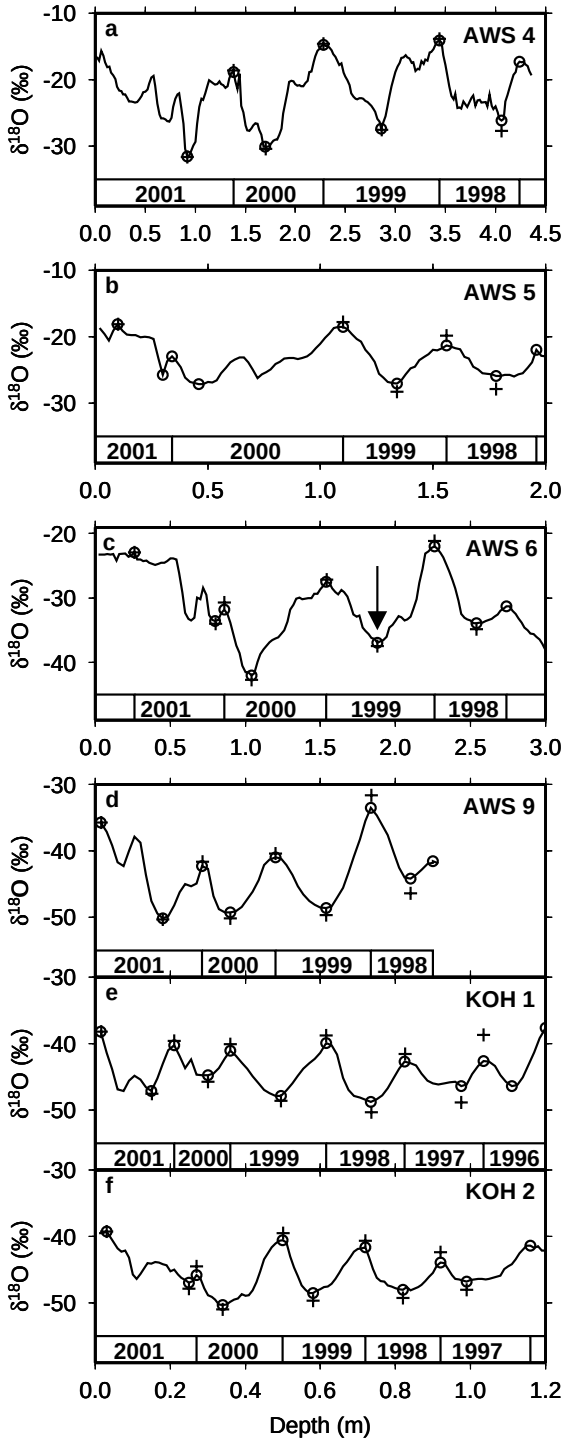

Figure 2.2: *The isotope records from the snow pits at AWS 4, AWS 5, AWS 6, AWS 9, KOH 1 and KOH 2. The data are plotted at sampling resolution, no filtering has been applied. The seasonal extreme values of each year are indicated by circles. The crosses show the back-diffused seasonal extreme values. Above the x-axis, a time indicator is shown, with a new year starting at each summer maximum.*

extended winter minima.

2.3 Reconstruction of the seasonal isotopic variability

To be able to compare the isotopic composition of snow with meteorological conditions prevailing during deposition on an event base, the accumulation should meet two conditions. Firstly, to separate events in the isotope record, the accumulation per event should be greater than the sample resolution. Due to the low accumulation at the Antarctic plateau, this condition probably is not always met at sites like AWS 9. Secondly, to allow neglecting the influence of isotopic diffusion in the firn, low temperatures and high accumulation rates are optimal. Unfortunately, this combination is unlikely. At the coastal ice shelf, accumulation is high, but the temperatures are high as well, which enhances isotope diffusion. On the Antarctic plateau, temperatures are lower, but due to the much thinner seasonal snow layers, diffusion will have a large influence as well, and affect longer time scales in the snow.

The shape of the isotopic records (Figure 2.2) indicates that the seasonal amplitudes decrease with depth. Therefore, we suspect that diffusion cannot be neglected in the study area, even though the time of sampling after deposition of the snow is relatively short ($<$ 4 years). Since the focus of this study is on seasonal variability, the original seasonal isotope signal should be reconstructed, which can be done by using a back-diffusion model.

Molecular mixing in air in the pores of the ice matrix dominates isotope diffusion in firn. Johnsen (1977) first described the physics of this process; this description was later improved by Whillans and Grootes (1985), Cuffey and Steig (1998) and Johnsen *et al.* (2000). The back-diffusion method we used is based on the diffusion theory of Johnsen *et al.* (2000), in which two earlier diffusion equations of Johnsen (1977) and Whillans and Grootes (1985) are combined successfully. Their model describes the smoothing of isotope profiles over time; this smoothing appears to be strongly dependent on temperature and firn density. Density and temperature gradients in the firn would theoretically also influence the magnitude of diffusion, but this effect is so small that it can be neglected (Whillans and Grootes, 1985). Following Johnsen *et al.* (2000), the isotopic composition δ of (not deforming) firn at a depth z changes over time t according to:

$$\frac{\partial \delta}{\partial t} = D(z,t)\frac{\partial^2 \delta}{\partial z^2} \tag{2.2}$$

The diffusivity D depends for each isotopic species on the temperature T and density ρ of the firn. For the diffusion of $\delta^{18}O$, Johnsen *et al.* (2000) defined D as follows:

$$D(z,t) = \frac{m e_{si}(T)\omega_{a18}(T,p)}{RT\alpha_{18}\tau}\left(\frac{1}{\rho} - \frac{1}{\rho_{ice}}\right) \tag{2.3}$$

Here, m is the molar weight of water, e_{si} is the saturation vapour pressure over ice, ω_{a18} is the diffusivity of the heavy isotope (i.e. $H_2^{18}O$) in open air, p is the

ambient air pressure, R is the universal gas constant, α_{18} is the ice-vapour equilibrium fractionation factor for ^{18}O and τ is the tortuosity. For all parameters in this equation, we use expressions as suggested by Johnsen *et al.* (2000).

Eq. 2.2 can be used to model the diffusion of the isotope signal over time. However, a back-diffusion model is needed to reconstruct the undiffused signal from the isotope record. Reversing the diffusion process numerically leads to unstable results because the input isotope record often shows high-frequency variations that quickly blow up to unrealistic values. Even in originally smooth isotope records, artificial intra-seasonal variations develop during back-diffusion modelling. Filtering of the original data is a solution to these problems (e.g., Johnsen, 1977; Cuffey and Steig, 1998; Bolzan and Pohjola, 2000), but has the drawback that it has the same effect as forward-diffusion: it leads to a small but unknown underestimation of the back-diffused amplitudes. Since our main objective was the reconstruction of the original seasonal amplitudes rather than sub-seasonal fluctuations, we preferred not not filter the data, but use a simpler numerical approach described by Bolzan and Pohjola (2000).

This approach only reconstructs the seasonal amplitude based on the extreme values of the isotope record (circles in Figure 2.2) and calculates the back-diffused values from this reduced data set. The second derivative needed in Eq. 2.2 is estimated by assuming that the isotopic variation around an extreme value is sinusoidal. At closely spaced seasonal extremes, this assumption may not hold, but this method generally leads to realistic reconstructions (Bolzan and Pohjola, 2000). The second derivative in Eq. 2.2 is then approximated by:

$$\frac{\partial^2 \delta}{\partial z^2} = \pm \frac{1}{2} \pi^2 \left(\frac{A_i}{\lambda_i^2} + \frac{A_{i+1}}{\lambda_{i+1}^2} \right) \tag{2.4}$$

$A_{i(+1)}$ is the isotopic amplitude above (below) extreme value i; $\lambda_{i(+1)}$ is the seasonal layer thickness above (below) an extreme value i. The plus (minus) sign indicates an isotopic trough (crest). Using this method, we solved the diffusion equation by keeping the upper boundary value fixed, which means that the surface snow is not altered by diffusion. We set the value of the second derivative of the lower boundary equal to the neighbouring extremum (but with the opposite sign), which may introduce a small error, but we omit the last extremum in each pit in the analysis discussed in section 2.6.

We let the calculation start at the moment of sampling, and step backward in time, in steps of one day. Since T and ρ are the key parameters that control the diffusivity coefficient, it is important to use the correct values. We used modelled daily subsurface temperatures from an energy balance model applied to the AWS data (Van den Broeke *et al.*, 2005, in press). For the density, we used a fitted function through our density measurements for each snow pit, and assumed that this density distribution is constant over time.

This back-diffusion method considers the firn as a closed system; eventual enhanced diffusion due to wind pumping (Neumann and Waddington, 2004) is neglected, nor is the influence of isotopic fractionation associated with snow metamorphism (Friedman *et al.*, 1991) taken into account. These assumptions will probably lead to a small underestimation of the back-diffusion in the upper part of the firn.

Table 2.3: *Summary of results of the back-diffusion model*

	Mean amplitude measured record (‰)	Mean amplitude back-diffused record (‰)	Change (%)
AWS 4	6.6	7.0	5
AWS 5	3.1	3.7	19
AWS 6	5.4	5.9	9
AWS 9	5.0	5.9	19
Pit KOH 1	3.6	4.4	22
Pit KOH 2	3.5	4.2	22

In Figure 2.2, the crosses indicate the back-diffused seasonal extremes. Although the differences between measured and modelled extremes do not appear to be very large, the diffusion cannot be neglected: Table 2.3 lists the average seasonal amplitudes of both the measured and the back-diffused records, as well as the relative increase in amplitude. These data show that the seasonal extremes at AWS 5 and at the Antarctic plateau (AWS 9, KOH 1 and KOH 2) have experienced the greatest relative change (∼20 %), which implies that these isotope profiles are most vulnerable to diffusion effects. Relative increases of the seasonal isotope amplitude directly result in equal relative increases of the seasonal $\delta^{18}O$-T slope.

Although the model yields consistent results both in forward and backward mode, the accuracy of the back-diffused seasonal extremes is difficult to assess, since the results cannot be validated. However, the calculations provide the most plausible estimation of the influence of diffusion on the annual isotope cycles. Sampling of snow pits over successive years would provide valuable data to test the robustness of the back-diffusion method.

In general, the model seems to have generated realistic values, with one exception: the seasonal extreme values at AWS 5 from the winter of 2000 to the winter of 2001 (not shown in Figure 2.2). The thin seasonal layer at this location did not allow the assumption of a sinusoidal shape of the δ curve near the extreme values. This resulted in an erroneous reconstruction, due to an overestimation of the second derivative in Eq. 2.4.

According to our results, diffusion has an almost negligible effect on the seasonal amplitude at AWS 4. However, the observed sub-seasonal variation in the record of AWS 4 has not been reconstructed, and it should be stressed that the method used here is not applicable to reconstruct sub-seasonal variability. Therefore, the original sub-seasonal variation may have been larger than the measured variation.

2.4 Accumulation record

The local meteorology and accumulation have been monitored with four similar AWSs (see Reijmer and Van den Broeke (2003) for a detailed description). Table 2.1 gives a summary of the topographic and climatic characteristics of the AWS sites.

For this study, we mainly used the results of the SHRs (Campbell SR50), which measured (the change in) surface height. Every two hours, the instruments measured a time lag between a downward sonic signal and the first received reflected upward sonic signal. Since temperature influences the speed of sound, a temperature correction was applied. The SHR data were filtered with a moving average over a day, after which the record was subdivided into 12-hour intervals.

The SHR records of the surface height change at the four AWSs are plotted in Figure 2.3a. All four records are characterised by discontinuous, sharp increases of the surface height, followed by longer periods of slowly decreasing or constant surface height. The sudden increases of the surface height are caused by snow deposition: a combination of snowfall and a net deposition of drifting snow. The SHR record does not distinguish between the two types of accumulation, but since most of the accumulation events occur simultaneously with events at at least one other AWS, accumulation appears to be predominantly the result of snowfall. During the periods without accumulation, the surface slowly subsides, as a result of settling of the snow and sublimation. Sharper decreases of the surface height are caused by net erosion due to snowdrift.

Note that not all snowfall events have been preserved in the snow pack, since sublimation and snowdrift may have partly removed the accumulated snow. Figure 2.4 displays a close-up of the SHR record. The surface of the snow that accumulated on 26 May 2000 slowly dropped (due to settling, sublimation or wind erosion), until a new accumulation event covered this snow on 29 May 2000, after which the cycle was repeated. An accumulation date was attributed to a snow layer as soon as new accumulation permanently buried the previous layer (Figure 2.4). The top level of this previous layer is then defined as the base level of the new layer. Due to settling of underlying snow, the distance between a certain snow layer and the SHR increases slowly with time. A depth correction using the density measurements was carried out on the SHR data to facilitate comparison with the isotope records. Unfortunately, not all isotope records were sampled at the exact same position as the SHR records (Table 2.2), which makes such a comparison not always straightforward since local accumulation variability can be large (e.g., Richardson *et al.*, 1997; Frezzotti *et al.*, 2002; King *et al.*, 2004).

All preserved accumulation events were identified from the record of the surface height change, as explained in Figure 2.4. Figure 2.3b shows an overview of the timing and magnitude of these events. The monitoring period is too short to draw strong conclusions about seasonality. Nevertheless, for AWS 9 we observe a tendency of increased accumulation in winter. This would explain the relatively broad winter minima in the isotope records, compared to the narrow summer peaks.

The intermittent character of accumulation in this area is apparent: only a few large events account for the bulk of the total accumulation. Reijmer and Van den Broeke (2003) have described the size distribution of accumulation events in more detail. The lack of accumulation over long periods over the year may result in an isotope record that is not representative for the mean annual temperature. This will be further investigated in the next section.

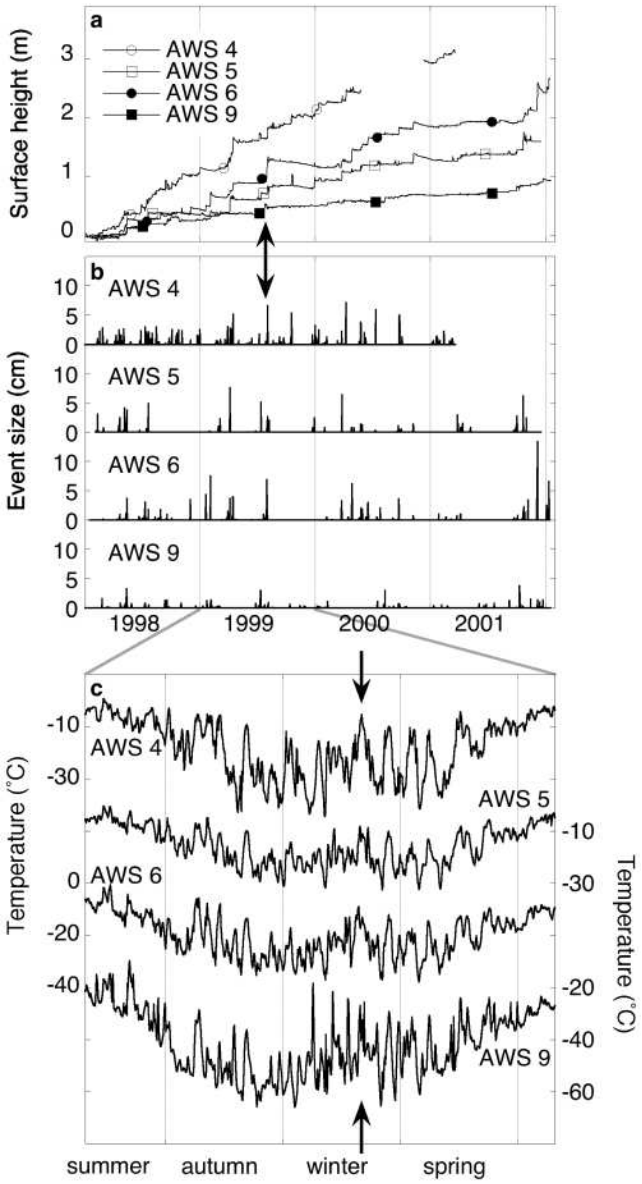

Figure 2.3: *Surface height (a) and identified accumulation events (b) from the AWSs over the period 1998-2001. Due to a malfunctioning SHR, the accumulation history of AWS 4 could only be established until early 2001, with a data gap in winter 2000. The temperature records (daily means) of 1999 are shown in (c). The arrows point to an accumulation event at all four sites in early August 1999.*

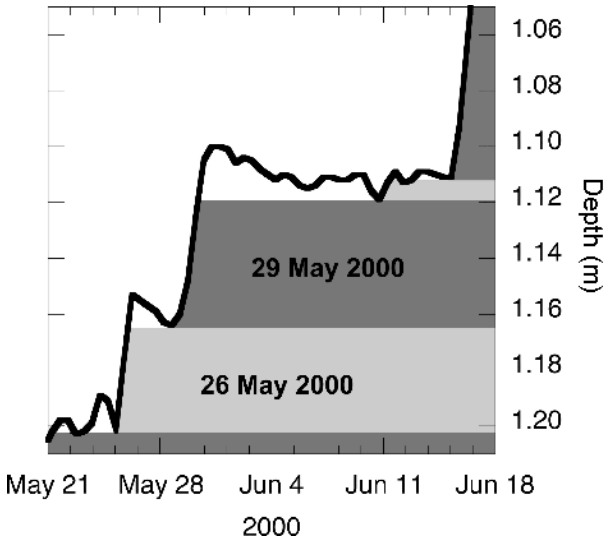

Figure 2.4: *Example of the attribution of an accumulation date to a snow layer. The thick line indicates the SHR data for AWS 6. As soon as the surface height data show a new accumulation event (e.g., at 12h on 29 May 2000), an accumulation date is given to the underlying snow.*

2.5 Temperature during accumulation

To investigate the temperature signal in the $\delta^{18}O$ records, it is valuable to compare them with the temperature records from the AWSs (e.g., Shuman *et al.*, 1995; Van Ommen and Morgan, 1997). However, as accumulation in DML is discontinuous and the $\delta^{18}O$ signal is determined by conditions during accumulation, a comparison with a continuous temperature record is not appropriate, since this study tries to reveal the local controls of the $\delta^{18}O$-T relation. Therefore, we analyse the the temperature records using the time series of the accumulation events. As an example, Figure 2.3c shows the daily temperatures of 1999 as measured by the AWSs. Especially in winter, the temperature is highly variable; higher than average temperatures often coincide with accumulation on DML. This is in agreement with earlier findings for this area by Reijmer and Van den Broeke (2003) and can be explained by the synoptic conditions that are characteristic for accumulation in this region: a low-pressure area over the Weddell Sea and a high-pressure area over eastern DML enhance advection of warm and humid air. The Antarctic plateau then forces the air to rise, inducing orographic precipitation (Noone *et al.*, 1999).

The arrows in Figure 2.3 highlight an example of these typical accumulation conditions. During this period in the middle of the Antarctic winter (August 1999), accumulation occurred at all four sites. Figure 2.3c shows that in that period all four AWSs recorded daily mean temperatures that are comparable to summer conditions. The difference in temperature between snowfall events and average seasonal condi-

tions causes a bias in the isotope record, since only snowfall conditions are preserved in the snow.

The temperature shown in Figures 2.3c is 2-metre temperature, T_{2m}, as measured by the AWSs. The isotopic composition of snow is not directly influenced by T_{2m}. Of greater importance is the temperature at the time and place of snow formation, i.e. the temperature during condensation, T_c. Therefore, we expect that a comparison of the $\delta^{18}O$ records with T_c should lead to a better understanding of the $\delta^{18}O$ relationship.

We obtained T_c from a Regional Atmospheric Climate MOdel, specially designed for the Antarctic region (RACMO2/ANT Reijmer *et al.*, 2005). The European Centre for Medium Range Weather Forecasts (ECMWF) ReAnalysis data set ERA-40 drives RACMO2/ANT at its boundaries. RACMO2/ANT simulates the Antarctic climate at a horizontal resolution of ∼55 km and with 40 vertical levels. RACMO2/ANT has proven to yield more realistic results for the Antarctic region than the ERA-40 data set itself (Reijmer *et al.*, 2005). In the following, we use vertical profiles from RACMO2/ANT at grid points close to the AWS locations in terms of location, elevation and slope.

Figure 2.5 depicts vertical profiles of temperature and condensed water (cloud water content, CWC) at the four AWS locations for two occasions. The solid lines represent the state of the atmosphere during warm conditions on 3 August 1999; the dashed lines show the clear-sky situation on 26 July 1999. These dates are representative examples of the state of the boundary layer during overcast and clear sky conditions, respectively.

During clear-sky conditions (no CWC in Figure 2.5), a temperature inversion develops in the atmospheric boundary layer, which explains the low surface temperatures. Cyclonic disturbances bring warmer and more humid air inland, which often leads to snowfall over the area. During these overcast conditions, no significant temperature inversion is present (Figure 2.5) as the result of an increase of the surface net radiation budget. After the low-pressure system has passed, a stable stratification can redevelop and the surface temperatures drop to low winter values again. Large temperature changes in wintertime (as shown in Figure 2.3c) are the result of switches between inversion and non-inversion conditions. The accompanying temperature differences at the surface can be greater than 30°C. For comparison, T_{2m} as measured by the AWS is plotted in Figure 2.5 as well, and shows that RACMO2/ANT is successful in simulating the near-surface layer. Only at AWS 4 is T_{2m} slightly underestimated.

With respect to the observed isotopic variability in the snow pits, we are interested in T_c during snow formation. For the definition of T_c, the profiles of CWC are of critical importance. A zone with nearly constant temperature can be found at the level of maximum CWC. This level of maximum CWC is defined as the level of snow formation, and the temperature at this level is T_c. Since RACMO2/ANT is only forced at its boundaries, it is free to simulate the climate within its domain. Consequently, it is possible that cyclonic systems arrive a few days later or earlier above DML than calculated. Therefore, we applied a search window of six days around the observed accumulation day to find the right moment of maximum CWC that is compared with the AWS data.

In comparison with the strong difference in T_{2m} between clear-sky conditions

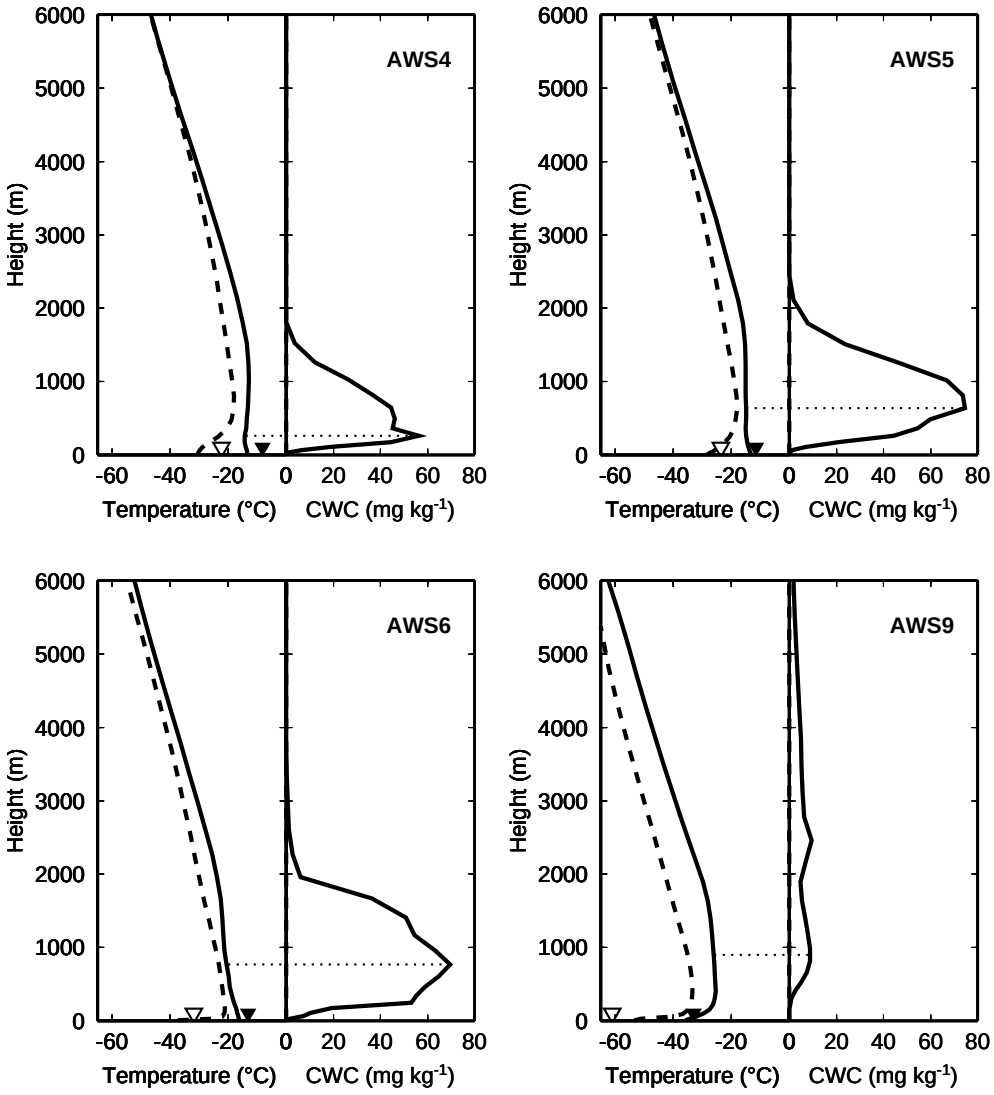

Figure 2.5: *Vertical profiles of temperature (left) and cloud water content (right) at the four sites. On 26 July (dashed lines), clear-sky conditions prevail over DML, which caused a temperature inversion in the atmospheric boundary layer. On 3 August (solid lines), warmer and more humid air brought snowfall to the area. For comparison, the 2-m temperatures as measured by the AWS are plotted as triangles. The levels of maximum CWC and accompanying T_c are indicated by the thin dotted lines.*

and accumulation conditions, we also see a somewhat higher temperature above the atmospheric boundary layer during snowfall, though not as large as for T_{2m}.

To investigate the link between the temperature history and the observed isotopic records further, we retrieved T_{2m} (from the AWSs) and the T_c (from RACMO2/ANT) for all events that were greater than the SHR event resolution (1 cm). These temperatures are plotted in Figure 2.6, and form synthetic temperature records at the resolution of sampling in the snow pits (T_{2m} as white dots and T_c as black dots). Due to the threshold of 1 cm, only relatively large accumulation events contribute to this temperature record. Especially at AWS 9, some of the events fell below this threshold, as a result of which no temperature is determined in some sample increments, resulting in a non-continuous record (indicated by the white zones). The discontinuities in the record for AWS 4 are caused by inferior data from the SHR of this AWS.

The horizontal white lines in Figure 2.6 represent the mean value of T_{2m} over the observed period for each site. For most precipitation events, T_{2m} is higher than this value, indicating that a bias is introduced in the isotope records relative to annual means. Focussing on the preserved amplitude of both T_{2m} and T_c (Figure 2.6; white and black dots, respectively), it appears that these amplitudes are smaller than the amplitude of the annual temperature cycles of T_{2m} in Figure 2.3c. As snow formation occurs during non-inversion conditions or above a possible temperature deficit layer, the seasonal amplitude of the temperature preserved in the isotope record is smaller than the amplitude observed in the seasonal signal of T_{2m}.

The background grayscale in Figure 2.6 indicate the season in which the snow accumulated. Only the data from AWS 4 represent all seasons during the observation period, i.e., no seasons are missing in the annual accumulation record. This is not surprising considering the relatively high accumulation rates at this site on the coastal ice shelf. In the records from AWSs 5, 6 and 9, all lower accumulation sites, the seasons are often very poorly resolved, or even lacking completely, e.g., the summer and winter of 2001 at AWS 5. This explains the lack of a pronounced seasonal cycle for 2001 in the isotope record of AWS 5 (Figure 2.2b), and the problems arising with the reconstruction of these seasonal extreme values.

Nevertheless, for most years the isotope records exhibit a clear seasonal cycle (Figure 2.2). However, the seasonal variations in the associated temperature records (Figure 2.6) are much less pronounced. A good example that illustrates this is the shape of the temperature record for AWS 6 for 1999 (Figure 2.6c) in comparison with the isotope record of AWS 6 (Figure 2.2c). The temperature during accumulation in autumn and winter 1999 (arrow in Figure 2.6) remained on a constant level, close to the mean temperature over the total observed period. Nevertheless, in Figure 2.2c the $\delta^{18}O$ record shows a clear winter minimum in the centre of the 1999 layer (arrow in Figure 2.2), much lower than the $\delta^{18}O$ value of the preceding autumn. This qualitative comparison between the measured isotope records and the synthetic temperature records shows that T_c does not explain all variability in the isotope record. Certainly during winter precipitation, T_c often remains too high to explain the observed isotopic values in the moisture.

It should be stressed that due to the limited accuracy of the SHR, we only used temperatures prevailing during the larger accumulation events (>1 cm) for the con-

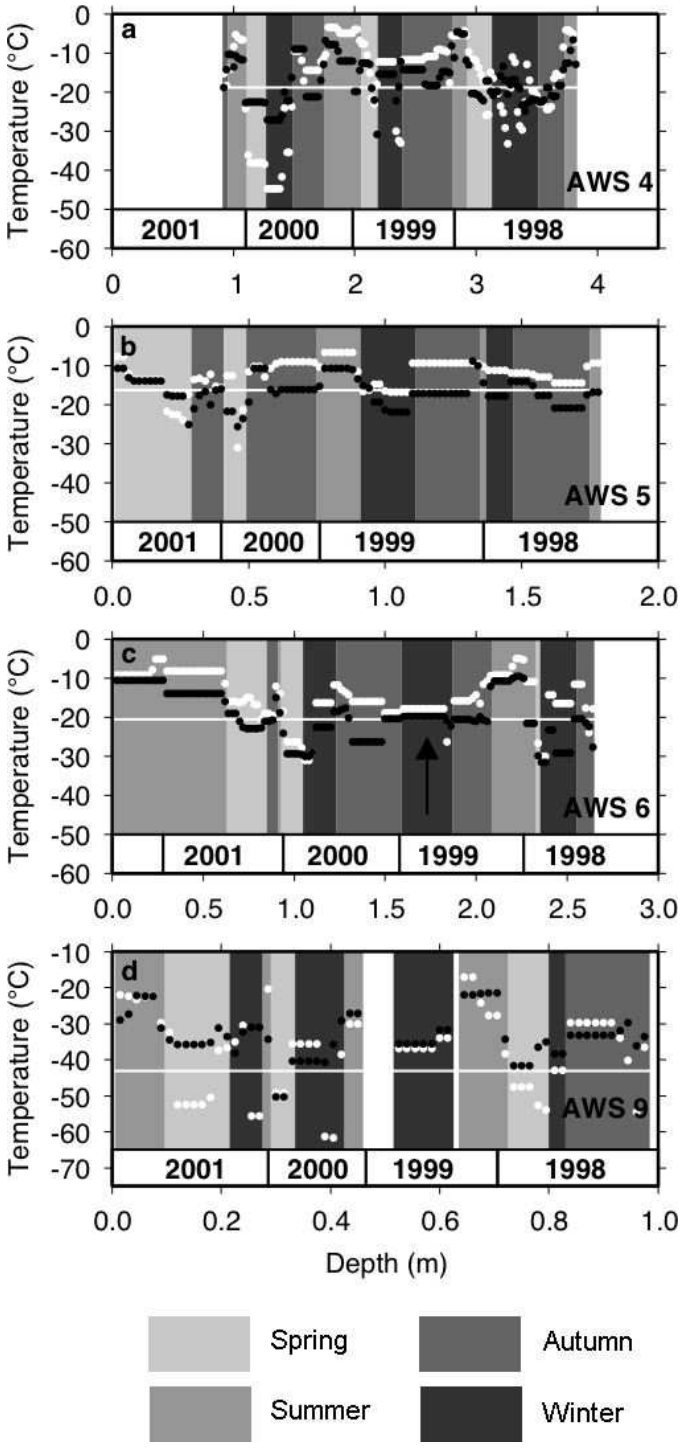

Figure 2.6: *T_{2m} (white dots) and T_c (black dots) during accumulation. The climatological value of T_{2m} is indicated by the horizontal white line. The background grayscale indicate the season of accumulation (Spring (SON), Summer (DJF), Autumn (MAM), Winter (JJA)). Above the horizontal axis, a time indicator is displayed.*

struction of the temperature records in Figure 2.6. Mainly for AWS 9, the exclusion of smaller events could potentially explain the lack of coherency between temperature and the $\delta^{18}O$ signal. However, we tested this potential error by also incorporating temperatures during accumulation events smaller than 1 cm. This barely changed the temperature records in Figure 2.6, which supports our conclusion that local temperature variability cannot entirely explain the observed isotopic variability.

Besides T_c, it is the temperature difference over the distillation path that determines the isotopic composition of the moisture (e.g., Jouzel *et al.*, 1997). An explanation for the observed values in the wintertime precipitation can be that the source region of this water vapour is situated more to the north, due to the increased sea ice extent in winter. For a better understanding of the observed isotopic variability, knowledge of the transport history is thus necessary.

2.6 Implications for the $\delta^{18}O$-T relationship

This section quantifies the warm bias that is introduced in the isotope record and discusses its implications for the interpretation of the isotope records. Furthermore, the seasonal amplitudes of T_{2m} and T_c are compared to the observed seasonal isotope cycle, by establishing seasonal $\delta^{18}O$-T relationships. Figure 2.7 visualises the temperature bias for the four-year period. Figure 2.7a shows a plot of the temperatures as measured by the AWSs during accumulation events, $T_{2m,event}$, against the average temperature of the month in which accumulation took place, $T_{2m,month}$. In general, $T_{2m,event}$ is higher than $T_{2m,month}$, and this effect becomes larger at lower temperatures. This indicates that the warm bias during accumulation is larger in winter an in the Antarctic interior. In addition, the scatter between $T_{2m,month}$ and $T_{2m,event}$ becomes larger with decreasing temperature, which makes a relationship between $T_{2m,month}$ and $T_{2m,event}$ not useful. This points out that with decreasing temperatures, the individual accumulation events contain less information about average monthly conditions.

We calculated the mean deviation of $T_{2m,event}$ from $T_{2m,month}$ for each site, shown as the white bars in Figure 2.7c. The magnitude of the introduced temperature bias is $\sim$4.5°C for AWSs 4, 5 and 6. For AWS 9, this bias is much larger: $\sim$8.5°C. This large bias is related to the low accumulation rate at this site: the deviation from average conditions will be relatively large at a site with little accumulation. However, the large magnitude of the standard deviation of this bias (also shown in Figure 2.7c) is of particular importance for the interpretation of the isotope records. This again points out that fluctuations in isotopic composition between individual accumulation events are not readily interpretable as local temperature fluctuations.

These results show that the isotopic composition of individual accumulation events does not contain consistent temperature information. The question that comes up is: what is the shortest timescale over which the isotope records in this area contain significant temperature information? Since our data only cover four years, we can only test the effect of annual averaging, and not for longer timescales. This effect is depicted in Figure 2.7b. All temperatures during accumulation are averaged over a

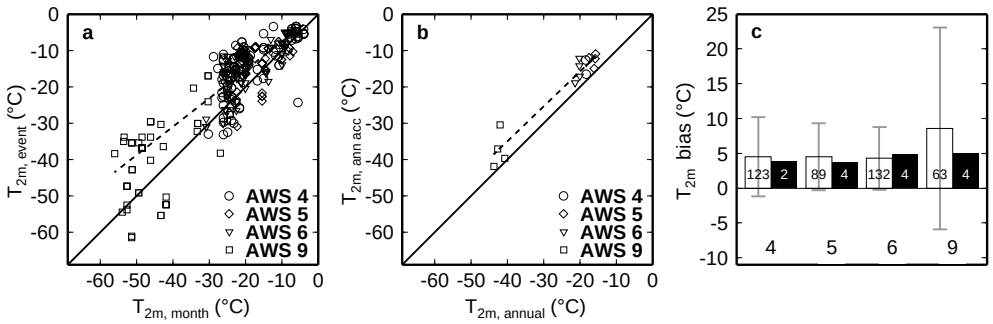

Figure 2.7: *(a) Mean monthly values of T_{2m} versus $T_{2m,event}$ for all events; (b) annual averaged values of T_{2m} versus mean annual values of $T_{2m,event}$; and (c) the total temperature bias introduced in the accumulation records with its standard deviation. White bars indicate the average temperature bias of $T_{2m,event}$ from $T_{2m,month}$ [data from (a)]. Black bars show the average temperature bias of $T_{2m,event}$ from $T_{2m,annual}$ [data from (b)]. The number of points used for the averaging is indicated in the bars.*

year, $T_{2m,ann\,acc}$, and plotted against the annual temperature of the site, $T_{2m,annual}$. In each of the observed years,$T_{2m,ann\,acc}$ is higher than $T_{2m,annual}$. The large scatter as observed in Figure 2.7a is no longer present. This results in an apparently better relationship between $T_{2m,annual}$ and $T_{2m,ann\,acc}$. On a spatial scale this holds true and we only see a spatially nearly constant offset of $T_{2m,ann\,acc}$ with $T_{2m,annual}$. This offset is depicted as the black bars in Figure 2.7c. We did not calculate the standard deviation as we had only a few data points. If the temperature bias per location were be equally large for each year, a simple correction could be made for the interpretation of isotope records (using the dotted line in Figure 2.7b). However, even after annual averaging, $T_{2m,ann\,acc}$ shows large differences between the years (over 10°C for AWS 9), in contrast to $T_{2m,annual}$, which shows at most 2°C difference. Furthermore, the AWS 9 data reveal that the warmest year according to $T_{2m,ann\,acc}$ is not the warmest year according to $T_{2m,annual}$ so, in other words, $T_{2m,ann\,acc}$ and $T_{2m,annual}$ do not covary. The implication for the interpretation of isotope records in this area is that annual shifts in $\delta^{18}O$ cannot be translated into changes in mean annual temperature, i.e., annual averaging of isotope data does not provide an accurate annual paleothermometer for DML on these short timescales. However, we expect that an increase of the period of averaging to, e.g., a decade, will lead to a more consistent relationship between temperature during accumulation and climate. This in turn would support the use of $\delta^{18}O$ as a climate proxy on these longer timescales.

This study also offers the possibility to address the relationship between annual mean values of T_{2m} and T_c during accumulation. This can be useful regarding the classical linear relation used in East Antarctica, linking inversion temperature and surface temperature (Jouzel and Merlivat, 1984). Although this transfer function is computed using spatial differences in the inversion strength, it is often used to translate changes in inversion strength over time. Although we only have a limited

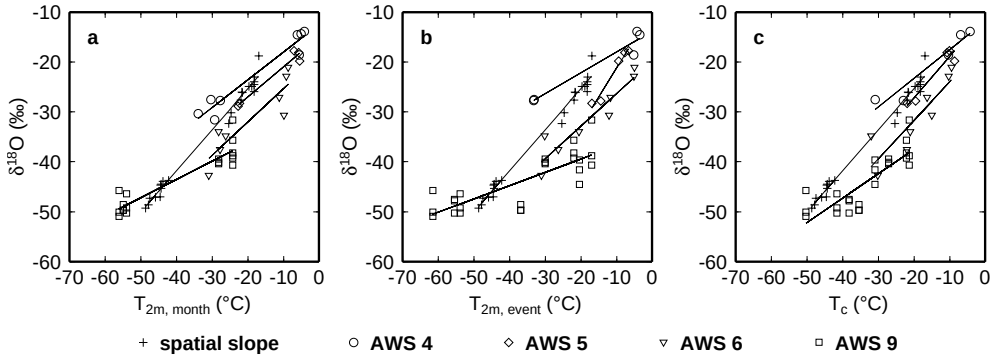

Figure 2.8: *$\delta^{18}O$-Temperature relationships, using (a) seasonal extreme values of $T_{2m,month}$, (b) $T_{2m,event}$, and (c) T_c. The spatial slope (crosses) is plotted as a reference.*

period of data, a comparison of time series of annual mean values of T_{2m} and T_c weighted with accumulation (not shown) demonstrate that annual means of T_c during snowfall are not covariant with mean annual values of T_{2m}. This is in agreement with results from Van Lipzig *et al.* (2002a), who pointed out that changes in the strength of the inversion layer can introduce large temperature biases on an inter-annual timescale.

Since the annual cycle in $\delta^{18}O$ and T is much larger than the inter-annual variation, a comparison of the annual isotopic cycle with the annual temperature cycle still seems valuable. To assess the relationship between the isotopic composition and the annual temperature cycle, we plotted the back-diffused seasonal extreme values of $\delta^{18}O$ against different associated temperatures. From these plots, we calculated the seasonal $\delta^{18}O$-T slope (Table 2.4). Firstly, for Figure 2.8a, we applied the method as described by Van Ommen and Morgan (1997), using the annual amplitude of monthly mean values of T_{2m}. All temperatures prevailing during the warmest and coldest months of the year have been used in this method, including non-accumulation days. The slopes from Figure 2.8a are based on two areas of data points far apart in the graph, a winter minimum and a summer maximum. As a reference, the spatial $\delta^{18}O$-T relationship for this area is also plotted (crosses). This spatial slope is based on the mean isotopic composition of shallow firn cores and 10-m firn temperatures from coastal sites and sites on the Antarctic plateau in western DML (Oerter *et al.*, 1999). The resulting slopes of the $\delta^{18}O$-T relationships are all smaller than the spatial slope of this area (Table 2.4), which can be attributed to the fact that the winter temperatures used in this plot are the temperatures of the coldest month of each year. This is in line with findings of, e.g., Van Ommen and Morgan (1997).

We then used $T_{2m,event}$ during accumulation as well as T_c during accumulation (Figure 2.8b and c, respectively); if T_c is used, the $\delta^{18}O$-T slopes become steeper, and more in line with the spatial slope, since condensation temperatures during accumulation are much higher than $T_{2m,monthly}$ in winter. Nevertheless, Figure 2.8b

Table 2.4: *Characteristics of the $\delta^{18}O$ relationships at the different snow pit sites.*

	$T_{2m,month}$		$T_{2m,event}$		$T_{c,acc}$	
	slope (‰ °C^{-1})	r	slope (‰ °C^{-1})	r	slope (‰ °C^{-1})	r
AWS 4	0.55	0.97	0.42	0.97	0.57	0.96
AWS 5	0.60	0.98	1.16	0.98	0.83	0.96
AWS 6	0.67	0.90	0.65	0.94	0.77	0.88
AWS 9	0.37	0.93	0.27	0.81	0.49	0.84

The spatial slope from Oerter *et al.* (1999) has a value of 0.83 ‰ °C^{-1} (R=0.99).

shows that when $T_{2m,event}$ is used as a reference temperature, AWS 4 and 9 still have a low seasonal $\delta^{18}O$-T slope. This is due to a persistent temperature inversion at these locations, since the slope of the regression line for AWS 4 and 9 is steeper if T_c is used. At AWS 5 and 6, no strong temperature inversions occurred during large accumulation events.

Although it should be emphasised that the relationships derived in Figure 2.8 are based on few data points, the seasonal $\delta^{18}O$-T slopes (Figure 2.8c) in general approach the spatial $\delta^{18}O$-T relationship from Oerter *et al.* (1999). It is not unexpected that the 'classical' derived seasonal slopes (Figure 2.8a) are all lower than the spatial slope, since the seasonal cycle will also influence temperature in the source area of the moisture. This will moderate the extra fractionation in winter, resulting in a smaller seasonal fluctuation in the $\delta^{18}O$ signal, and a low $\delta^{18}O$-T slope. It is not likely that the spatial slope is influenced by this correlation of source and site temperature. Due to the use of T_c (Figure 2.8c), the seasonal $\delta^{18}O$-T slope increases, since the annual cycles of T_c are only small.

Although the newly derived seasonal slopes are comparable to the spatial slope, this result cannot be considered as support for the use of the spatial $\delta^{18}O$-T relationship as a paleothermometer on a seasonal scale, since as demonstrated above, the isotopic composition of individual events does not contain accurate information about monthly mean temperatures. Furthermore, selecting only temperatures during accumulation also leads to a weaker correlation coefficient r (Table 2.4) of the $\delta^{18}O$-T relationship. The temperature at or above the accumulation site does not explain all of the observed isotopic variability. Besides, the established $\delta^{18}O$-T relationships are sensitive to the inclusion or exclusion of one or more summer or winter maxima, indicating that the seasonal $\delta^{18}O$ variations in this area cannot reliably be interpreted as strictly variations in either 2 m temperature or temperature at the level of snow formation.

2.7 Summary and conclusions

In this study, the relationship between isotopic composition of snow and temperature during snow formation has been assessed. The seasonal extremes of isotopic composition were reconstructed by using a back-diffusion model. AWS data revealed that

during accumulation, temperature is above average. This effect is most pronounced in winter and at low-accumulation sites such as the Antarctic plateau. This is in line with earlier findings of, e.g., Peel *et al.* (1988), Noone *et al.* (1999) and McMorrow *et al.* (2001). More important for the climatic interpretation of isotope records is the high inter-annual variability in the temperature during accumulation, compared to the inter-annual variability in annual mean temperature. These results show that isotope records in this area are a poor indicator of local temperature on timescales of days to several years. The number of years over which averaging should be performed to obtain an isotope record that better covaries with temperature cannot be determined from a limited data set such as we used here.

Van Lipzig *et al.* (2002a) used the temperatures at the level where precipitation is formed to quantify the possible effects of the warm bias and the effects of seasonality in precipitation. In this chapter, we have presented a comparison between observed seasonal isotopic variations and temperatures at the level of snow formation. This comparison indicates that temperatures during accumulation are not able to explain the observed isotopic variability. This in turn points out that the isotope signal is not just determined by the local temperature, but is a more complex regional signal, influenced by for instance conditions along the transport path of the water vapour and in the source region.

With regard to seasonal variability, our results indicate that the slope of the seasonal $\delta^{18}O$-T relationship depends to a large extent on which temperature is considered. The slope is lowest when the annual cycle of monthly average values of T_{2m} is used (Figure 2.8a). If cloud temperatures during accumulation are considered, the slopes are greater and more comparable to the spatial $\delta^{18}O$-T relationship (Figure 2.8c), but correlation coefficients are lower. This again indicates that in contrast to the apparent firm $\delta^{18}O$-T relationship on a spatial scale, the seasonal variability of the isotopic composition in this area cannot just be explained by changes in 2-m temperature or even by the temperature at the level of snow formation. This leads us to conclude that, on a timescale of days to several years, the direct interpretation of isotope shifts in terms of temperature change is not recommended for this area. To derive a better physical relationship between observed meteorological data and isotopic variability, a better understanding of the relative contribution of the different stages of depletion along the water vapour transport path is crucial. Such an approach will be adopter in the following chapters.

Chapter 3

Modelling the isotopic composition of snow for a particular precipitation event in Dronning Maud Land

Abstract

We consider a specific accumulation event that occurred in January 2002 in Western Dronning Maud Land, Antarctica. Snow samples were obtained a few days after accumulation. We combine meteorological analyses and isotopic modelling to describe the isotopic composition of moisture during transport. Backward trajectories were calculated, based on European Centre for Medium-Range Weather Forecast operational archive data so that the history of the air parcels transporting water vapour to the accumulation site could be reconstructed. This trajectory study showed that the air masses were not (super-) saturated along the greater part of the transport path, which is in contrast with assumptions in Lagrangian fractionation models and probably true for most precipitation events in Antarctica. The modelled fractionation along the trajectories was too limited to explain the measured isotopic content of the snow. It is shown that the observed isotopic composition of precipitation resulted from fractionation of initially more depleted water. This lower initial isotopic composition of water vapour might result from atmospheric mixing with more depleted air along the trajectory or from earlier condensation cycles, not captured by the trajectories. This is in accordance with isotope fields resulting from general circulation models, indicating a gradient in isotopic composition from the equator towards Antarctica.

This chapter has been published as: Helsen, M.M., R.S.W. van de Wal, M.R. van den Broeke, E. Kerstel, Masson-Delmotte, V. H.A.J. Meijer, C. Reijmer and M.P. Scheele. Modeling the isotopic composition of Antarctic snow using backward trajectories: a particular accumulation event in Dronning Maud Land, Antarctica. 2004. *Ann. Glaciol.* **39**, 293-299.

3.1 Introduction

The isotopic composition of precipitation is regarded as a powerful tool to investigate palaeoclimate (e.g. Jouzel *et al.*, 1997). The empirical link between the isotopic ratios $\delta^{18}O$ and δD of precipitation (hereafter called δ) and local temperature (T) is the basis of reconstructions of climate fluctuations and has been synthesised by Dansgaard (1964). Although the water isotope ratios are regarded as a valid temperature proxy, there is some debate to what extent this proxy can be used as a climate indicator, because the δ-T relationship appears to vary in space and time (e.g. IAEA, 1992; Cuffey *et al.*, 1994; Johnsen *et al.*, 1995; Boyle, 1997; Jouzel *et al.*, 1997; Dahl-Jensen *et al.*, 1999; Hoffmann *et al.*, 2000; Holdsworth, 2001; Van Lipzig *et al.*, 2002a).

To give the isotope thermometer a better physical basis, attempts have been made to model the fractionation process of water in the atmosphere. This has either been done using general circulation models (GCMs) with water isotope tracers or using Lagrangian parcel models, based on Rayleigh distillation. The GCM approach is promising, and has been able to reproduce the global variation of δ in precipitation (e.g. Jouzel *et al.*, 1997; Hoffmann *et al.*, 1998, 2000; Mathieu *et al.*, 2002; Noone and Simmonds, 2002a,b; Werner and Heimann, 2002). An advantage of this approach is that it includes all physical processes involved in the determination of the δ value: from evaporation at the oceanic source region, mixing of air masses, cloud formation, droplet re-evaporation, to condensation conditions. Also the impact of seasonality of the snowfall can in this way be calculated. However, the complexity of GCMs reduces their usefulness in terms of interpretation. Furthermore, the resolution of GCMs is still a limiting factor especially in describing crucial processes like cloud formation, and precipitation in polar regions. Besides that, the coarse resolution (order of 1°-3°) does not allow a direct comparison with observations of a single snowfall event (Hoffmann *et al.*, 2000), which hampers full validation.

The other major class of models are Lagrangian parcel models, based on Rayleigh fractionation. These models consider moisture fractionation in an isolated air parcel. They describe condensation and fractionation from a single source area to polar regions assuming immediate removal of precipitation (Dansgaard, 1964; Jouzel and Merlivat, 1984). They are useful because they can by-pass the need to account for details of the cloud processes (including the microphysics) that influence the fractionation. Thus, they can easily be tuned to accurately quantify the bulk effect of cloud processes on isotopic content. A drawback of Lagrangian parcel models is that due to their descriptive nature, they do not realistically describe individual precipitation events, since they do not take into account potentially important factors like mixing of air masses and evaporative recharge of moisture. However, such simple models are easily modified to test the sensitivity to the inclusion of more complicated physics. Finally, the Lagrangian parcel models are poorly constrained by meteorological data.

In this study, we examine the possibilities of combining meteorological data with an isotope distillation model. The Mixed Cloud Isotopic Model (MCIM; Ciais and Jouzel, 1994) is used, and three dimensional, five days backward air parcel trajectories are used as an input for this model. The trajectories are calculated with European Centre for Medium-Range Weather Forecasts (ECMWF) operational data. The

MCIM is a derivate of a Rayleigh distillation model (Merlivat and Jouzel, 1979; Jouzel and Merlivat, 1984), and treats processes occurring in idealised air masses, accounting for the mean behaviour of cloud micro-scale physics. This model has proven to generate realistic δ values in East Antarctica (Ciais and Jouzel, 1994) and is a valuable tool in studies about source region characteristics of both present day snow (Ciais *et al.*, 1995) as well as precipitation from the last deglaciation in East Antarctica (B. Stenni *et al.*, 2001).

Previously, the MCIM treated the history of the moisture in a descriptive way. Here, the trajectory approach serves to describe the meteorological history of the moisture in a more realistic way, which enables the comparison of isotope-modelling results with an observed snowfall event.

A problem arising when such a model is used for regional studies is the definition of the initial isotopic composition of the vapour. Jouzel and Koster (1996) suggested to use a GCM generated isotope distribution as initial conditions. In this study, we calculate initial isotopic ratios of the vapour, necessary to explain the observed δ value of the snow, by an iterative modelling exercise. In this way, the variation in initial isotopic composition of water vapour is explored.

3.2 Observations

A large snowfall event in Western Dronning Maud Land (DML) in January 2002 has been chosen for this study. This system extended over a large part of DML, and is typical for accumulation events in the region (Noone *et al.*, 1999; Reijmer and Van den Broeke, 2001).

Within the framework of the European Project for Ice Coring in Antarctica (EPICA) the climate of DML is monitored using several Automatic Weather Stations (AWS). Sensors employed on these AWSs include a sonic height ranger that measures changes in surface height (e.g. Reijmer and Oerlemans, 2002). In the austral summer of 2001-02, some of the AWSs were visited and snow samples were collected directly under these sonic height rangers. These samples offer the possibility to compare the timing and related meteorological conditions during accumulation events with associated isotopic composition of the snow. Here we use the results of a snow pit at AWS 6 (74°28.9'S, 11°31.0'W).

AWS 6 is situated in DML at an elevation of 1160 m a.s.l. at the foot of the steep slope towards the high plateau (Heimefrontfjella). The average accumulation of this location is 268 mm w.e. year^{-1}, based on sonic height ranger measurements over the period 1998-2002 and measured snow density. The mean annual temperature is -20°C, and mean annual surface pressure is 854 hPa (Reijmer and Oerlemans, 2002). Snow sampling up to 3 meters depth was carried out, in order to obtain an isotopic record that is at least as long as the AWS's record of meteorological data (i.e. 4 yr). The sampling increment was 2 cm, so an average annual cycle is expected to be represented by $\sim$32 samples. However, due to unequal timing of precipitation the thickness of annual cycles is expected to vary. The snow samples are analysed for isotopic composition at the Centre for Isotope Research in Groningen, the

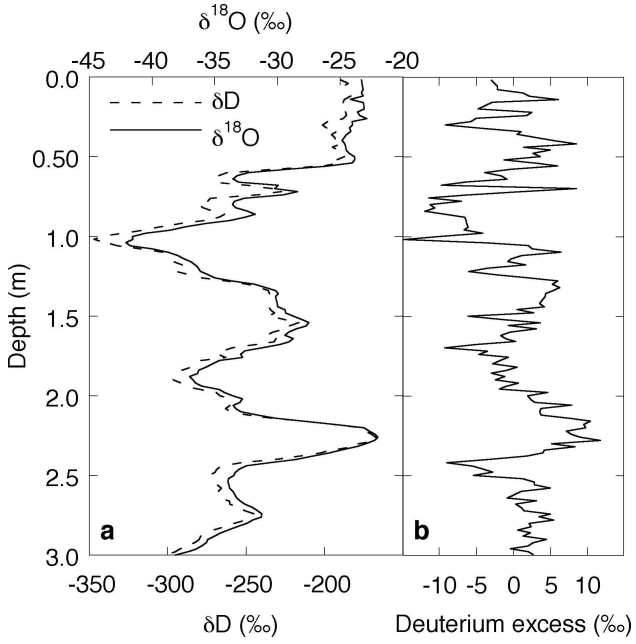

Figure 3.1: *Isotope profile from snow pit at AWS 6. (a) $\delta^{18}O$ (solid line) and δD (dashed line; (b) the deuterium excess signal.*

Netherlands. The precision of the mass spectrometer used to determine the isotopic composition of the samples is in the order of 0.1‰ in $\delta^{18}O$ and 2.0‰ in δD, which results in an accuracy for the deuterium excess (d-excess = $\delta D - 8\delta^{18}O$) of 2.2‰. The results are presented in Figure 3.1.

The main measured isotopic variations can be attributed to annual cycles, although not all summer and winter extremes are equally pronounced in the record. This is due to the event type nature of precipitation and to post-depositional removal of the snow (wind erosion and sublimation), as can be concluded from the 4 year record of the sonic height ranger on the AWS. For this site, approximately 10 precipitation events can be identified per year, but only ∼5 per year contribute substantially to the change in surface height (Reijmer and Van den Broeke, 2003).

Apart from the annual cycles, a top layer of 0.5 m with a fairly constant isotopic composition can be distinguished. The AWS data shows that at least the first 0.2 m of this snow layer has accumulated only a few days before sampling, during a major storm event in Western DML (Figure 3.2). This event lasted from 9 to 13 January and had its maximum on 11 January. Sampling took place on 14 January, so there was insufficient time for diffusion processes to modify the isotopic composition of the snow. The deuterium excess value, usually used as an indicator for evaporation conditions in the source region of the moisture, shows a rather irregular signal in the upper 0.2 m (Figure 3.1b). It varies between −5‰ and +6‰. On a seasonal

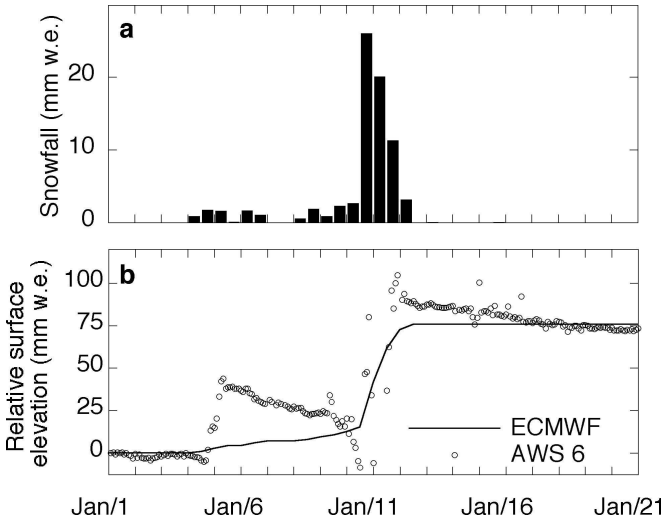

Figure 3.2: *Measured and modelled snowfall at AWS 6. (a) Snowfall from ECMWF model output; (b) observed (AWS; circles) compared to calculated (ECMWF; solid line) surface height change in mm w.e.*

scale however, coherence with the $\delta^{18}O$ an δD signal can be observed in Figure 3.1; with lower excess values in the winter precipitation, and higher values in summer precipitation, ranging from $-15‰$ to $+11‰$. The average isotopic composition of the upper 0.2 m of snow from the precipitation event in January 2002 ($\delta^{18}O = -23.3‰$ and $\delta D = -187.0‰$) is used in the remainder of this study.

3.3 Isotope modelling along trajectories

The model used in this study is the Mixed Cloud Isotopic Model (MCIM) described by Ciais and Jouzel (1994). The MCIM is an extension of earlier Lagrangian models based on Rayleigh distillation, presented by Merlivat and Jouzel (1979) and Jouzel and Merlivat (1984). It describes isotopic processes from its oceanic source region to the precipitation site on the ice sheet and it has proven to be able to reproduce the main characteristics of stable isotope variability in the middle and high latitudes (Jouzel *et al.*, 1997). Depending on the temperature, the MCIM allows for a zone of mixed clouds, where liquid droplets and ice crystals can coexist. During cooling of the air the liquid droplets either evaporate and subsequently condensate to ice, or these super cooled droplets directly freeze onto an ice crystal. This feature is known as the Bergeron-Findeisen process and it is associated with kinetic fractionation effects. The importance of these kinetic effects in fractionation is mainly determined by the amount of super saturation. The isotopic composition of different phases of an isolated air parcel is calculated along a prescribed transport path.

In the original model (Ciais and Jouzel, 1994) this transport path was prescribed

in terms of temperature and pressure. An important assumption in the MCIM is that the air parcel is transported in (super-) saturated conditions, from its source region to the precipitation site, implying continuous fractionation.

Here, the air parcel history will be derived from a trajectory study. From these trajectories, not only temperature and pressure are obtained, but also information on specific humidity, so that we can estimate whether or not the air is saturated. In this respect it is worthwhile to keep in mind that the humidity of a trajectory parcel is likely to be a small underestimate of the true parcel humidity, since instabilities have been removed in the atmospheric model. This probably introduces a small error in the calculations. Nevertheless, we consider the saturation values from the trajectory study to be representative for the saturation values at the cloud microphysical scale. In case of saturation, we calculate the isotopic fractionation along the trajectories with the MCIM. In case of under-saturation no condensation is expected, so the water vapour will not change its isotopic composition over this part of the trajectory, provided that there is no evaporative recharge.

3.4 Trajectory model

We used the Royal Netherlands Meteorological Institute trajectory model (TRAJKS) to calculate five days air-parcel backward trajectories. This model computes the large-scale three-dimensional displacement of an air parcel. A description of this model can be found in Scheele *et al.* (1996). The trajectory model has previously been used to calculate backward trajectories to the EPICA drilling site in DML (Reijmer and Van den Broeke, 2001) and to several other deep drilling sites in Antarctica (Reijmer *et al.*, 2002).

As input for the trajectory model the ECMWF operational data is used. This numerical weather prediction analysis is generally regarded as the best available for the Antarctic region (e.g. Cullather *et al.*, 1997; Connolley and Harangozo, 2001). The horizontal resolution of this archive is T511 (0.36°), but for the trajectory model the resolution of the input data is kept constant at 1.0° in the horizontal plane, 60 levels in the vertical and six hours in time. Interpolation in space and time is therefore necessary. The spatial interpolation is bilinear in the horizontal and linear in the logarithmic value of the air pressure in the vertical. The time interpolation is quadratic. However, for temperature and specific humidity the quadratic time interpolation produced unrealistic variations over time. For these parameters a linear interpolation is therefore applied, which unfortunately produces less smooth output, but no spurious signals. A test run has been performed with a spatial resolution of 0.5°, which has pointed out to result in only marginal changes in the trajectory- or isotope modelling results.

The uncertainty in the calculated trajectories can be considerable. The choice of the type of trajectory, interpolation schemes and spatial resolution of the wind fields introduces an uncertainty in the order of 1000 km after five days backward calculation (Stohl *et al.*, 1995). In reality, the error can be even larger, due to the presence of convective systems (e.g. fronts, convective storms) or the vicinity of the

earth surface, which can cause the parcel to loose its identity. These errors are difficult to quantify and not included in the uncertainty estimate, so computed trajectories must be interpreted with care.

Apart from the above-mentioned difficulties, an additional problem of this trajectory approach that can influence the isotope modelling is that not the moisture itself, but an air parcel containing moisture is traced. Possible mixing of moisture along the trajectory is not taken into account, since the isotopic content of the ambient water vapour is not known. It should be kept in mind that neglecting this mixing can be a substantial source of error in the results. Nevertheless, we apply the trajectory method because we consider it the best estimate of the transport history. Moreover, it enables the opportunity to compare modelled and observed δ values of precipitation.

3.5 Results

3.5.1 The snowfall event of 10-11 January 2002

In January 2002 several precipitation episodes occurred in western DML (Figure 3.2). A small accumulation event took place on 6 January, which was followed by a major event on 10-11 January. The average density of this snow as measured on 14 January was 372 kg m^{-3}, which is used to scale the elevation change from the sonic height ranger to mm w.e. (Figure 3.2b). Close observation shows a removal of snow in the first few hours of the storm (10 January, lowering the surface below the value of 1 January. This is followed by a sharp increase to a value of around 80 mm w.e.

As a first indication of the capability of the ECMWF model to reproduce the local conditions, the modelled snowfall at the grid-point closest to AWS 6 is compared to the measured snowfall by the AWS. The horizontal distance between the model grid-point and AWS 6 is only 2 km so a comparison with the AWS site seems acceptable. Modelled snowfall is based on the cumulative snowfall in the first 12 forecast hours and suffers from model spin-up. Snowfall from the 0 to 12 hours forecast is about 9 % less than the amount from the 12 to 24 hours forecast (Turner *et al.*, 1999). Due to the orographic nature of Antarctic precipitation, the influence of errors in model orography can be substantial. The location of the study site is near the escarpment region, but the difference between model elevation (1302 m a.s.l.) and actual elevation (1160 m a.s.l.) is regarded as acceptable.

Figure 3.2a presents the snowfall as predicted by the ECMWF model at the grid-point nearest to AWS 6. Over the first half of January, the ECMWF predicts 75.8 mm w.e. (sum of the bars in Figure 3.2a). Looking at Figure 3.2b, the underestimation of the ECMWF surface height change is only 10 %. However, in more detail we can see that the ECMWF model largely misses the snowfall on 6 January, and if we only consider the snowfall during the storm of 10-11 January, the underestimation is 30 %. This may seem large, but it is much better than earlier estimates of snowfall by the ECMWF reanalysis data, ERA-15 (1979-93). Reijmer *et al.* (2002) show that ERA-15 dataset underestimates snowfall for Kohnen station in DML by more than 50 %. It should be kept in mind that ECMWF analyses concern grid average precipitation, and do not account for inhomogeneous surface conditions.

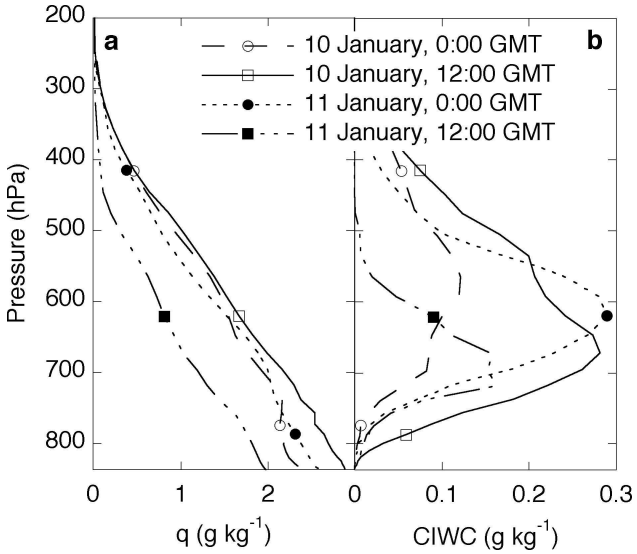

Figure 3.3: *(a) Vertical profiles above AWS6 of specific humidity (q) and (b) cloud ice water content (CIWC) at four moments during the storm event.*

The peak in snowfall according to ECMWF took place between 10 January, 12:00 GMT and 11 January, 0:00 GMT. Vertical profiles presented in Figure 3.3 show a maximum of moisture in the column of air at the grid-point closest to the sampling site around this date. These vertical profiles are used as an indicator from which pressure levels the backward trajectories should be calculated in order to find the right transport path of the moisture arriving at the sampling site. In Figure 3b, a clear maximum in the profiles of cloud ice water content (CIWC) can be seen. We assume that precipitation formed predominantly at these levels. On 10 January, 12:00 GMT, the peak in CIWC was at 675 hPa, while on 11 January, 0:00 GMT, this peak can be observed close to 625 hPa.

3.5.2 Trajectories

Six trajectories were calculated five days back in time for two arrival times: 10 January, 12:00 GMT and 11 January, 0:00 GMT, starting at pressure levels ranging from 725 hPa to 600 hPa, with intervals of 25 hPa (Figure 3.4). The trajectories with the same arrival time but different starting height do not differ much, but there is a major difference in the trajectories arriving 10 January, 12:00 GMT compared to those arriving 11 January, 0:00 GMT. For 10 January all air parcels were located above the Pacific Ocean five days before the precipitation event, whereas for 11 January the air parcels all originated from the South Atlantic. Important to note is the passage of the 10 January trajectories over South America, three days before arrival.

Pressure, temperature, specific- and relative humidity along the trajectories ar-

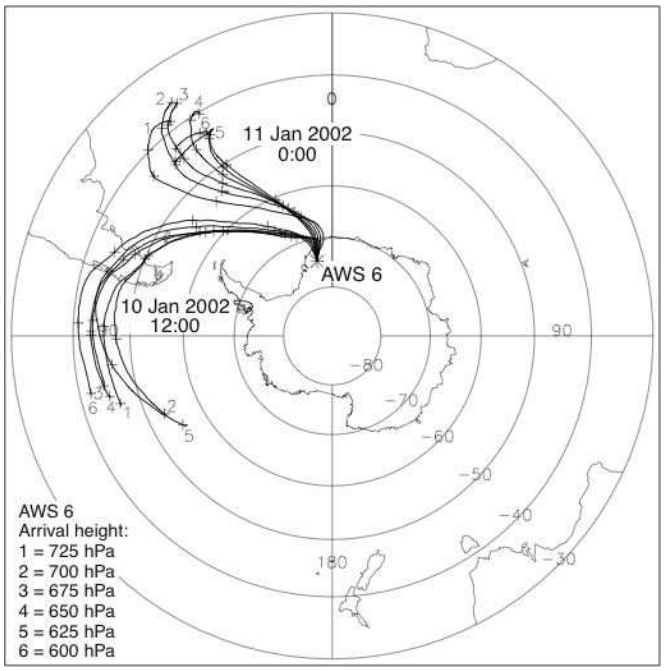

Figure 3.4: *Five days backward trajectories arriving above AWS 6 at 10 January, 1200 GMT and 11 January, 0000 GMT starting at six different pressure levels above the surface (P_0=820 hPa). Each day is marked with a plus sign.*

riving at the level of maximum CIWC are plotted in Figure 3.5. Looking at the trajectory of 10 January (open circles in Figure 3.5), the passage over the southern Andes three days before arrival forced the air to rise and cool, whereby it lost part of its moisture. After passing South America, this air parcel did not descent sufficiently to pick up any moisture from the South Atlantic Ocean. The specific humidity decreased until AWS 6 is reached. This indicates a moisture source region in the Pacific Ocean. Nevertheless, indications exists that the South Atlantic Ocean is also a source region, since three out of five other trajectories calculated for 10 January (not shown here) show a substantial increase in specific humidity over the South Atlantic Ocean.

The trajectory arriving on 11 January (black dots in Figure 3.5) shows a small increase in specific humidity from three days to 12 hours before arrival. This represents a source region of the moisture in the South Atlantic Ocean between 44° and 67° S. Trajectories from the other pressure levels, which are not shown, indicate a sharper increase of specific humidity north of 50°S or they already contained a high amount of moisture five days before arrival.

A remarkable but consistent result is that saturated conditions occurred only hours before arrival at AWS 6, i.e. hardly any fractionation has taken place previous to that time due to condensation. Only 3 of the trajectories travelling over South

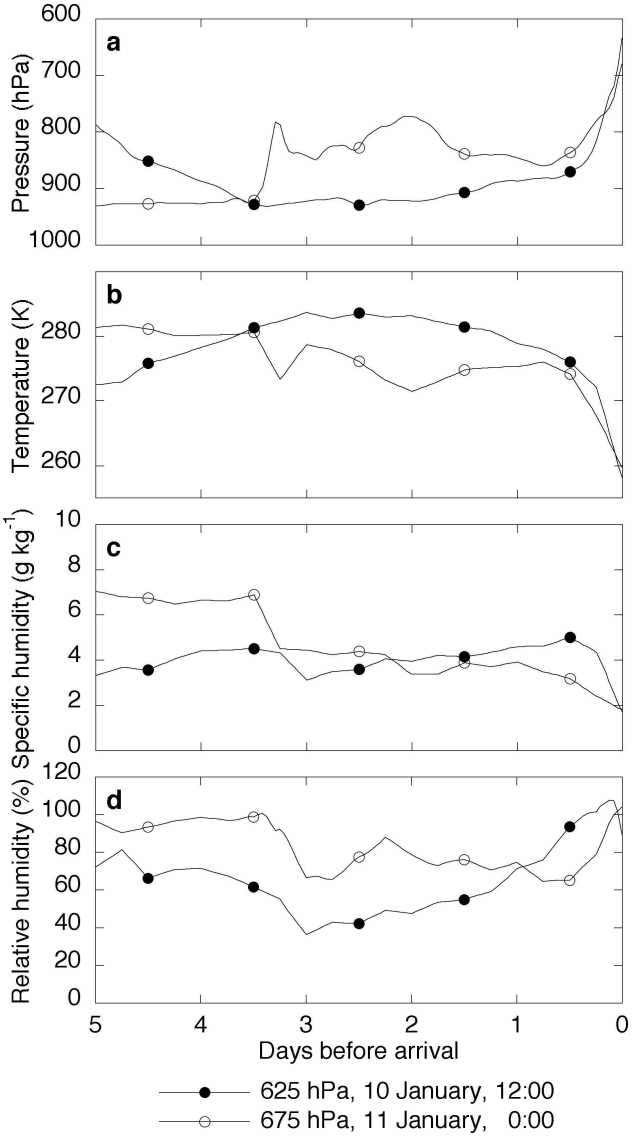

Figure 3.5: *Air-mass properties along the trajectories arriving at the level of maximum CIWC (Figure 3.3b) for (a) pressure, (b) temperature, (c) specific humidity, (d) relative humidity.*

America show saturation over the time while rising over the Andes. These are the only air parcels that could have experienced isotopic depletion before fractionation over Antarctica begins. Otherwise, air parcels travelled southward in under-saturated conditions, until they started their ascent onto the ice sheet.

3.5.3 Isotope modelling results

The modelled isotopic depletion is basically a function of the difference in water content between the locations of first saturation and the precipitation site. Along most trajectories in this study, condensation does not start north of 67°S. As a consequence, the modelled vapour content at this point has a δ value equal to that of five days before arrival, at the starting point of the trajectories. If we assume that the δ value at this point is equal to the value at the moment of evaporation (approximately -10 ‰), then the isotopic depletion due to the rain out between the locations of first saturation and final precipitation is in this case in the order of $\sim$13 ‰ for $\delta^{18}O$, i.e. the water vapour attains a $\delta^{18}O$ value of -23 ‰. Upon subsequent condensation, this leads to precipitation with a $\delta^{18}O$ value of -11 ‰. Keeping in mind the observed isotopic value of the snow at AWS 6 ($\delta^{18}O = -23.3$ ‰), we conclude that water vapour in the air parcels approaching Antarctica is by far not sufficiently depleted to explain the observed isotopic composition of the snow. Even when fractionation during the passage over South America is incorporated, the resulting δ values are too high in comparison with the observed values. In other words, incorporating (under-) saturation conditions along the transport path of the air parcel in the MCIM shows that there is not sufficient condensation for the fractionation to be realized. This result is observed in all identified trajectories, and does not seem to suffer from uncertainties in the trajectory calculations.

Atmospheric mixing along the trajectories with air containing more depleted vapour could lead to a lower δ value at the point where condensation first took place. Another factor that might play a role is that in some cases the water vapour at the starting point of the trajectory has already experienced some fractionation after evaporation from its oceanic source.

To estimate the required δ value of the vapour at the moment of first condensation, an iterative modelling exercise was performed for the 12 trajectories shown in Figure 3.4. The initial $\delta^{18}O$ value of the water vapour needed to achieve snowfall at AWS 6 with a $\delta^{18}O$ value of -23.3 ‰ was calculated. The fractionation along these trajectories is shown in Figure 3.6, as a function of specific humidity, both for vapour (dashed lines) and for the precipitation (solid lines). The $\delta^{18}O$ values for initial vapour range roughly from -24 ‰ to -35 ‰. As can be seen from Figure 6b, the air parcels arriving 11 January all show a comparable fractionation over 3 g kg^{-1}, in contrast to the air parcels arriving 10 January. The latter have a much shorter range over which fractionation takes place (Figure 3.6a), owing to the different moment of first saturation along the transport path, which is further south on 10 January.

The needed initial isotopic composition of vapour seems to be strongly dependent on the spatial position of the air parcel (Figure 3.7). With this empirical relation between latitude and δ value as an indication for the initial δ value of the vapour,

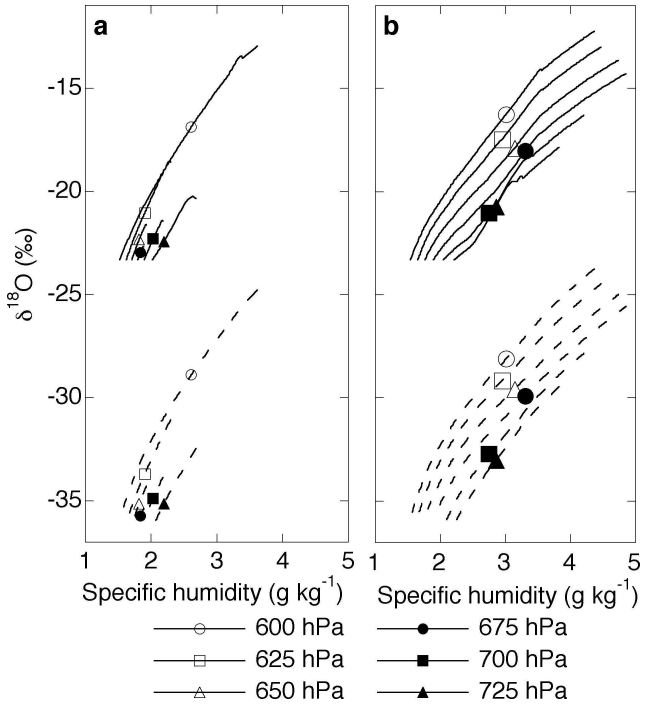

Figure 3.6: *$\delta^{18}O$ content of the precipitation (solid lines) and vapor (dashed lines) as a function of specific humidity along trajectories. Fractionation along six trajectories arriving at 10 January, 1200 GMT (a) and 11 January 0000 GMT (b) is plotted. The model has been tuned to the δ values of the vapour as the fractionation begins.*

the MCIM was used again, to recalculate $\delta^{18}O$ value of precipitation at AWS 6. This leads to an average $\delta^{18}O$ value precipitation of 23.0 ‰, in accordance with observed values (weighted with CIWC from Figure 3.3).

3.6 Discussion and Conclusion

Our study shows that, at least for this particular accumulation event, vapour concentration in air is not saturated for the greater part of its transport from the source to the deposition site, according to the ECMWF-based trajectories. Only during the final rise onto the continent does (super-) saturation occur. Continuous saturation is an important assumption in isotope models based on Rayleigh fractionation in order to estimate temperature changes. As our results show, this assumption is not fulfilled along all transport paths of the vapour. We expect this to be the rule rather than the exception in Antarctica. Only with a spatially dependent isotope field that serves as a starting value for the δ value of the water vapour, Rayleigh type fractionation models can reproduce the observed δ values at the precipitation site.

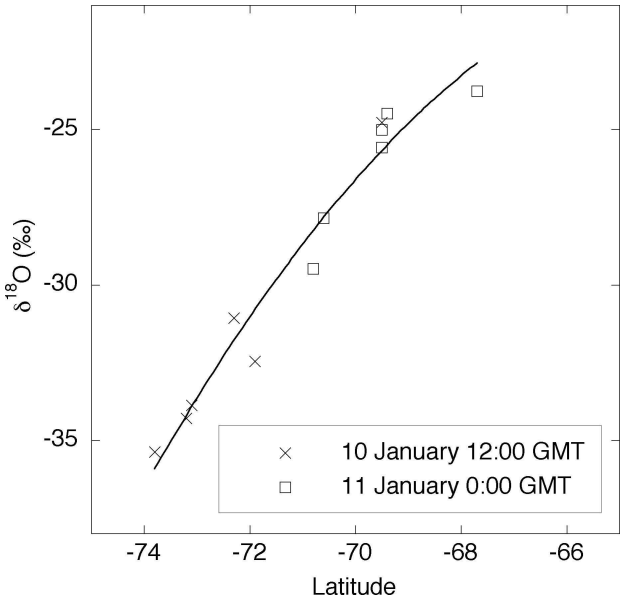

Figure 3.7: *Required initial $\delta^{18}O$ values of water vapour as function of latitude.*

The question is which processes are responsible for the isotopic depletion of the moisture before fractionation due to condensation occurs. A plausible explanation seems to be atmospheric mixing (by turbulence and convection) during transport to the polar region and its associated isotopic depletion due to eddy transport (e.g. Eriksson, 1965; Fisher and Alt, 1985; Kavanaugh and Cuffey, 2003). Besides this, before the trajectories describe the distillation history of the air parcels (i.e. more than five days before arrival), a condensation process could have occurred. This cannot be excluded either, and it can influence the isotopic content of the precipitation as well. The magnitudes of these influences are not known, since these processes are not captured by this trajectory approach.

It is worthwhile to compare this spatial relation of δ values of water vapour with instantaneous isotope fields of water vapour in GCMs, and to estimate the natural variability of these isotope gradients in reality. The magnitude of the natural variability of this spatial variation of the isotope field should be studied, for example by vapour sampling for δ measurements on a ship trip to DML. This variability determines the possibility of success of this approach to isotope modelling and understanding the δ-T relation in time and space.

Chapter 4

A Rayleigh-type isotope distillation model along backward trajectories

4.1 Introduction

The Mixed Cloud Isotopic Model (MCIM) (Ciais and Jouzel, 1994) is a one-dimensional model that describes the isotopic fractionation of water vapour as a function of temperature and pressure, from its (oceanic) source area to the (polar) precipitation site. It is able to account for moisture in its three phases: vapour, liquid and ice.

In principle, it is a derivative of the Rayleigh model as described by Dansgaard (1964), in which the condensate is supposed to be formed in isotopic equilibrium with the vapour phase and is immediately removed from the cloud after condensation. However, the Rayleigh model does not explain experimental results concerning the $\delta D - \delta^{18}O$ relationship (Gat, 1980), nor does it explain the temperature-isotope gradient in a satisfying way, especially at low temperatures, such as encountered over central Antarctica (Jouzel *et al.*, 1983).

Therefore, improvements to the theory have been developed by e.g. Merlivat and Jouzel (1979), who modelled the isotopic effects associated with evaporation of water from the ocean surface. They included kinetic fractionation during evaporation by considering the effect of relative humidity (RH), sea surface temperature and wind speed. They showed that the deuterium excess parameter (d-excess= $\delta D - 8\delta^{18}O$) is strongly influenced by these parameters in the moisture source region.

Another improvement on the theory of isotopic fractionation was proposed by Jouzel and Merlivat (1984), who introduced the Rayleigh Model including the Kinetic fractionation effect (RMK). This kinetic isotopic fractionation effect occurs during

Chapter 4 and 5 combined are a manuscript under review: Helsen, M.M., R.S.W. van de Wal, M.R. van den Broeke, V. Masson-Delmotte, H.A.J. Meijer, M.P. Scheele and M. Werner. Modeling the isotopic composition of Antarctic snow: Simulation of snow pit records. *Submitted to J. Geophys. Res.*

snow formation, as a result of the fact that vapour deposition at low temperatures occurs in supersaturated conditions with respect to ice. The magnitude of supersaturation (S_i) has a large influence on the d-excess, which decreases strongly with increasing values of S_i.

An additional problem that arises when dealing with both warm evaporation conditions and precipitation in cold regions is the switch between vapour-liquid transition and the vapour-ice transition at the onset of snow formation. This is due to the fact that these two phase changes are associated with different isotopic fractionation coefficients. Ciais and Jouzel (1994) have improved the theory of isotopic distillation by describing isotopic fractionation in mixed clouds; both liquid droplets and ice crystals can coexist and are able to interact following the so-called Bergeron-Findeisen process (Bergeron, 1935; Findeisen, 1938).

The three improvements on the classical Rayleigh theory mentioned above are incorporated in the MCIM. In order to do so, this model has been developed as a conceptual model, to describe isotopic evolution of water vapour towards the polar regions in an isolated air parcel, as a function of constantly decreasing temperature and pressure. It is used to interpret mean values and tendencies of the isotopic composition of snow. This implies that the prescribed transport history of the moisture also should be interpreted as a mean pathway. In this work, the purpose of the use of an isotope model is that it can describe the isotopic changes of moisture along realistic trajectories for specific snowfall events. Along such trajectories, temperature (T) and pressure (p) do not decrease constantly but rather fluctuate. Another aspect of the MCIM that is not in line with realistic moisture transport is the assumption of constant saturation along the transport path from the source region to the deposition site. Therefore, there is a need to adjust the MCIM such that it is capable to describe isotopic changes along individual trajectories.

In Section 4.2, some key-results of the original model of Ciais and Jouzel (1994) are reproduced. Then, the adaptations on the model are described and tested for some idealised scenarios. Section 4.3 describes changes in the formulation of the initial isotopic composition of the vapour. As conditions during moisture transport are not always favorable for condensation (and associated isotopic fractionation), Section 4.4 describes how the MCIM is adjusted whereby it can deal with these changing moisture conditions. Furthermore, Section 4.5 presents modifications to the MCIM related to isotopic recharge, i.e. increases of specific humidity (q) which are associated with strong isotopic changes of the moisture. Finally, results from a test-run using a trajectory case study are evaluated.

4.2 The original MCIM

A description of the original MCIM is given by Ciais and Jouzel (1994). For a comprehensive description of modifications to the original model, the capability of the model to reproduce the results of Ciais and Jouzel (1994) is outlined in this section.

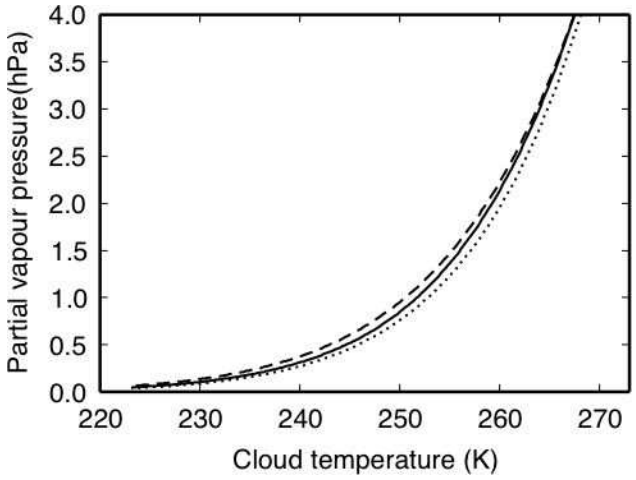

Figure 4.1: *Partial pressure of water vapour (e_w) in the MCIM (solid line). Below 268 K, e_w lies between the saturation vapour pressure with respect to liquid water ($e_{s,l}$, dashed line) and the saturation vapour pressure with respect to ice ($e_{s,i}$, dotted line).*

4.2.1 Supersaturation function

The partial water vapour pressure (e_w) is an important parameter in the MCIM, since it drives the amount of different airborne phases. According to the Bergeron-Findeisen hypothesis (Bergeron, 1935; Findeisen, 1938), e_w lies between the saturation vapour pressure with respect to liquid water ($e_{s,l}$) and the saturation vapour pressure with respect to ice ($e_{s,i}$). This is shown in Figure 4.1. When T is close to the melting point, e_w is close to $e_{s,l}$. As the temperature drops, e_w approaches $e_{s,i}$. However, it does not reach $e_{s,i}$, which becomes more clear in Figure 4.2. In this figure, the function for S_i used in the MCIM is shown (black line). Three different T ranges can be recognised. First, with T higher than 268 K, saturation with respect to liquid water is assumed. Below 248 K, S_i is described by a straight line, i.e. $S_i = 1.02 - 0.0038T$. Between 248 K and 268 K, a function that connects these two lines is prescribed. This function ensures continuity for the supersaturation (Ciais and Jouzel, 1994). In comparison to previous work, the advantage of this approach is that there is no abrupt switch between functions for S_i when $T >$268 K and when $T <$ 248 K. However, there does seem to be a slight discontinuity at 248 K, which also appears in Figure 3 from Ciais and Jouzel (1994).

4.2.2 Mixing ratios

The amount of the different components of water in the cloud is shown in Figure 4.3. The amount of water vapour is controlled by the amount of supersaturation (previous section) and the temperature and pressure. This is indicated by the solid line in Figure 4.3. We further see that liquid water (dashed line) disappears at 248K, in

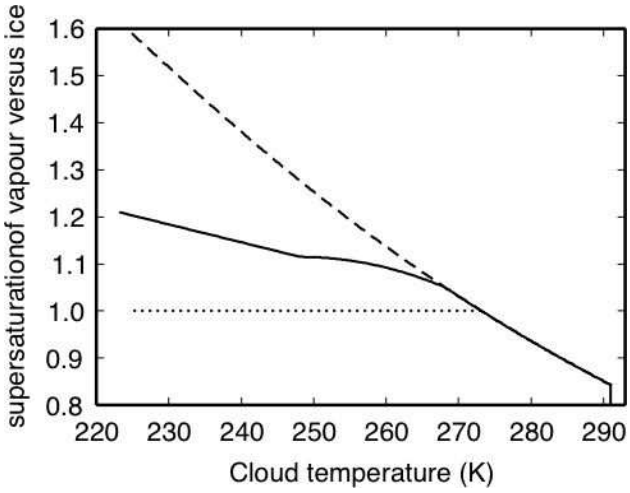

Figure 4.2: *Supersaturation functions of the vapour with respect to the cloud ice in the MCIM. The dotted line represents the saturation at equilibrium, the dashed curve is the supersaturation value if $e_{s,l}$ is used as the amount of water vapour in the air. The solid line shows the S_i function used in the MCIM.*

accordance with our settings that mixed clouds are present between 248K and 268K. At cooler temperatures, only cloud ice (dotted line) exists, and also drops towards 0.

Above 268 K, only vapour and liquid water are allowed to exist in the cloud. As the temperature drops below 268 K, cloud ice appears. The amount of cloud liquid water and ice is controlled by some parameters that do not have a physical basis but should be tuned by trial and error (Ciais and Jouzel, 1994). When using the values mentioned in Ciais and Jouzel (1994) ($C_{1,prec}$=0.2 and $C_{2,prec}$=0.01), too much cloud ice is kept in the cloud, as shown by the gray dotted line in Figure 4.3. With the values $C_{1,prec}$=0.3 and $C_{2,prec}$=0.1, the results as displayed in Figure 5 from Ciais and Jouzel (1994) are correctly simulated, so these values are used in the remainder of this work.

4.2.3 Simulated isotopic composition

A simulation of the isotopic distillation is described for a linear decreasing temperature ($T_{initial}$=291 K; T_{final}=223 K) and pressure ($p_{initial}$=1015 hPa; p_{final}=650 hPa). Figure 4.4 shows the isotopic composition (δD) of all the airborne phases in the air parcel, as a function of temperature. The δD value of newly formed liquid is more negative as the value of cloud ice. This is due to a different (larger) fractionation factor for the vapour-ice transition compared to the vapour-liquid transition. Moreover, since the MCIM allows a fraction of the ice to be kept in the cloud, this ice will hold an "isotopic memory" of the previous condensation steps, whereas the liquid is completely equilibrated with the vapour, each step (Ciais and Jouzel, 1994). The δD

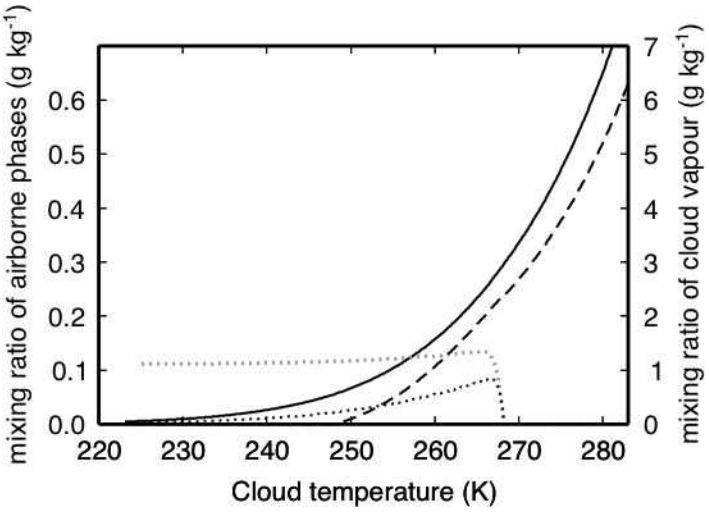

Figure 4.3: *Mixing ratios of the different constituents on the cloud in the MCIM. The solid line shows the mixing ratio of water vapour (right axis). The dashed line is the amount of cloud liquid and the dotted line is the amount of cloud ice. The gray dotted line is obtained when using the settings from Ciais and Jouzel (1994).*

of the precipitation follows the liquid line when $T > 268K$, it follows the solid line when $T < 248K$ and it lies in between these curves in the temperature zone of mixed clouds. Figure 4.5 shows the resulting values of the deuterium excess parameter, which are in agreement with the results of Ciais and Jouzel (1994).

4.2.4 Isotope distillation excluding the mixed cloud effect

As explained in Section 4.1, the MCIM is derived from the "Rayleigh model including the isotopic kinetic effect" (RMK; Jouzel and Merlivat, 1984). This was the first model that took into account kinetic fractionation at low temperatures, due to the fact that vapour deposition occurs in an environment supersaturated over ice. However, it did not allow vapour, liquid and ice to coexist, i.e. all the newly formed precipitation was immediately removed from the cloud.

To illustrate the difference between the MCIM and the RMK, Figure 4.6 and 4.7 show results from the RMK, which can be compared with the MCIM results in Figure 4.4 and 4.5. An abrupt jump between the vapour - liquid transition and the vapour - solid transition is clearly visible in Figure 4.6. The place of this transition is now (arbitrarily) chosen at 248 K. The effect of a sudden switch between different condensation transitions is even more dramatic when looking at the deuterium excess parameter in Figure 4.7. This problem is solved by the MCIM with the introduction of a temperature interval in which mixed clouds exist. The Bergeron-Findeisen process accounts for the gradual transition of "liquid clouds" to "ice clouds".

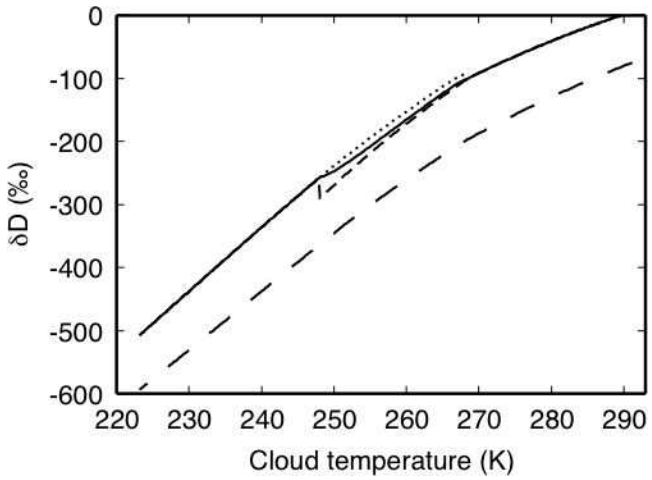

Figure 4.4: *Deuterium content (δD) in the different constituents of the cloud as a function of cloud temperature in the MCIM. Long dashed line = vapour; short dashed line = cloud liquid; dotted line = cloud ice; solid line = precipitation.*

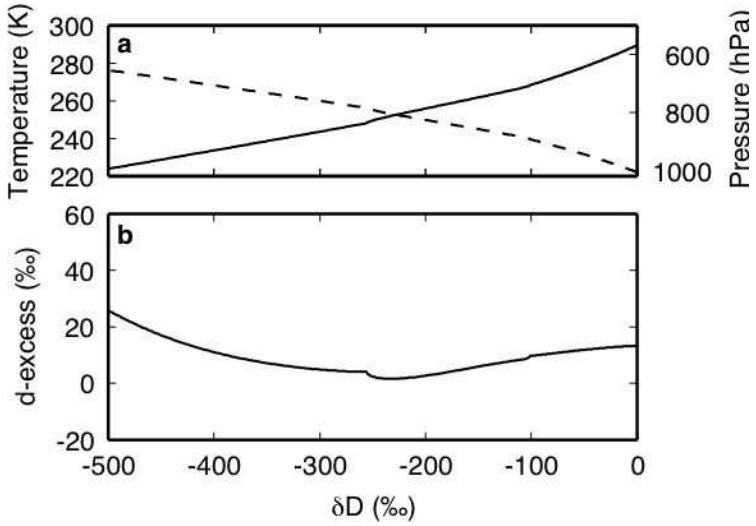

Figure 4.5: *(a) Temperature (solid line) and pressure (dashed line) history of an air parcel that serves as input for the MCIM. (b) Modelled deuterium excess content (d-excess) in precipitation plotted against δD, as a function of the temperature and pressure history in (a).*

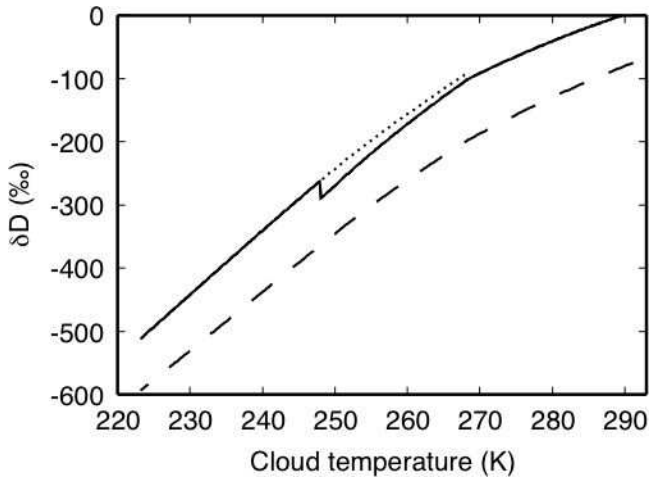

Figure 4.6: *Deuterium content (δD) in the different constituents of the cloud as a function of cloud temperature in the RMK model. Long dashed line = vapour; short dashed line = cloud liquid; dotted line = cloud ice; solid line = precipitation.*

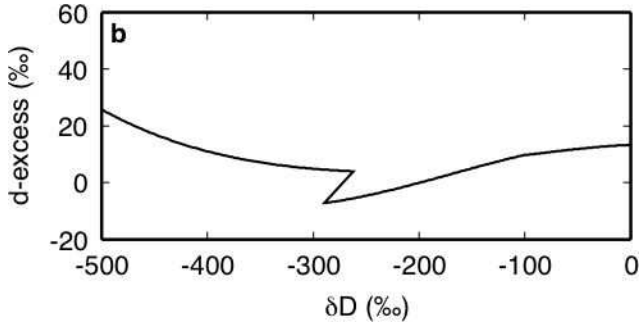

Figure 4.7: *Deuterium excess content (d) in precipitation plotted against δD in the RMK model.*

Another difference of between RMK and MCIM is the magnitude of the fractionation. In the MCIM, some of the condensate is kept in the cloud, which slightly suppresses the distillation. Indeed, the final δD value of the precipitation in Figure 4.4 (-508 ‰) is slightly higher than in Figure 4.6 (-512 ‰).

4.3 Initial isotopic composition

The initial isotopic composition of vapour (δ_{v0}) in a Lagrangian air parcel is not easily estimated because the vapour and the ocean surface are not in isotopic equilibrium. More specifically, the value of δ_{v0} differs from the isotopic content of evaporating water (δ_e) (Craig and Gordon, 1965). However, many Rayleigh-type distillation models assume δ_{v0} and δ_e to have the same value, using global-scale balance considerations between evaporation and precipitation. This enables the calculation of δ_{v0} from conditions at the ocean surface (Merlivat and Jouzel, 1979) and this approach is known as the global-scale closure equation. However, Jouzel and Koster (1996) pointed out that, although evaporation and precipitation are in balance on a global scale, this might not be justified at the regional scale. Therefore, they recommend to use results from a general circulation model (GCM), i.e. the simulated isotopic composition of water vapour (δ_v), overlying the ocean surface (as in e.g. Delmotte *et al.*, 2000).

Moving towards a trajectory approach, the value of $\delta^{18}O_v$ cannot directly be taken from such two dimensional GCM-generated fields, since air masses are typically located 1-3 km above the ocean surface when the calculations start. This is well above the marine atmospheric boundary layer, and the moisture in these air masses is expected to be more depleted compared to the moisture in the surface layer, due to earlier condensation cycles. Helsen *et al.* (2004) (Chapter 3) showed that moisture approaching the Antarctic continent has indeed a more depleted $\delta^{18}O_v$ value than can be expected from evaporation from the local ocean surface. Furthermore, they showed that the required isotopic composition of the vapour strongly depends on latitude.

Therefore, we make use of three dimensional GCM-generated isotope fields, from which the value of δ_{v0} is taken as a starting point for the isotope model. A 20-year present-day climate run is performed with the Hamburg atmospheric climate model ECHAM4 (Roeckner *et al.*, 1996), which includes tracers for the isotopic species $\delta^{18}O$ and δD (Hoffmann *et al.*, 1998; Werner and Heimann, 2002). The spectral resolution is T106 (1.1°lat x 1.1°lon) with 19 vertical levels. This run provides monthly mean values of the isotopic composition of water vapour for $\delta^{18}O$ and δD. These fields are regarded here as an isotope climatology. With the present resolution, ECHAM4 has proven to yield a realistic spatial distribution of isotope variability (Vuille *et al.*, 2003).

To sketch the character of this isotope distribution, Figure 4.8a and b show modelled isotopic values of vapour ($\delta^{18}O_v$) of the near-surface level in January and July, respectively. Over the ocean, $\delta^{18}O_v$ remains relatively constant, whereas strongly depleted values are visible over the Antarctic continent. Very low values of <-80 ‰ are found over central Antarctica, during winter, but whether these low values also occur in reality is not sure, since this would require strong, continuous condensation

near the surface.

Figure 4.8c and d show vertical cross sections from the ECHAM4 isotope fields, along the 0° E/W meridian. The large vertical gradient in $\delta^{18}O_v$ is apparent, and indicates that the vertical position of the starting point of the trajectory will be of great influence for the initial isotopic value of the moisture. Furthermore, the moisture just above the ocean surface is much more depleted in July than in January, which is partly caused by an increased sea ice extent and lower SSTs in winter.

From the cross section in July it becomes clear that the anomalously low values over the Antarctic continent only show up in a shallow layer covering the surface. For our purpose, the ECHAM4 isotope fields are used to define the initial value of δ_{v0} (mostly over the ocean) and therefore, these possibly spurious parts of the model data will not affect our isotopic modelling results.

Figure 4.9 shows d-excess values of vapour in the ECHAM4 climatology. For the winter situation (Figure 4.9b and d) very high values are found over the Antarctic continent. These high vapour d-excess values also produce anomalous high d-excess values in central Antarctic precipitation, which are not in agreement with observed d-excess patterns. This points to problems in the parameterisation of kinetic fractionation effects occurring during snow formation in ECHAM4 (Werner *et al.*, 2001). Nevertheless, as explained above, these data are not expected to affect our results, since it is the isotopic composition at lower latitudes that determines the initial isotopic value of the moisture in the air parcels.

However, the d-excess variability over the ocean is important for our purpose, since it determines the initial d-excess signature of the moisture in the air parcels. Over the ocean surface, ECHAM4 produces a gradient in d-excess values of the vapour, with increasing values with altitude. Since the initial altitude of the trajectories (five days before arrival) can vary considerably, the vertical gradient in d-excess is obviously of large influence for our modelling results.

It should be noted that the use of climatological mean ECHAM4 isotope values as initial isotopic values can introduce a significant error in our final modelling results. Isotopic values in single storm events can show large variability compared to the mean state (Hoffmann *et al.*, 1998). Especially in regions where cyclonic disturbances occur only occasional, the isotopic composition during intense storms might deviate substantially from the mean state. However, while there exist no reanalyses of atmospheric isotope fields, climatological values are considered to be the best estimate for defining the initial isotopic composition in four dimensions.

4.4 Fractionation threshold

Chapter 3 showed that an air mass bringing extensive snowfall towards Antarctica was not saturated along its entire transport path from the source area to the precipitation site. Especially during the final part of the transport, when the air was orographically lifted onto the Antarctic continent, RH approached saturation conditions. It is not expected that moisture in an under-saturated air mass exhibits isotopic fractionation. However, the original MCIM simulates the isotopic evolution only as a function of

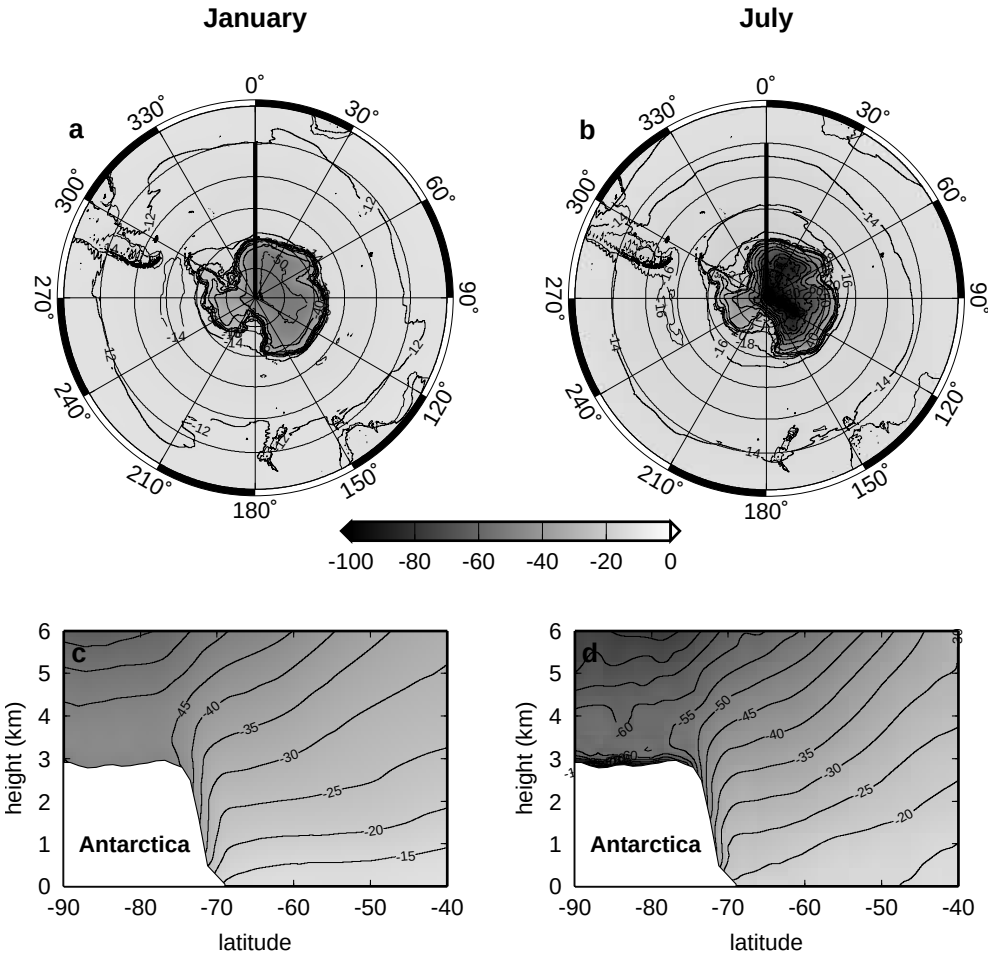

Figure 4.8: *Mean monthly $\delta^{18}O_v$ values of water vapour in January (left) and July (right) from ECHAM4. (a) and (b) show the $\delta^{18}O_v$ distribution in the level closest to the surface; (c) and (d) show vertical cross sections along the 0° E/W meridian. The white area in the lower left corner represents the Antarctic continent.*

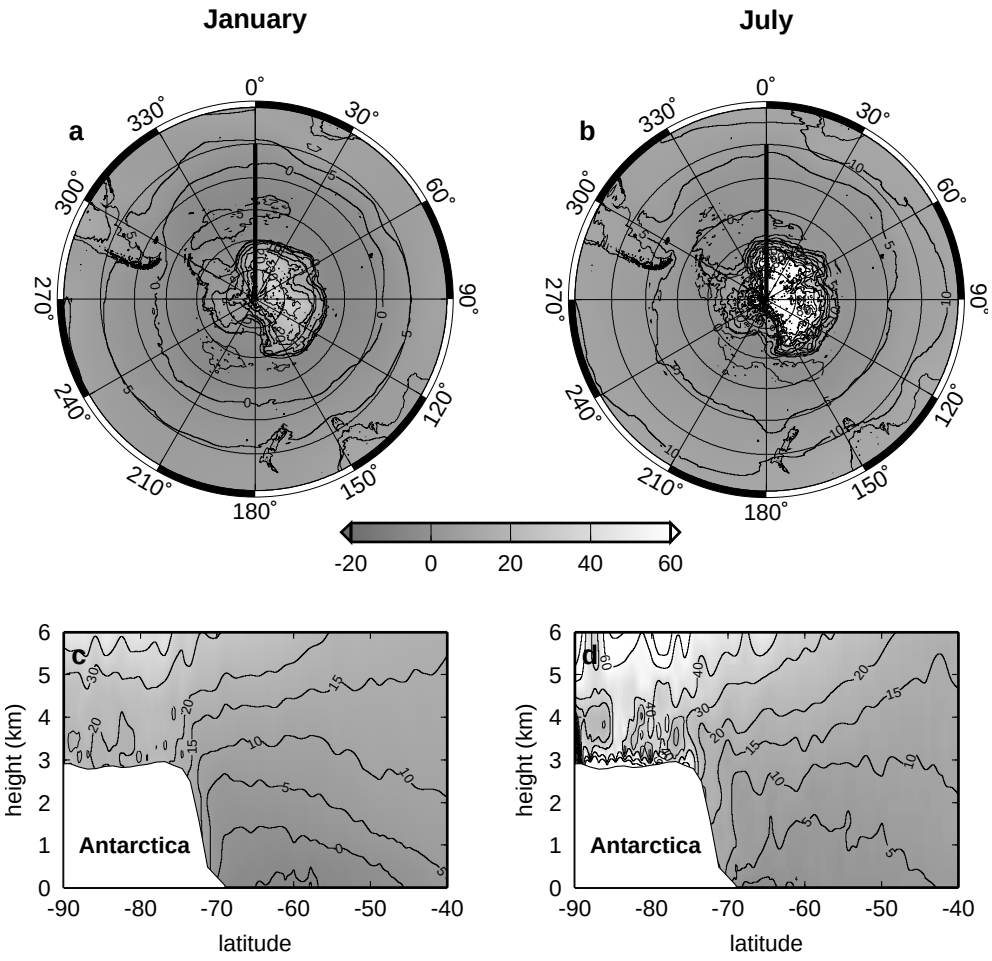

Figure 4.9: *As Figure 4.8, but now for mean monthly d-excess values of water vapour in January (left) and July (right) from ECHAM4. (a) and (b) show the d-excess distribution of the level closest to the surface; (c) and (d) show vertical cross sections along the 0° E/W meridian.*

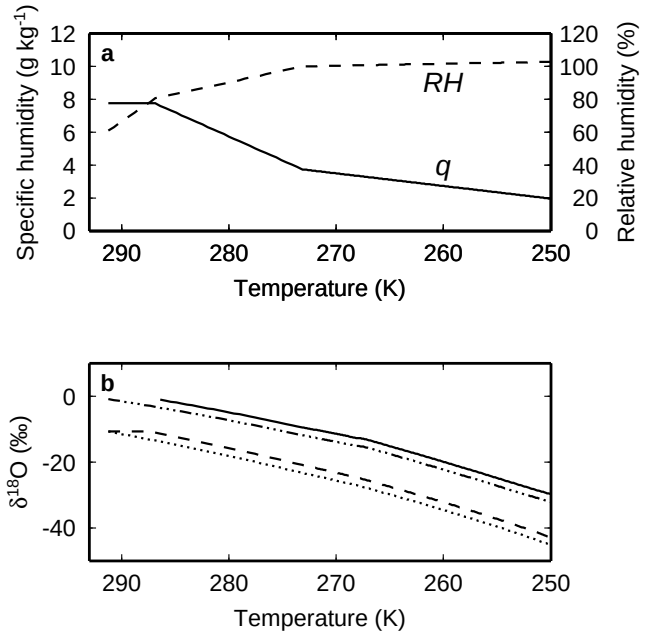

Figure 4.10: *Output from the adapted MCIM showing the effect of a threshold value of RH for isotopic fractionation. (a) Schematic moisture changes along trajectory: specific (solid line) and relative (dashed line) humidity as a function of T; (b) isotopic changes of the moisture as a function of T. The dashed line represents vapour in the adapted model, the solid line the resulting precipitation. The dotted line is the vapour if the original MCIM is used, and the dash-dotted line is the accompanying precipitation.*

temperature (T) and pressure (p), assuming continuous saturation from the source region to the deposition site. This is not in line with our moisture data along the trajectories, which forces us to make modifications to the isotope model.

In the ECMWF model (and many other GCMs), cloud water is assumed to form when RH exceeds a specified threshold (Tiedtke, 1993; Jakob, 1999). In analogy with these models, we included a parameter $RH_{threshold} = 80$ % as an indicative value for the presence of clouds. The RH value obtained from the trajectories can be considered representative for grid-average conditions, but not necessarily on cloud micro-physical level. This in an important difference, since the MCIM calculates kinetic fractionation effects as a function of the amount of super-saturation with respect to ice (S_i) on a cloud micro-physical level (i.e. RH >100%). To overcome this discrepancy, we follow the original MCIM in defining a super-saturation value as a function of T (using the parameterisation of Petit *et al.*, 1991), to ensure realistic modelling results for d-excess, while we follow our trajectory data as an indicator for the presence of clouds.

The implication of this threshold is schematically explained in Figure 4.10. We

impose a schematic T, p and specific humidity (q) on an air parcel (Figure 4.10a). Initially, the air parcel is well below saturation ($RH = 60\%$). As T decreases and q is kept constant, RH increases. As soon $RH > RH_{threshold}$ is reached, condensation is assumed to occur, and although the RH values according to the imposed humidity history are still below 100%, on a cloud micro-scale level supersaturated conditions are defined as a function of T. The key element is that during these conditions isotopic fractionation starts. The fractionation follows the same gradient as would occur using the original MCIM (dotted and dash-dotted lines in Figure 4.10b). Clearly, the impact of threshold is that the newly modelled isotopic fractionation depends on the temperature difference between $T_{RH=80\%}$ and T_{final}. In the original MCIM, the air parcel was lifted until saturation was reached, and then followed until the final point of the trajectory. Hence, the difference in temperature between the source area (at the level of saturation) and the arrival location was the main controlling parameter. It is not expected that the introduction of $RH_{threshold}$ has large implications for d-excess, since in this parameter does not change much at high temperature (Figure 4.4)

4.5 Isotopic recharge

Apart from the above-mentioned difficulties associated with the combination of trajectories and a theoretical isotope distillation model, realistic transport histories often show subsequent increases in q before the final rain-out towards the precipitation site. These increases of q are associated with isotopic recharge, i.e. the uptake of moisture with a different isotopic composition. Since the original MCIM maintains mass conservation between the moisture source area and the final precipitation site, it only allows an increase of moisture resulting of the re-evaporation of cloud water. Any increase of q that exceeds the total amount of water in the air parcel will result in model failure. To enable realistic description of the isotopic evolution of air parcels, the MCIM has been modified to account for such increases of q, assuming that this moisture is mixed into the air parcel from ambient air.

Similarly as for the initial isotopic composition of the vapour (δ_{v0}), we use the ECHAM4 isotope fields to determine the isotopic composition of the ambient water vapour ($\delta_{v,ECHAM}$). As soon as all available cloud water and/or ice is re-evaporated, the additional increase of q is 'extracted' from ambient air, and the resulting $\delta_v(t)$ value is calculated by mixing $\delta_{v,ECHAM}(t)$ with $\delta_v(t - \Delta t)$. Using this approach, a strong increase of q will result in a value of δ_v close to the value of $\delta_{v,ECHAM}$ at that particular location, which is schematically illustrated in Figure 4.11.

In this figure, a schematic history of T and q is shown, in which an isotopic recharge occurs between four and three days before arrival. Here, we kept the isotopic composition of the ambient moisture constant ($\delta^{18}O_{v,ECHAM} = -20‰$, dotted line in Figure 4.11b). Between five and four days before arrival, fractionation occurs in the same way as in the original MCIM. Then, between four and three days before arrival, T (solid line in Figure 4.11a) and q (dashed line in Figure 4.11a) in the air parcel increase, and the isotopic composition of the vapour ($\delta^{18}O_v$, dashed line in Figure 4.11b) increases as well. The value of $\delta^{18}O_v$ approaches $\delta^{18}O_{v,ECHAM}$ but

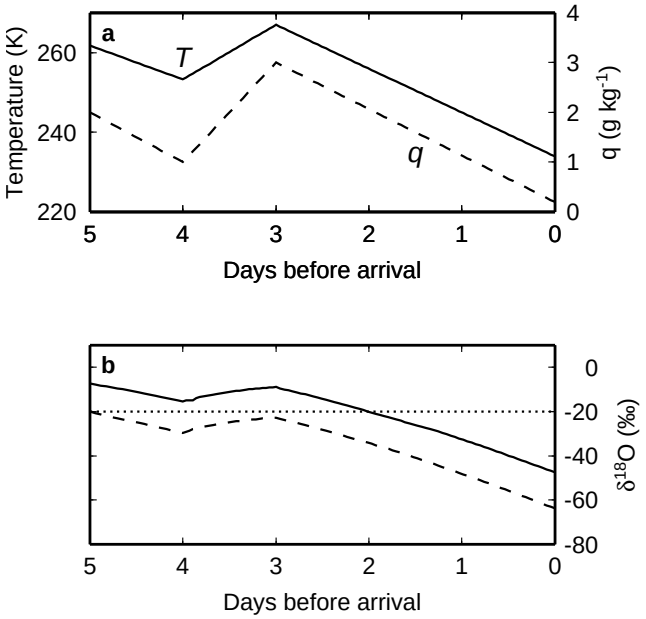

Figure 4.11: *Output from the adapted MCIM showing the effect of isotopic recharge with a constant isotopic composition of the ambient moisture. (a) Imposed T (solid line) and q (dashed line) history as a function of time; (b) isotopic composition of the ambient moisture (dotted line) and the resulting isotopic changes in vapour (dashed line) and precipitation (solid line).*

will never entirely reach its value due to the presence of the depleted vapour at four days before arrival. After this recharge, a drop in T causes a distillation comparable to the original model. The resulting final isotopic composition is slightly lower compared to the case without an earlier condensation cycle, which is a result of the recharge process.

In practice, the ambient value of $\delta^{18}O_{v,ECHAM}$ is not constant, but fluctuates both in time and space (see Section 4.3). Therefore, a realistic history of T, p, q and $\delta^{18}O_{v,ECHAM}$ is shown in Figure 4.12. In this particular case, the air parcel is situated above the Antarctic continent, five days before arrival. This causes an initially low q content, and the initial vapour (from ECHAM4) has a depleted value (i.e. $< -50‰$). The initial RH value however indicates that the air parcel is extremely under-saturated, so no precipitation is modelled during the first modelled day. As soon as RH exceeds the threshold value of 80%, isotopic fractionation begins and precipitation starts to form. The associated isotopic composition of the precipitation is shown in Figure 4.12d (solid line). Between three and two days before arrival, the air parcel undergoes a sharp descent in the atmosphere, which is accompanied by a strong increase of T, under-saturated conditions, and an increase of q. Here, the air parcel undergoes an almost complete isotopic recharge, since q increases from almost

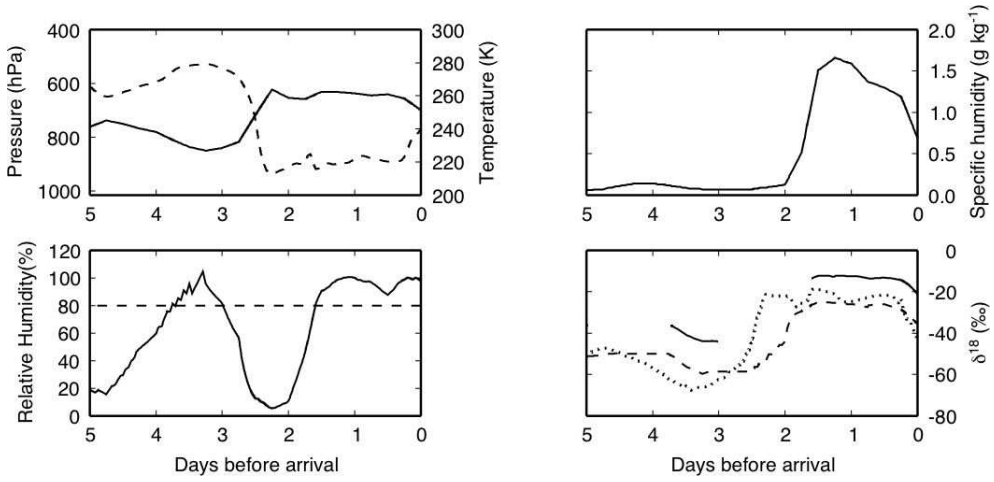

Figure 4.12: *Output from the adapted MCIM showing the effect of isotopic recharge along a realistic trajectory. (a) the imposed T (solid line) and p (dashed line) history of the air parcel; (b) the imposed q history; (c) the associated RH along the trajectory. The threshold value of RH = 80% is indicated with the dashed line; (d) the modelled isotopic evolution of the vapour (dashed line) and associated precipitation (solid line). The dotted line indicates the isotopic composition in the ECHAM model, at that particular location.*

0 to ∼1.7 g kg^{-1}. The strong increase of q is associated with the pathway of the trajectory: in this case, the air parcel flows from the Antarctic continent towards the ocean, and mixing with moisture from humid air over this area occurs. To account for this effect, $\delta^{18}O_{v,ECHAM}$ (dotted line in Figure 4.12) is used as the value of the isotopic composition of the 'new' moisture. Just before the strong increase of q, modelled $\delta^{18}O_v$ is still low, while $\delta^{18}O_{v,ECHAM}$ attains a much higher value at the air parcel's position. Because of this recharge, the modelled value of $\delta^{18}O_v$ almost attains the value of $\delta^{18}O_{v,ECHAM}$ (∼−25 ‰) at the end of the strong increase of q. Finally, during the last day before arrival, some isotopic depletion occurs, which is associated with just a minor temperature decrease towards the precipitation site. The 'final' modelled value of $\delta^{18}O_p$ is ∼ −20 ‰.

4.6 Summary

Through the years, the theory of isotopic distillation (Dansgaard, 1964) has been improved, which has resulted in an increased capability of such models to describe observed spatial gradients (Jouzel and Merlivat, 1984) and seasonal variations (Ciais *et al.*, 1995). Ciais and Jouzel (1994) presented the mixed cloud isotopic model (MCIM), which is a one-dimensional model that describes isotope distillation of water vapour as a function of temperature and pressure, and allows vapour, liquid and ice

to coexist in the cloud. This enables a full simulation of isotopic distillation from the moisture source area toward the (polar) precipitation site, including a smooth transition from liquid to solid precipitation. However, for a combination of such a one-dimensional isotope model with realistic moisture transport, some modifications of the MCIM are necessary. In this chapter, these modifications are described.

The initial isotopic composition of the moisture is no longer calculated from evaporation from the ocean surface (as described by Merlivat and Jouzel, 1979), but is determined using monthly mean (three-dimensional) isotope fields from a general circulation model (ECHAM4). These fields show vertical gradients in $\delta^{18}O$ and in d-excess above the oceanic source area. Therefore, the initial height of the air parcel will have an influence on the isotopic composition of the final modelled precipitation.

The original MCIM assumes continuous saturation along transport. Realistic meteorological conditions are in contrast with this assumption. In analogy with GCMs, we use a relative humidity value of $RH_{threshold} = 80\%$ as an indicator for condensation and hence associated isotopic distillation conditions.

Lastly, the original MCIM was modified to enable isotopic recharge associated with increases of specific humidity along transport. We assumed that this additional moisture is mixed into the air parcel from ambient air. Similar as for the initial moisture in the air parcel, the isotopic ratio of the additional moisture along transport is determined from monthly mean ECHAM4 isotope climatology.

The above mentioned changes have resulted in a modified version of the MCIM that can be used to describe isotopic changes of moisture along realistic transport paths. In the following chapters, this model will be used in combination with backward trajectories, to simulate the isotopic composition of snow pit records (Chapter 5) and to simulate the mean isotope pattern over the entire Antarctic ice sheet (Chapter 6).

Chapter 5

Simulation of snow pit records in Dronning Maud Land for the period 1998-2002

Abstract

The quantitative interpretation of isotope records ($\delta^{18}O$, δD and d-excess) in ice cores can benefit from a comparison of observed meteorology with associated isotope variability. For this reason we studied four isotope records from snow pits in western Dronning Maud Land (DML), Antarctica, covering the period 1998-2001. Timing and magnitude of snowfall events on these locations was monitored using sonic height rangers. For the distinguished snowfall events we evaluated the isotopic composition of the moisture during transport by combining backward trajectory calculations with isotopic modelling, using a Rayleigh-type distillation model (MCIM). The initial isotope ratio of the moisture was determined from monthly mean isotope fields from a general circulation model (ECHAM4). The trajectory analysis showed that the southern Atlantic Ocean is the major moisture source for precipitation in DML. Modelling results along the trajectories revealed that most of the isotopic depletion occurred during the last day of transport. Finally, a diffusion model was applied to describe diffusion in the firn layer such that modelled isotopic composition of snow could be compared with observed isotope records. The resulting modelled isotope profiles were mostly in good agreement with the observed seasonal variability in the snow. However, at low temperatures (especially on the Antarctic interior), magnitude of the total distillation was underestimated. Regarding d-excess, our results show a large influence of advection height on the final value of d-excess in precipitation. This in turn points to the importance of the vertical structure of d-excess over the oceanic source region, which obscures the classical interpretation of this parameter in terms of temperature and relative humidity in the moisture source region.

Chapter 4 and 5 combined are an article under review: Helsen, M.M., R.S.W. van de Wal, M.R. van den Broeke, V. Masson-Delmotte, H.A.J. Meijer, M.P. Scheele and M. Werner. Modeling the isotopic composition of Antarctic snow: Simulation of snow pit records. *Submitted to J. Geophys. Res.*

5.1 Introduction

Ice cores from polar regions contain a wealth of paleoclimatic information (e.g. GRIP Members, 1993; Petit *et al.*, 1999; North Greenland Ice Core Project members, 2004; EPICA community members, 2004). The most important parameter from these ice cores used as a proxy for temperature (T) changes is the isotopic composition of water ($\delta^{18}O$ and/or δD, usually expressed in ‰ as the deviation from the Vienna Standard Mean Ocean Water, VSMOW). The strong empirical relationship between mean annual T and the isotopic composition of snow (δ) is the basis of the use of stable water isotopes as a climate proxy. Furthermore, the second-order parameter deuterium excess ($d = \delta D - 8\delta^{18}O$, hereafter called d-excess) contains additional information about non-equilibrium fractionation of moisture, as was first synthesised by Dansgaard (1964). As such, d-excess is often used to infer climatic information from both the source region of the moisture and of the precipitation site (e.g. B. Stenni *et al.*, 2001; Cuffey and Vimeux, 2001; Masson-Delmotte *et al.*, 2003).

Although water isotope ratios are regarded as a powerful tool to investigate paleoclimate (e.g. Jouzel *et al.*, 1997, 2003), some controversy exists to what extent this proxy can be used as a T indicator, since the δ-T relation varies in space and time (e.g. Robin, 1983; IAEA, 1992; Cuffey *et al.*, 1995; Johnsen *et al.*, 1995; Jouzel *et al.*, 1997, 2003; Masson-Delmotte *et al.*, 2003; Landais *et al.*, 2004). Moreover, in low accumulation areas, the short term correlation (i.e. over several years) between δ and local T is not strong enough to translate isotope records with confidence into T changes (e.g. Helsen *et al.*, 2005b).

Apart from local T, numerous other factors influence the isotopic composition of precipitation, such as condensation temperature (e.g. Dansgaard, 1964; Aldaz and Deutsch, 1967; Peel *et al.*, 1988), changing conditions in the water vapour source area (Boyle, 1997; Cuffey and Vimeux, 2001), microphysical processes in clouds during snow formation (Fisher, 1991; Ciais and Jouzel, 1994), changes in magnitude of the ratio between advective and diffusive transport (Kavanaugh and Cuffey, 2003), changes in strength of the inversion layer (Van Lipzig *et al.*, 2002a), seasonality in precipitation (Werner *et al.*, 2000).

To provide the δ-T relationship with a better physical basis, attempts have been made to model the isotopic fractionation of atmospheric water, either using Lagrangian parcel models based on Rayleigh distillation or using general circulation models (GCMs) equipped with water isotope tracers. The GCM approach is very suitable for the validation of the δ-T relationship since it offers the possibility to take into account all the relevant processes involved in the determination of the δ value. Moreover, with increasing resolution GCMs are increasingly capable to reproduce global and regional patterns of isotope variability (e.g. Joussaume *et al.*, 1984; Hoffmann *et al.*, 1998; Werner and Heimann, 2002; Noone and Simmonds, 2002a; Vuille *et al.*, 2003). However, the complexity of GCMs reduces their usefulness in terms of interpretation. Besides that, GCMs in climate mode generate their own internal variability of e.g. timing of accumulation, which hampers direct comparison with observed isotope records.

On the other hand, Lagrangian parcel models describe isotopic distillation of mois-

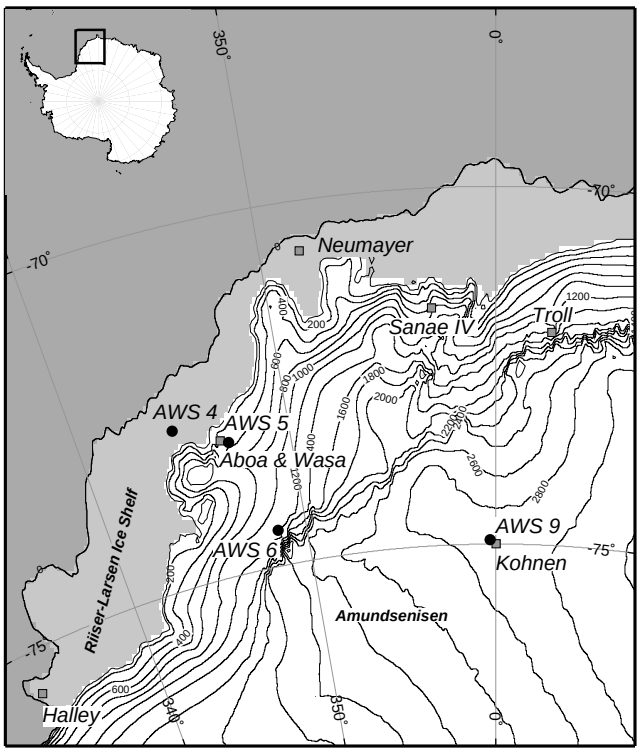

Figure 5.1: *Map of Western Dronning Maud Land, with the locations of the automatic weather stations.*

ture in an isolated air parcel, from a single moisture source towards a precipitation site. In these models, details of cloud processes are often parameterised, which enables them to account for the bulk effect of cloud processes on kinetic isotopic fractionation (Jouzel and Merlivat, 1984; Ciais and Jouzel, 1994). Due to their relative simplicity, these models are suitable to study the influences of different processes along transport. Moreover, the influence of non-equilibrium fractionation (both in the moisture source region and along transport) on the *d*-excess is largely based on results from this type of Lagrangian parcel models (Merlivat and Jouzel, 1979; Johnsen *et al.*, 1989; Ciais *et al.*, 1995; Vimeux *et al.*, 1999). However, these models are often poorly constrained by meteorological data. In an attempt to improve this, Helsen *et al.* (2004) combined back-trajectory calculations with isotopic modelling using a Lagrangian parcel model, for a major snowfall event in Dronning Maud Land (DML), Antarctica. They revealed a general inconsistency in assumptions in this type of model, regarding the (non-continuous) saturation of air masses that transport moisture to the polar regions. Furthermore, they showed that the moisture overlying the south Atlantic Ocean was initially more depleted than expected from local evaporative conditions.

In the present study we aim to increase our knowledge about the controls on polar

Table 5.1: *AWS topographic and climate characteristics, 1998-2001*[a]

	AWS 4	AWS 5	AWS 6	AWS 9
Start of observation	22 Dec 1997	3 Feb 1998	15 Jan 1998	1 Jan 1998
End of observation	21 Dec 2001	2 Feb 2001	14 Jan 2002	31 Dec 2001
Location	72°45.2' S, 15°29.9' W	73°06.3' S, 13°09.9' W	74°28.9' S, 11°31.0' W	75°00.2' S, 0°00.4' E
Elevation (m a.s.l.)	34	363	1160	2892
Surface slope (m km^{-1})	0.1	13.5	15.0	1.3
SSMB[b] (kg m^{-2} yr^{-1})	393	179	267	74
Snow density (kg m^{-3})	406	383	396	307
Temperature (K)	253.4	256.8	252.6	230.0
Relative humidity(%)	93	83	78	93
Specific humidity (g kg^{-1})	1.03	1.01	0.72	0.17
10 m wind speed (m s^{-1})	5.7	7.9	7.7	4.8

[a]Source: Van den Broeke *et al.* (2004). [b]SSMB, specific surface mass balance.

isotopic variability, by extending the approach of Helsen *et al.* (2004), combining isotopic modelling with meteorological data, to be able to compare modelling results with observed isotope records. We use four years of automatic weather station (AWS) data to infer the accumulation history of four different sites in western DML (Figure 5.1). After establishing the accumulation history (section 5.2), we use back-trajectory calculations to trace the transport history of the moisture (section 5.3). Then, we combine this meteorological data with isotope distillation modelling, using a Rayleigh-type fractionation model, which is able to deal with the occurrence of under-saturation and evaporative recharge (section 5.4). This gives us modelled isotopic values of the detected snowfall events, which still cannot readily be compared with the observed isotope records from the snow pits, since post-depositional diffusion has smoothed the original values of the individual events. Therefore, we simulate the diffusion process in section 5.5, and the resulting modelled isotope records are compared with observations in section 5.6. In section 5.7 a discussion follows, whereupon conclusions are drawn in section 5.8.

5.2 Study area and accumulation history

The mass balance of western DML has been monitored for several years using AWSs (Reijmer and Van den Broeke, 2003). For the present study, we use results from four AWSs situated along a transect connecting the coastal area (AWS 4), with the high Antarctic plateau (AWS 9) (Figure 5.1). The escarpment region (AWS 5 and 6) forms the transition between these two areas. The accumulation is relatively low in this area, and ranges from 74 kg m^2 yr^{-1} on the Antarctic plateau (AWS 9) to 393 kg m^2 yr^{-1} on the ice shelf (AWS 4). Table 5.1 gives a summary of the topographic and meteorological characteristics of these sites.

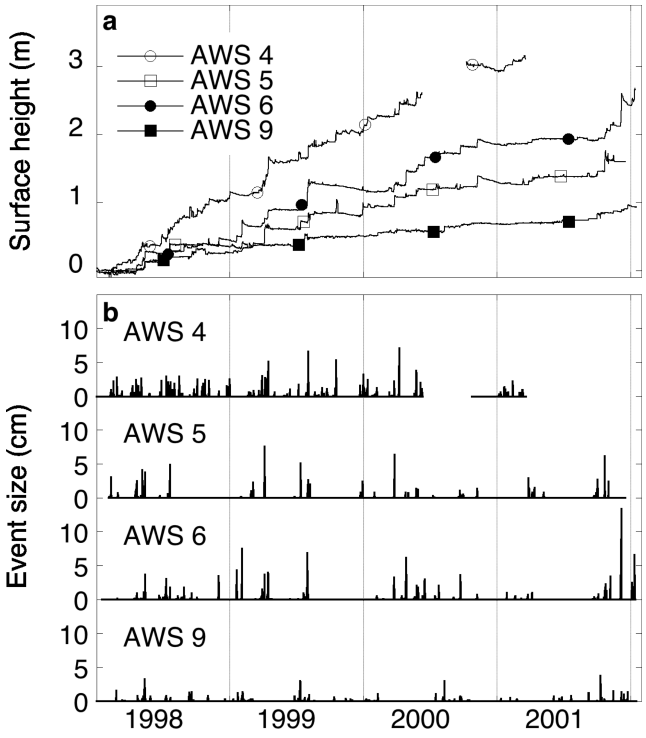

Figure 5.2: *Surface height (a) and identified accumulation events (b) from the AWSs over the period 1998-2001. Due to a malfunctioning SHR, the accumulation history of AWS 4 could only be established until early 2001, with a data gap in winter 2000.*

The AWSs are equipped with a sonic height ranger (SHR) (Campbell SR50) that measured the local (change in) surface height. This instrument enables us to retrieve the exact timing of snowfall events (Helsen *et al.*, 2005b). The SHR record of the surface height change is plotted in Figure 5.2a. The accumulation is discontinuous; sudden increases of the snow surface are followed by longer periods of slowly decreasing or constant surface height. The sudden increases of the surface are most likely the result of snowfall. However, a net deposition of drifting snow cannot be ruled out. The surface slowly subsided during periods without accumulation, as a result of settling of the snow and sublimation. Sudden decreases of the surface height are most likely caused by wind erosion.

From these records, accumulation events that are preserved in the snow are distinguished following the procedure described in Chapter 2. The accumulation history of each site is hereby resolved in 12-hour intervals. Due to compaction of the underlying snow, the distance between a certain snow layer and the SHR increases slowly through time. We corrected for this effect using measured density profiles, to give a best estimate of the depth of each layer at the end of the monitoring period. This was

Table 5.2: *Characteristics of samples taken from snow pits in the field season 2001-02*

	AWS 4	AWS 5	AWS 6	AWS 9
Location	15 m from AWS 4	2 m from AWS 5	under SHR	under SHR
sampling date	25 Dec 01	17 Dec 01	14 Jan 02	17 Jan 02
depth of the pit (cm)	450	200	300	91.5
δ sampling interval (cm)	2.0	2.0	2.0	1.5
ρ sampling interval (cm)	5.0	5.0	5.0	2.5

done to facilitate a comparison with measured isotope records (Table 5.2, see Section 5.6). However, due to unknown changes in the density profiles through time, the final depth of each snowfall event is only an estimate, which hampers an event-based comparison of observed and modelled isotope records (see Section 5.6).

Figure 5.2b displays an overview of the timing and magnitude of the preserved snowfall events. The intermittent character of the accumulation is apparent, resulting in only few large snowfall events that account for the bulk of the total accumulation. This has resulted in the exclusion of entire seasons from the isotope records, which can hamper the interpretation of isotopic variability on a seasonal scale. At AWS 4, 5 and 6 the accumulation is highest in autumn and winter (with 65-75 % of annual accumulation). AWS 9 shows a more evenly distribution of accumulation through the year (Reijmer and Van den Broeke, 2003). The relation between local T and the isotope records is further discussed in Chapter 2. In the present study, we follow an alternative approach, by explicitly modelling the isotopic composition of each accumulation event.

5.3 Trajectories

In order to model the isotopic composition of snowfall, information is needed about the transport history of the moisture. We obtained this information by using a trajectory model, that calculates five days backward trajectories for air parcels arriving at the locations of the AWSs. This trajectory model was developed by the Royal Netherlands Meteorological Institute (KNMI; Scheele *et al.*, 1996) and it computes the large-scale three-dimensional displacement of an air parcel during a time step Δt, using an iterative scheme:

$$X_{n+1} = X_0 + \frac{\Delta t}{2}[v(X_0, t) + v(X_n, t + \Delta t)] \tag{5.1}$$

where X_0 is the position vector of the air parcel at time t, X_n is the n^{th} iterative approximation of the position vector at $t + \Delta t$, and $v(X, t)$ is the three-dimensional wind vector at position X and time t. The iteration time step Δt is -10 min. The iteration stops when the horizontal distance between X_n and X_{n+1} is less than 300m, and the relative vertical (pressure) difference $(p_{n+1} - p_n)/p_{n+1}$ is less than 10^{-4}. For comparison, the mean horizontal displacement in 10 min. is typically 4-5 km.

As an input for the trajectory model we used the European Centre for Medium-range Weather Forecasts (ECMWF) reanalysis (ERA-40) data set. We used the analysed fields, to obtain the most accurate estimate of the 'true' state of the atmosphere. The spectral resolution of this archive is T159 (corresponding to ∼125 km horizontal spatial resolution and 60 vertical levels), but as input for the trajectory model these data are gridded on a constant 1.0° resolution in the horizontal plane, 60 vertical levels, and six-hourly data. Interpolation in space and time was therefore necessary. The spatial interpolation of the trajectory model is bilinear in the horizontal, and linear with $\log(p)$ in the vertical. The interpolation in time is quadratic, but for temperature and moisture this produced unrealistic variations, which made us apply a linear interpolation for these parameters.

Uncertainties in the resulting trajectories can be considerable. The choice of trajectory type, interpolation schemes and spatial resolution of the wind fields introduces an uncertainty in the order of 1000 km after five days backward calculation (Stohl *et al.*, 1995). In reality, the error can be even larger, due to the presence of convective systems (e.g. fronts, convective storms) or the vicinity of the earth surface, which can cause the parcel to lose its identity. These errors are difficult to quantify and not included in the uncertainty estimate, so computed trajectories must be interpreted with care.

Apart from the above-mentioned difficulties, an additional problem that can influence the isotope modelling is that a trajectory model only traces the advective pathway of an air parcel. This is not necessarily equal to the pathway of the moisture itself, since diffusive moisture fluxes are neglected. Nevertheless, we apply the trajectory method because we consider it the best available estimate of transport histories for individual snowfall events.

For the Antarctic region this trajectory model has previously been used to define moisture source regions for several deep drilling sites (Reijmer *et al.*, 2002), whereas Helsen *et al.* (2004) (Chapter 3) used the trajectory model in combination with an isotope model to investigate the isotopic distillation of Antarctic moisture along transport.

To capture the best estimate of the transport history of the moisture that brings snowfall to the study sites, the trajectories for air parcels should ideally be calculated from arrival locations at the exact time and location of the snow formation above the accumulation sites. For the timing of the snowfall events, we used the accumulation records from the SHRs (Figure 5.2). These records consist of accumulation amounts in 12-hour intervals, which are bounded by 0600 and 1800 GMT; if accumulation occurred in such an interval, we defined the moment of snow fall either at 0000 or 1200 GMT. To determine the vertical (pressure) level of snow formation, vertical profiles of cloud water content (CWC) from ERA-40 were considered. We defined the height of snow formation as the level with maximum CWC. If successive 12-hour intervals showed accumulation, the interval with the highest maximum CWC was considered to be the interval with most snow fall, and in addition, this moment is regarded to be the representative timing of snow formation of this event. Then, five-days backward trajectories were calculated from five pressure levels (-50, -25, 0, 25 and 50 hPa) centred around this pressure level with maximum CWC.

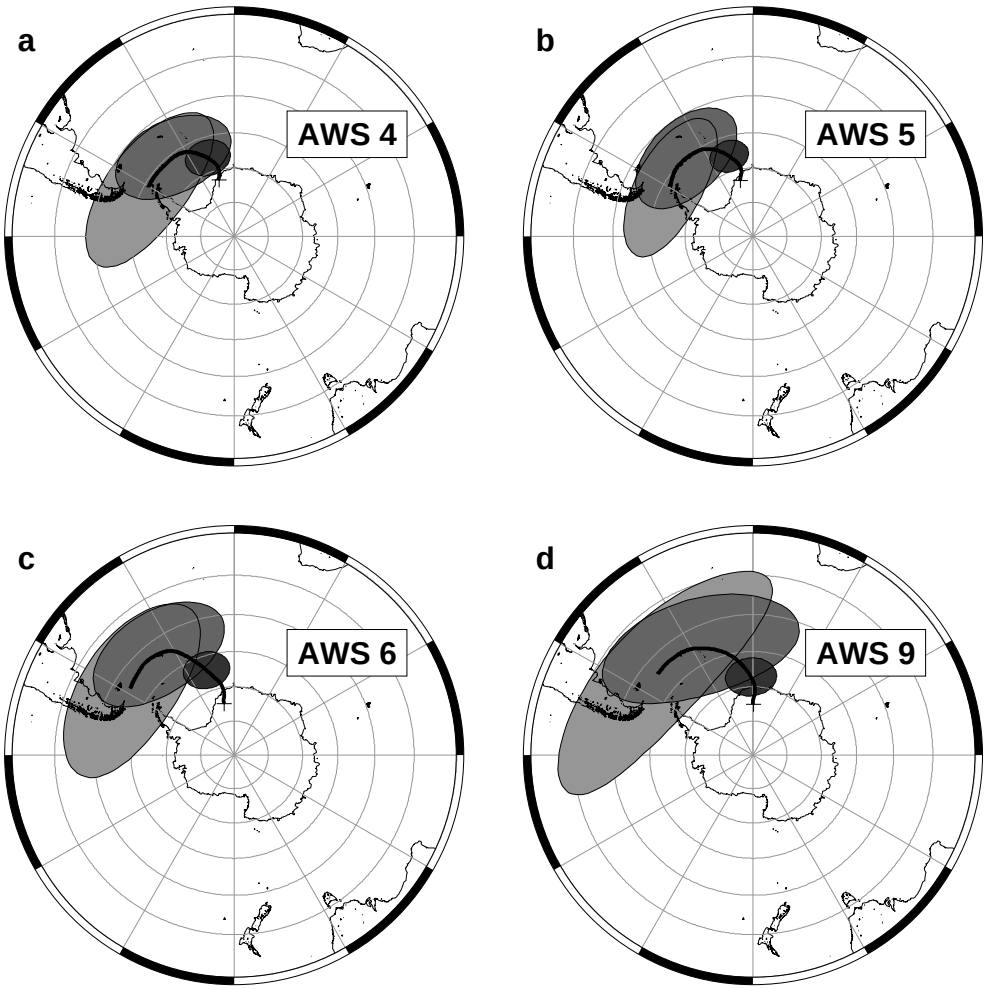

Figure 5.3: *Weighted mean five-days backward trajectories (thick lines) and covariance ellipses for days when snowfall occurred at AWS 4 (a), AWS 5 (b), AWS 6 (c) and AWS 9 (d). Covariance ellipses are associated with air parcel locations at five days (light gray), three days (medium gray) and one day (dark gray) before arrival at the study sites. Weighting is performed using the magnitude of snowfall events from Figure 5.2.*

Figure 5.3 shows the weighted mean of the trajectories calculated for all snowfall events at the AWSs. The magnitude of each accumulation event detected by the SHR (Figure 5.2b) is used as a weighting factor (w_i). In this way, a weighted mean pathway of the moisture could be calculated. The main picture for all four AWSs shows a cyclonic transport path over the southern Atlantic Ocean, which is in agreement with earlier studies of moisture transport to DML (Noone *et al.*, 1999; Reijmer *et al.*, 2002) To indicate the variability of the air parcel positions, covariance ellipses are plotted around the mean locations at one, three and five days before arrival (Figure 5.3). The size, shape and angle of these ellipses are based on the weighted variances (σ_x^2 and σ_y^2) and covariances (σ_{xy}) of the position vector components (x, y, in km), in analogy with Kottmeier and Fay (1998),

$$\sigma_x^2 = \frac{\sum_1^n w_i(x_i - \bar{x})^2}{\sum_1^n w_i} \tag{5.2}$$

$$\sigma_y^2 = \frac{\sum_1^n w_i(y_i - \bar{y})^2}{\sum_1^n w_i} \tag{5.3}$$

$$\sigma_{xy} = \frac{\sum_1^n w_i(x_i - \bar{x})(y_i - \bar{y})}{\sum_1^n w_i} \tag{5.4}$$

using σ_x and σ_y as lengths for the major and minor axis of the ellipse, respectively. The orientation of major axis of the ellipse is determined by σ_{xy}/σ_x^2.

As expected, the trajectories converge from a large variability at five days before arrival towards a confined area one day before they reach their final destination. Although the pathways for the four study sites look quite similar, there is a major difference in the air parcels' position at five days before arrival. While the trajectories for the site on the ice shelf (AWS 4, Figure 5.3a) are located at ∼61°S, at five days before arrival, the trajectories for the Antarctic plateau (AWS 9, Figure 5.3d) show a position at ∼54°S at five days before arrival.

Generally, the air parcel positions are more northward for destinations higher on the Antarctic plateau. This pattern reflects an increase in advection speed. One should keep in mind that the trajectories shown here are weighted with accumulation at the arrival location. The larger advection speed of the trajectories for the plateau compared to the coastal sites can be attributed to the scarcity of cyclonic activity (and associated snowfall) in the Antarctic interior. Only intense cyclones penetrate onto the Antarctic plateau and bring snowfall to this area. Hence, a large snowfall event will be associated with strong advection, which explains the more distant origin. This difference in transport paths can have implications for the source area of the moisture, and its isotopic composition, especially regarding the *d*-excess parameter (discussed in Section 5.7).

The difference in intensity of advection is further explained by Figure 5.4a, which shows the pressure level of the air parcel during transport towards the arrival sites. The higher altitude of AWS 9 results in a higher starting level, and this higher transport level is maintained during all five days before arrival. The longer advection path

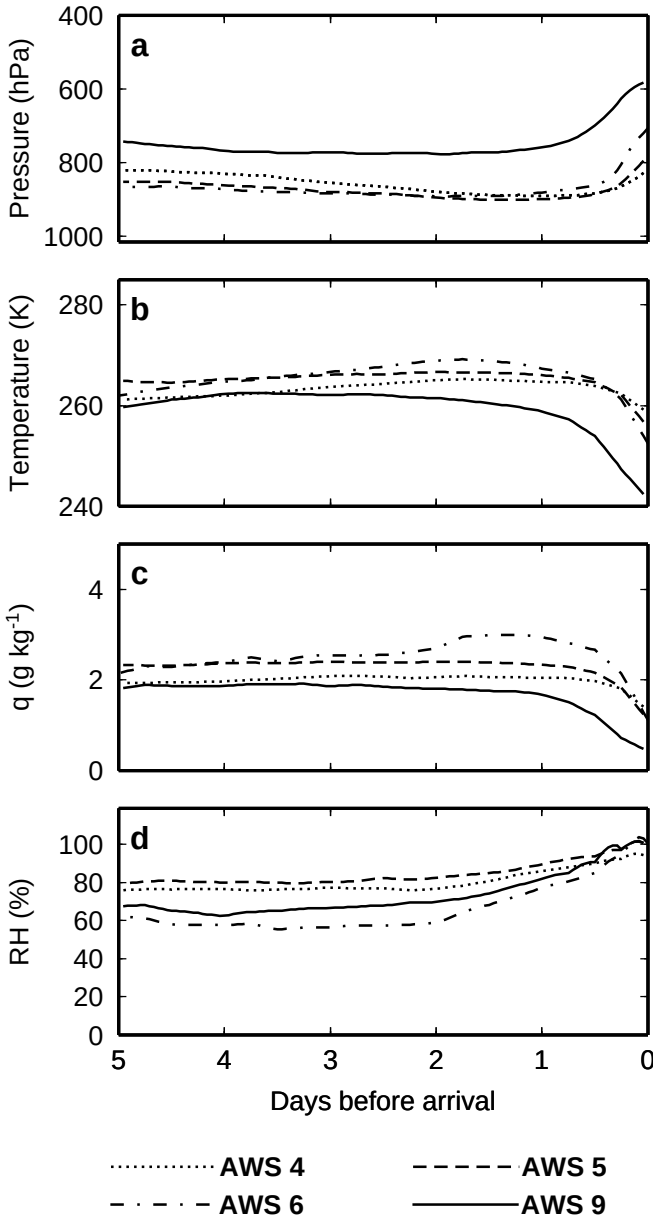

Figure 5.4: *Weighed mean values of air pressure (a), temperature (b), specific- (c) and relative humidity (d) along trajectories for the four study sites.*

of the trajectories arriving at AWS 9 is obviously also associated with the higher transport path.

The temperature evolution along the trajectories is shown in Figure 5.4b. During the major part of the transport path, T remains constant, or increases slightly. Only during the final stage of the transport (last day before arrival), T decreases strongly. This is the case for all sites, but most pronounced for AWS 9.

The changes in specific humidity (q, Figure 5.4c) during transport towards the arrival site are very similar to the T pattern. Increases of q occur either between five and one day before arrival (implying moisture uptake), or the moisture has already entered the air parcel more than five days before arrival. The strong decrease of T in the final stage of transport causes a similar drop in q. This decrease of T and q during the approach towards the Antarctic continent is of primary importance for the final isotopic composition of the moisture (see Section 5.4).

Using the variation of q along the trajectories, we can find the region of maximum moisture uptake for the four study locations, by weighting the location of moisture uptake with the amount of increase of q, multiplied by the weighting factor for each trajectory (as in the procedure for the calculation of the weighed mean trajectories). This gives us mean values and covariance ellipses of the moisture uptake locations, which can be interpreted as the moisture source regions for the four study sites (Figure 5.5). The dominant moisture source regions are located over the south Atlantic ocean, which is in line with earlier findings of e.g. Reijmer *et al.* (2002). It should be kept in mind that these source areas are determined using only moisture increases during the last five days of transport. The percentages in the ellipses in Figure 5.5 indicate the portion of the total moisture that has entered the air parcel during these last five days of transport. The remaining part of the moisture was already present in the air parcel at five days before arrival, which hampers an estimation of the source area of this moisture.

The difference in trajectory length that was noticed in Figure 5.3 has a consequence for the moisture source regions, which is clearly visible in Figure 5.5. Snow that is transported far onto the Antarctic plateau has a more distant moisture source than coastal precipitation: the moisture source for AWS 4 is located between ∼45°S and 70°S, while the moisture source for AWS 9 is between ∼40°S and 65°S. This is in agreement with different GCM studies (Werner *et al.*, 2001; Delaygue *et al.*, 2000) that also showed an increasing contribution of low latitude moisture towards the Antarctic interior.

Figure 5.4d presents values of relative humidity (RH). The value of RH is indicative for the presence of saturated conditions, which are crucial for the occurrence of condensation and associated isotopic fractionation. We note fairly high values of RH for the trajectories of AWS 4 and 5, while the trajectories for AWS 6 and 9 show a lower value over the first part of transport, slowly increasing towards saturated values. This indicates that air parcels bringing snowfall to the coastal area of DML tend to experience more frequent saturation during the last five days of transport than those that travel to the more elevated interior. The latter air parcels only show saturated conditions during the final phase of transport (∼1 day). These differences in RH can have consequences for the isotopic distillation process, since we do not expect

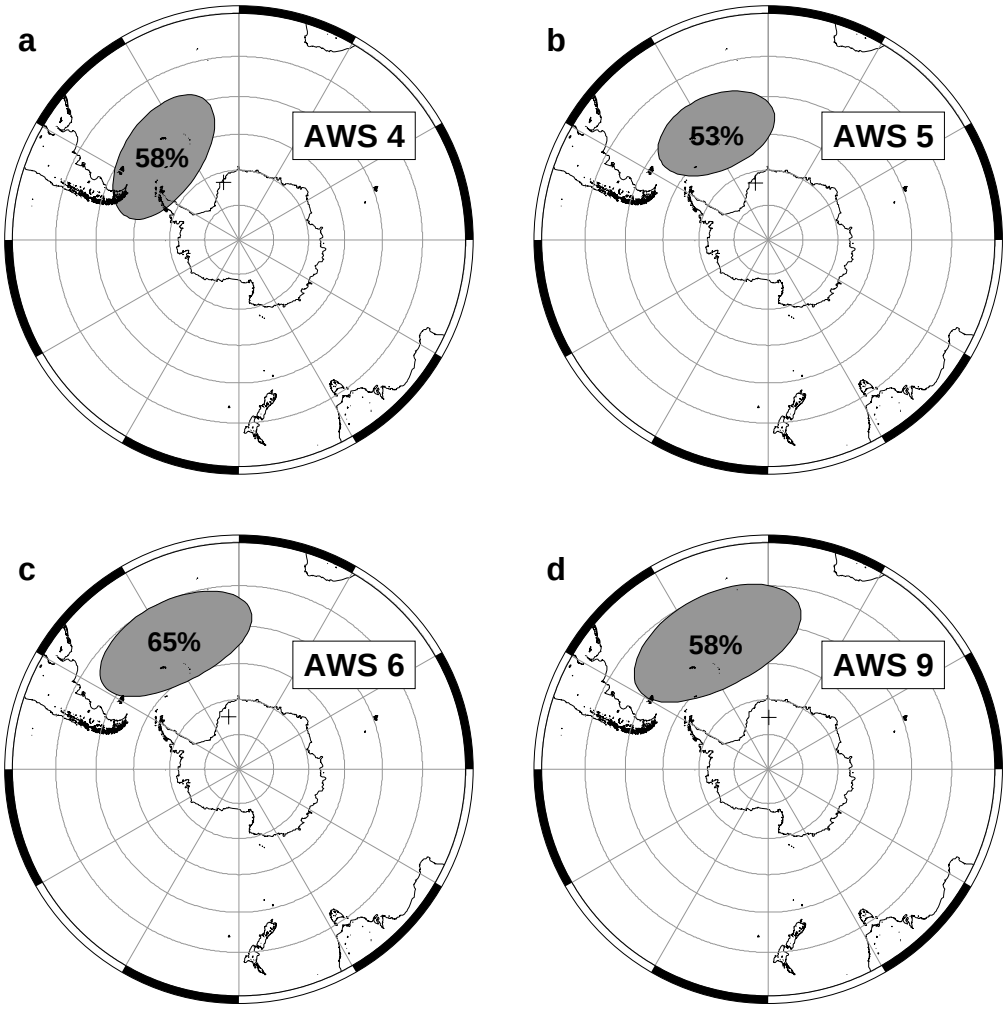

Figure 5.5: *Covariance ellipses representing the location of moisture uptake along trajectories for AWS 4 (a), AWS 5 (b), AWS 6 (c) and AWS 9 (d). The percentages in the ellipses show the portion of the total moisture that has entered the trajectory during the last five days of transport.*

condensation (nor isotopic fractionation) during undersaturated conditions.

5.4 Isotopic distillation

To simulate the isotopic fractionation process of moisture in air parcels, we use the Mixed Cloud Isotopic Model (MCIM; Ciais and Jouzel, 1994), which describes isotopic changes in an isolated Lagrangian air parcel. In principle, this model is derived from a Rayleigh distillation model as described by Dansgaard (1964). However, improvements on the Rayleigh distillation theory (regarding the kinetic fractionation effect) have been incorporated both in the source area (Merlivat and Jouzel, 1979) and in the description of snow formation at low temperatures (Jouzel and Merlivat, 1984). Furthermore, Ciais and Jouzel (1994) introduced a description of the processes occurring in mixed clouds, allowing the interaction of vapour, liquid and ice. These improvements have resulted in the MCIM, which has succeeded in reproducing the main characteristics of stable-isotope variability in the middle and high latitudes (e.g. Jouzel *et al.*, 1997). In addition, the MCIM has been used to support the interpretation of the seasonal cycle at Law Dome, Antarctica (Delmotte *et al.*, 2000; Masson-Delmotte *et al.*, 2003).

Difficulties arise when a conceptual isotope distillation model like the MCIM is combined with a backward trajectories of air parcels, since some of the assumptions made in the MCIM are not always met in reality (Chapter 3, Helsen *et al.*, 2004). Therefore, the MCIM has been modified, which is extensively addressed in Chapter 4. This modified MCIM obtains its initial isotopic composition from three-dimensional isotope fields generated by a 20 yr climate run of the ECHAM4 GCM. Furthermore, the modified MCIM is able to describe isotopic recharge, associated with increases of q along transport. Lastly, in analogy with GCMs, a threshold value of RH ($RH_{threshold} = 80\%$) is included, as an indicator for condensation and associated isotopic distillation.

We used this modified MCIM for a simulation of the isotopic distillation along trajectories for all snowfall events as identified by the AWSs. Weighted mean isotopic distillation histories are shown in Figure 5.6 for the trajectories calculated for the four study sites. As for the trajectory results presented in Figure 5.4, weighting for the averaging are obtained from accumulation amounts (Figure 5.2).

The mean isotopic change along transport of both $\delta^{18}O$ (left panels in Figure 5.6) and d-excess (right panels in Figure 5.6) are shown for both vapour (dashed lines) and precipitation (solid lines). Also shown are corresponding values of monthly mean isotope values of vapour from the ECHAM4 isotope climatology (Chapter 3), at the location of the air parcels (dotted lines). Minimum and maximum values of the final precipitation are also indicated with the gray bars.

The general picture from the fractionation histories in Figure 5.6 is that the modelled $\delta^{18}O$ value of the moisture is relatively constant during most of the transport, whereas during the last day of transport the major part of the fractionation takes place. This is very well explained by the changes in T and q (Figure 5.4) during the last day of transport. The isotopic amplitude is only minor at AWS 5, since most

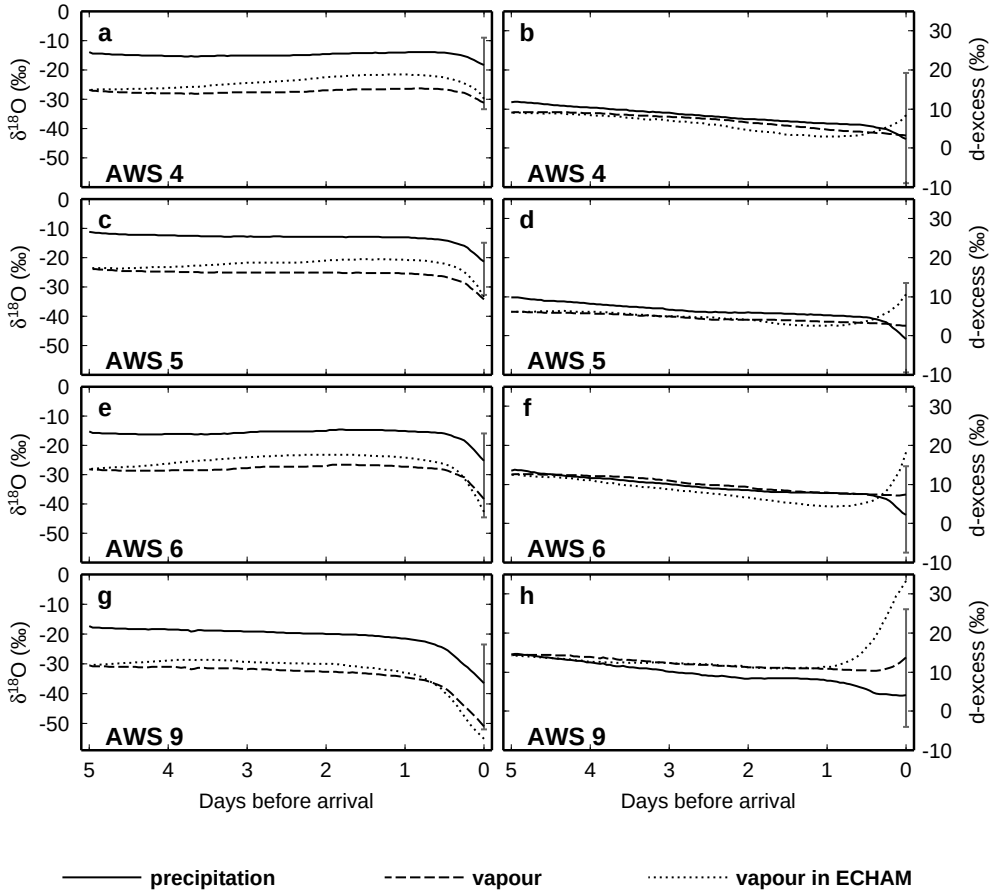

Figure 5.6: *Mean isotopic distillation histories along trajectories for AWS 4 (a,b), AWS 5 (c,d), AWS 6 (e,f) and AWS 9 (g,h). Left panels show weighted mean fractionation history for $\delta^{18}O$; right panels for the d-excess. Minimum and maximum values of the final isotopic value of the snow are plotted at the end of each distillation history, to indicate the variability.*

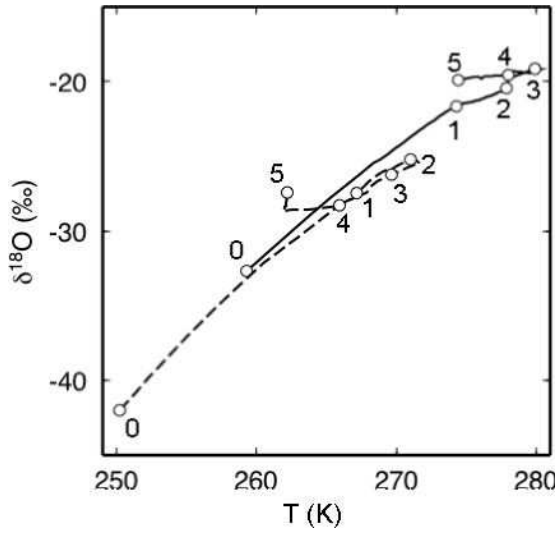

Figure 5.7: *Seasonal mean $\delta^{18}O_v$ distillation paths for AWS 6 as a function of T. Solid line represents summer (DJF) distillation, dashed line for winter (JJA). Numbers indicate day before arrival.*

precipitation occurred in spring or autumn (Chapter 2, Helsen *et al.*, 2005b), while AWS 9 shows the largest amplitude.

It is interesting to compare modelled $\delta^{18}O_v$ and ambient $\delta^{18}O_{v,ECHAM}$ from the ECHAM4 fields. Due to the definition of the initial state, the values of $\delta^{18}O_{v,ECHAM}$ and $\delta^{18}O_v$ are equal when the simulation starts (Chapter 4). From that moment onward, $\delta^{18}O_{v,ECHAM}$ slowly increases, while $\delta^{18}O_v$ hardly changes, due to (on average) constant values of T, p and q. However, during the last day of transport, $\delta^{18}O_{v,ECHAM}$ plunges to more negative values than $\delta^{18}O_v$ for AWS 6 and 9.

This can be understood, since the values of $\delta^{18}O_{v,ECHAM}$ are climatic mean values of a certain latitude and altitude. On the other hand, the values of $\delta^{18}O_v$ are only calculated for snowfall events. In Antarctica, snowfall is generally associated with advection of much warmer air than average (e.g. Noone *et al.*, 1999; Helsen *et al.*, 2005b). A comparison of T values from both our trajectories and in the ECHAM4 fields (not shown) indeed points to a difference in T. Therefore, the lower gradient of $\delta^{18}O_v$ compared to $\delta^{18}O_{v,ECHAM}$ is associated with a smaller drop in T during accumulation, compared to the mean temperature distribution over the Antarctic region, and hence explains why $\delta^{18}O_v$ is higher then $\delta^{18}O_{v,ECHAM}$.

Focussing on the seasonal amplitude, Figure 5.7 shows the seasonally averaged distillation of $\delta^{18}O_v$ as a function of T for trajectories to AWS 6. The drop in T (which is strongest during the last day of transport) produces a strong distillation of the moisture. The average δ/T gradient increases from 0.6 ‰ K^{-1} around the freezing point to 1.0 ‰ K^{-1} at 253 K. Between five and three days before arrival, increases in T are accompanied by isotopic recharge, which causes a somewhat irregular pattern

Table 5.3: *Characteristics of seasonally averaged distillation paths.* $\delta^{18}O_p$ *denotes final isotopic composition of the precipitation,* ΔT *is the difference in* T *over which distillation has occurred,* $\delta^{18}O_{\Delta T}$ *is the amount of distillation explained by* ΔT*. The final 3 columns give the total seasonal isotopic difference in the snowfall (*Δ_{tot}*), the amount of this difference explained by* ΔT *(*$\Delta_{\Delta T}$*), and the (remaining) difference explained by the initial isotopic composition of the moisture (*$\Delta_{\delta_{v0}}$*), respectively.*

	DJF			JJA			DJF−JJA		
	$\delta^{18}O_p$ (‰)	ΔT (K)	$\delta^{18}O_{\Delta T}$ (‰)	$\delta^{18}O_p$ (‰)	ΔT (K)	$\delta^{18}O_{\Delta T}$ (‰)	Δ_{tot} (‰)	$\Delta_{\Delta T}$ (‰)	$\Delta_{\delta_{v0}}$ (‰)
AWS 4	−13.2	7.1	5.6	−19.9	11.2	8.3	6.7	2.7	5.0
AWS 5	−17.0	11.2	7.5	−22.7	15.2	12.3	5.7	4.8	0.9
AWS 6	−20.5	20.9	12.2	−28.8	21.4	15.2	8.3	3.0	5.3
AWS 9	−26.0	20.7	13.7	−37.3	32.2	23.3	11.3	9.6	1.7

of the average values of T and $\delta^{18}O_v$.

Interestingly, looking at the difference in T over which condensation occurs (ΔT) over the seasonally averaged trajectories, Figure 5.7 shows that ΔT_{JJA} is hardly larger than ΔT_{DJF}. Since ΔT determines the magnitude of the isotopic distillation, not much difference would be expected in the final isotopic composition, notwithstanding that there is a seasonal difference in the $\delta^{18}O$ value of the initial moisture in the air parcel. This implies that the seasonal amplitude of $\delta^{18}O$ can only to a small extent be explained by seasonal changes in ΔT. To a much larger extent it is a reflection of a more regional signal in $\delta^{18}O$ of atmospheric moisture.

We summarised the relative contribution of ΔT to the total isotopic distillation in Table 5.3. The isotopic composition of the moisture that enters the air parcel appears to make a large difference for AWS 4 and 6, whereas ΔT can explain the bulk of the seasonal isotopic cycle for AWS 5 and 9. The large isotopic differences in this initial moisture along trajectories to AWS 4 and 6 are not due to large shifts in source areas, but can partly be attributed to seasonal changes in the isotopic composition of vapour around Antarctica and also to differences in initial height of the air parcels (which can be of large influence as explained in Chapter 4).

The changes in d-excess along the trajectories are shown in the right panels of Figure 5.6. In the first phase of transport, when the air parcels are located over the ocean, a gradual decrease can be observed in the d-excess values of both the moisture in our modelled air parcels as in the ECHAM4 fields. In the last part of the transport, when T strongly drops when the parcel approaches the Antarctic continent, our modelled d-excess values of the vapour do not react strongly, whereas the ECHAM4 fields show strongly increasing d-excess values. The modelled d-excess values in the precipitation along the trajectories show a decrease during the T drop in the final stage of transport.

This drop of d-excess in precipitation during the final stage of transport of the air parcels appears to be in conflict with the general pattern of increasing d-excess values with decreasing T over Antarctica, which is present in both observations (Petit *et al.*, 1991; Dahe *et al.*, 1994) and in model results (Hoffmann *et al.*, 1998). If we

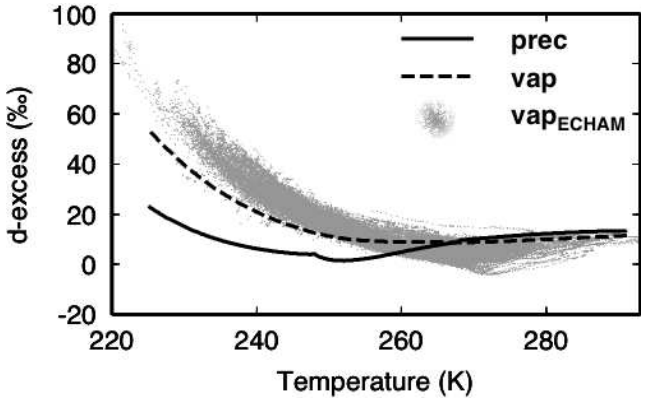

Figure 5.8: *Modeled d-excess of vapour (dashed line) and precipitation (solid line) as a function of temperature along an idealised trajectory; d-excess values of vapour from ECHAM are plotted in gray against temperature in ECHAM for all air parcel positions for AWS 9.*

focus on the general behaviour of d-excess in precipitation as a function of T in our model (Figure 5.8, which shows results of a model run using a linear decreasing T), it appears that d-excess slowly decreases down to T ~250K, and subsequently increases at lower T. Furthermore, changes in p also play a role in the exact shape of the d-excess curve. On average, our trajectories did not encounter low enough T to reach the increasing branch of the d-excess curve. This is the reason that the d-excess does not increase (yet) in the direction of the Antarctic interior. We thus expect higher values of d-excess for trajectories towards more remote regions in Antarctica.

An indication of higher d-excess values with low T can be found in the variability in d-excess (shown as the grey bars in Figure 5.6). Much more deviations from the mean value on the positive side of the d-excess range occur compared to deviations on the negative side. This is most evident for AWS 9 and the explanation for this is that events leading to such high d-excess values are associated with lower T than average. Since these cold accumulation events are typically associated with only a small amount of snowfall, the weighted mean d-excess is much lower than would be expected from the minimum and maximum value.

We can also compare our modelled values of d-excess in the vapour phase with ECHAM4. In Figure 5.8, mean monthly d-excess values of the vapour in ECHAM4 are plotted in grey as a function of mean monthly temperatures in ECHAM4 for pathways towards AWS 9. For the sake of clarity, modelled d-excess is plotted against trajectory T only for an idealised temperature history. This comparison shows that the two parameters generally behave in a comparable way. Only at very low T, the d-excess in ECHAM4 increases stronger than our modelled d-excess. These results point out that the apparent large difference in d-excess in ECHAM4 and in our modelling results in Figure 5.6 is caused by T differences between the ECHAM4 climatology (all conditions) on the one hand and the trajectories for snowfall events on the other

hand, during which warm conditions prevail. The different behaviour of d-excess at very low T can be attributed to a slightly different parameterisation of the degree of supersaturation in ECHAM (Hoffmann *et al.*, 1998) compared to the one we applied (Ciais and Jouzel, 1994).

5.5 Firn diffusion

To enable a comparison of modelled isotopic composition of precipitation with that measured in snow pits, the diffusion in the firn should be taken into account. We use the firn diffusion model as described by Johnsen *et al.* (2000), and refer to their work for a full explanation of the theory. This model is able to realistically describe the smoothing of isotope records through time.

Considering a coordinate system with a vertical z-axis and an origin at the surface, the isotopic composition δ_i of non-deforming firn changes over time t according to:

$$\frac{\partial \delta_i}{\partial t} = \frac{m e_s \omega_{ai}}{RT\alpha_i \tau}\left(\frac{1}{\rho_f} - \frac{1}{\rho_{ice}}\right)\frac{\partial^2 \delta_i}{\partial z^2} \tag{5.5}$$

where m being the molar weight of water, e_s the saturation vapour pressure over ice, ω_{ai} the diffusivity of the isotopic species i in open air, R the universal gas constant, T temperature, α_i the ice-vapour equilibrium fractionation factor for the isotopic species i, τ the tortuosity factor, ρ_f the density of the firn and ρ_{ice} the density of ice. Using Equation 5.5, the diffusion rate is especially sensitive for T and ρ_f. We obtained subsurface values of T from energy balance calculations by Van den Broeke *et al.* (2005). During sampling, ρ_f has been measured. We used a fitted power law function for ρ_f at each site, and assumed that this relation is constant over time. For all other parameters in Equation 5.5 we used expressions as suggested by Johnsen *et al.* (2000).

To minimise the effects of boundary conditions, we added one artificial sinusoidal seasonal cycle and started the diffusion model at 1 January 1998. Each day when accumulation occurred according to the SHR record, this snow is added on top of the diffusion domain, and the origin of the z-axis is shifted to the surface. We account for the densification of the snow by calculating new density values for the modelled domain each time a shift of the z-axis occurs (i.e. after each accumulation event).

In Figure 5.9, modelled growth of the $\delta^{18}O$ record at AWS 6 is shown. The $\delta^{18}O$ record is plotted for each modelled year, starting with the prescribed sinusoidal seasonal cycle at 1 January 1998, followed by four subsequent years of accumulation and diffusion, and ending on the day when the snow pit samples were taken, early 2002.

Figure 5.9 clearly shows that the isotope record is initially irregular and often includes several sub-seasonal variations. However, firn diffusion quickly smoothes these features, and after some years the only remaining signal is the annual cycle. Striking are also the differences in decrease of seasonal amplitudes, which are largely dependent on the second derivative term in Equation 5.5: the diffusion process has a

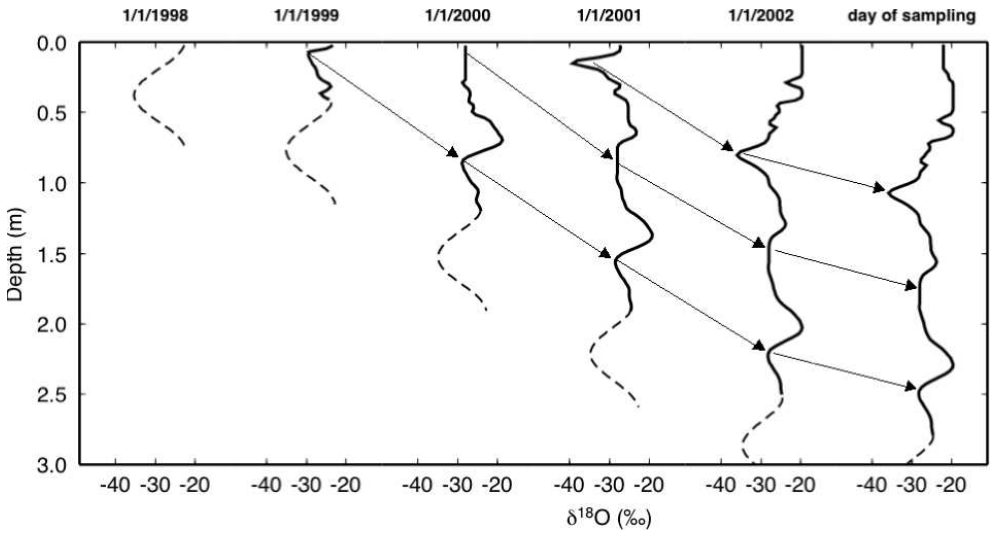

Figure 5.9: *Evolution of the $\delta^{18}O$ record at AWS 6. Arrows indicate the vertical shifts of winter minima in subsequent years.*

much larger effect on the strongly negative $\delta^{18}O$ winter 2000 minimum, compared to the broader minimum of winter 1999 (Figure 5.9).

5.6 Simulated snow pit records

By modelling both isotopic distillation during atmospheric transport and post-depositional diffusion occurring in the firn layer, we have obtained simulated isotope records that can be compared with the isotope records, as sampled in the Antarctic field season 2001-02 (Table 5.2). A comparison of modelled and observed records can reveal the validity of our modelling approach.

Both modelled (solid lines) and observed records (dashed lines) are shown in Figure 5.10. Furthermore, we summarised our results in Table 5.4 in terms of mean values and standard deviations (which can be interpreted as an indicator for the seasonal amplitude). Table 5.4 also shows a column with isotope values from ECHAM4. These values result from an experiment using monthly mean isotope values in precipitation from ECHAM4 (not shown in Figure 5.10), instead of our model experiment using backward trajectories.

5.6.1 $\delta^{18}O$

The results for the $\delta^{18}O$ records differ from site to site. For the coastal site AWS 4 (Figure 5.10a) it was not possible to reveal the entire accumulation record, due to failure of the SHR, which prohibited a reconstruction of the upper 1.5 m. The

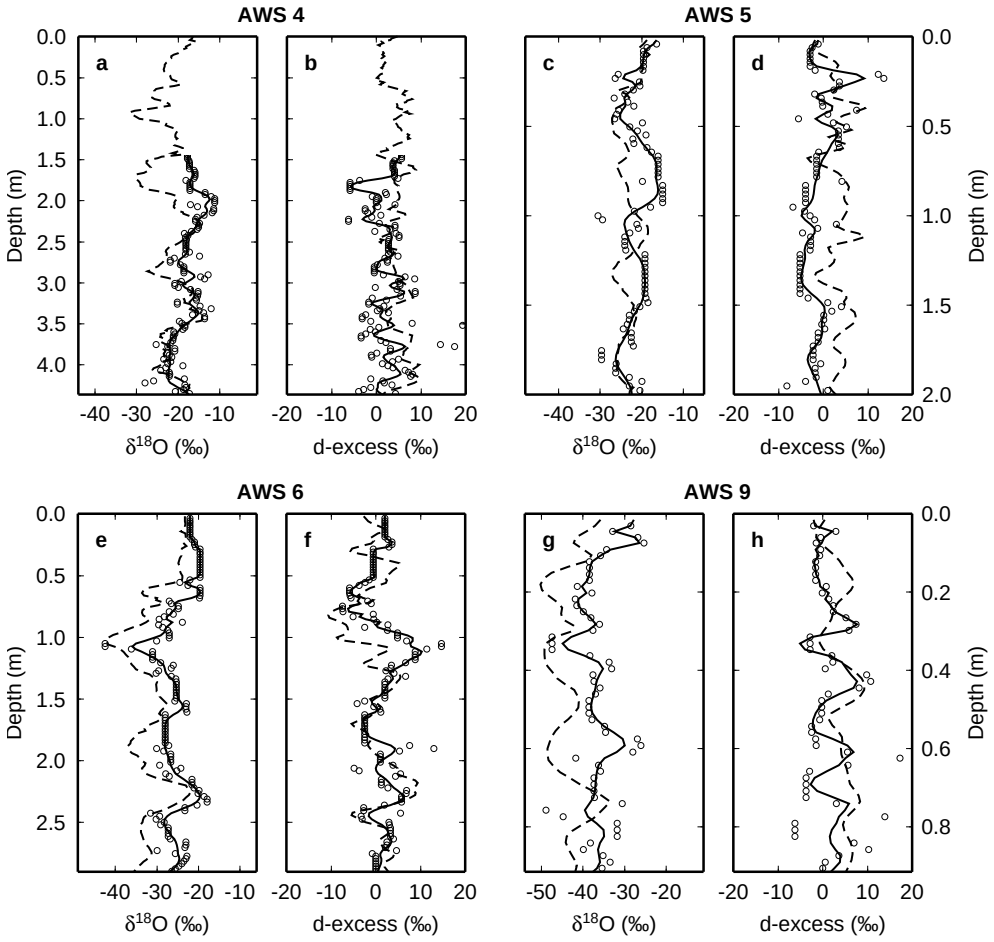

Figure 5.10: *Modelled and observed isotope records at the four sites. Dashed lines represent the observations, open circles are the modelled undiffused values and the solid lines show the modelled isotope records after diffusion.*

Table 5.4: *statistical properties of modelled and observed isotope records.*

	mean			σ		
	obs (‰)	ECHAM (‰)	MCIM (‰)	obs (‰)	ECHAM (‰)	MCIM (‰)
$\delta^{18}O$						
AWS 4	−21.4	−16.4	−17.7	4.2	0.8	2.7
AWS 5	−23.3	−19.3	−21.3	2.5	0.9	2.9
AWS 6	−30.4	−27.2	−25.1	5.1	2.3	3.7
AWS 9	−43.6	−38.9	−35.4	3.4	2.5	3.6
d-excess						
AWS 4	4.9	2.3	1.5	2.6	1.5	2.5
AWS 5	3.3	2.2	−1.2	3.0	0.9	2.7
AWS 6	0.0	3.8	1.3	4.6	2.3	3.4
AWS 9	4.0	11.5	2.8	3.4	1.9	3.4

remaining part of the reconstructed record resembles the observations reasonable, although the winter values are not as depleted as the observations. This results in a less negative mean value compared to the observations (Table 5.4).

Modeled and observed records are out of phase over a large part of the record of AWS 5 (between ∼0.5 m and ∼1.5 m; Figure 5.10c). The most probable reason for this is that for AWS 4 and 5, the snow pit samples were extracted somewhat away from the AWSs (Table 5.2). This implies that the SHR might have recorded a different accumulation history than was sampled in the snow pit, since spatial accumulation variability can be substantial at very short distances due to sastrugi formation (Isaksson *et al.*, 1996; Frezzotti *et al.*, 2002; King *et al.*, 2004). Nevertheless, both mean value and seasonal amplitude of the record at AWS 5 are well reconstructed.

The snow pit samples at AWS 6 and 9 were taken exactly under the SHR (Table 5.2), which should lead to a much better correspondence between modelled and observed isotope profiles. For AWS 6, this is indeed the case: the shape of the modelled $\delta^{18}O$ record at AWS 6 (Figure 5.10e) agrees well with the measured record. However, over the entire period, modelled $\delta^{18}O$ is shifted compared to the observed record, i.e. fractionation along the trajectories is underestimated by 5.3 ‰ on average (Table 5.4). This underestimation of the fractionation is larger in winter, since the modelled winter minima are less pronounced than the observed winter minima.

Agreement is not so good for AWS 9. The mean modelled $\delta^{18}O$ is not depleted enough (difference is 8.2 ‰ on average), and although the samples were taken directly under the SHR, the location of the seasonal maxima do not coincide with the observed record. However, the magnitude of the seasonal amplitude (expressed by σ in Table 5.4) does agree with the observations. Possible reasons for the underestimation of the isotopic distillation will be addressed in Section 5.7.

If we compare our model results to the records obtained using monthly mean values from the ECHAM4 climatology (Table 5.4) it appears that our model results match the mean observed records better for AWS 4 and 5, while the ECHAM-records

are closer to the observed mean values for AWS 6 and 9. However, looking at the seasonal amplitude, we see that our approach is much more successful in reproducing the magnitude of the seasonal cycle compared to ECHAM4.

A robust measure for the comparison between model results and observations is of course the correlation coefficient r. However, for a sound estimation of r, it is important that modelled and observed isotope values correspond to the same event. Due to uncertainties concerning the estimation of the depth of each event (see Section 5.2), and taken into account that the snow pits at AWS 4 and 5 are not sampled directly under the SHR, a comparison of the records only resulted in an acceptable correlation between modelled and observed isotope records for AWS 6 ($r = 0.86$). At AWS 9, a combination of the low accumulation (only 74 kg m^{-2} yr^{-1}) and the (unknown) influence of redistribution of snow by snow drift is probably the reason for the low resemblance between the modelled and observed record.

5.6.2 Deuterium excess

The precision of the mass spectrometer used to determine the isotopic composition of the samples is in the order of 0.1‰ in $\delta^{18}O$ and 2.0 ‰ in δD. Due to the relatively high uncertainty in the resulting d-excess parameter (2.2 ‰), the raw d-excess records were somewhat noisy. We applied a 3-point running average on d-excess data to smooth the records (dashed lines in Figure 5.10).

In general, the modelled d-excess variations are rather close to the observed records. Only at AWS 5 a bias is found from the observed record, but this can be explained by the difference in sampled snow and monitored accumulation by the SHR, as mentioned above. Even at AWS 9, where the modelled $\delta^{18}O$ record was not correctly reproduced, the d-excess values are close to the observed record. This means that δD deviates in a comparable way from the observations as $\delta^{18}O$. While for the mean $\delta^{18}O$ values our approach agreed best with AWS 4 and 5, the mean d-excess is better reproduced for AWS 6 and 9. As for the $\delta^{18}O$ records, the seasonal amplitude in d-excess is successfully reproduced (Table 5.4).

A comparison with the d-excess values resulting from the ECHAM4 climatology reveals a large deviation from the observed d-excess value at AWS 9. Clearly, ECHAM4 produces too high d-excess values at low temperatures, which is not in line with our observations. Generally, d-excess records are deconvoluted into a local forcing (site temperature) and a forcing due to changes in the moisture source area (sea surface temperature, RH, and wind speed) (e.g. B. Stenni *et al.*, 2001; Masson-Delmotte *et al.*, 2004). In Section 5.7 we will address to what extent d-excess is determined by the source area, compared to changes during transport.

5.7 Discussion

There is a tendency in our results obtained using the MCIM to underestimate isotopic distillation at lower site temperatures. This is most clearly shown at AWS 9 (Figure 5.10, where the difference between the mean modelled and observed $\delta^{18}O$ value at this

site is 8.2 ‰ (Table 5.4). To a lesser extent, the observed $\delta^{18}O$ record at AWS 6 also shows more depleted values than the modelled isotope record, especially in winter. There are several possible explanations for this underestimation.

Firstly, we imposed a $RH_{threshold}$ value of 80 % as an indicator for condensation to occur. From Figure 5.4 it appears that especially the trajectories to AWS 6 and 9 show lower RH values along a major part of the transport. To investigate the influence of $RH_{threshold}$, we repeated the MCIM runs for AWS 9 with $RH_{threshold}$=60 %. The resulting mean modelled $\delta^{18}O$ value decreased only 2.1 ‰ to −37.5 ‰. This is only a minor improvement, especially since it is not expected that condensation will occur in reality when RH is only 60 %. From Figure 5.4d it appears that RH generally is higher than 80 % during the last day of transport, when the major drop in T occurs. This explains the relatively small influence of the threshold value of RH on the total depletion of the moisture. These results point towards another reason for the large difference between model results and observations at AWS 9.

Secondly, the MCIM assumes that part of the water that forms during condensation is kept in the cloud. This slightly reduces the isotopic distillation compared to a distillation history when all newly formed condensed water of ice is immediately removed from the cloud. In principle, this latter model scenario is followed when the Rayleigh Model including the isotopic Kinetic effect (RMK Jouzel and Merlivat, 1984) is used. Applying the RMK, the final $\delta^{18}O_p$ value for AWS 9 decreases by only 1.9 ‰. Hence, choice of the distillation-type cannot explain the difference in observed and modelled $\delta^{18}O$ values either. A pure Rayleigh distillation (i.e. neglecting the kinetic fractionation effects during snow formation) would yield much lower $\delta^{18}O$ values, but would also produce unrealistically high d-excess values. Which prohibits the use of this distillation type.

Thirdly, the quality of the ERA-40 data-set as an input for the trajectory model can be a reason for the underestimation of the fractionation. ERA-40 is badly constrained by observations in a data-sparse region like the high Antarctic plateau. An underestimation of the T difference between $T_{RH=80\%}$ and $T_{c,final}$ in ERA-40 could well explain the lack of sufficient fractionation towards high elevation sites like AWS 9. However, it is not possible to test this hypothesis, since no independent information of $T_{RH=80\%}$ is available. We can only compare the final condensation temperature in the trajectories ($T_{c,final}$) with results from the regional climate model RACMO2/ANT (Reijmer *et al.*, 2005). This model is forced by ERA-40 at its boundaries, but it simulates the Antarctic climate at a much higher resolution (∼55 km). We defined condensation temperature in the regional climate model ($T_{c,RACMO}$) as the temperature with maximum CWC above the location of the AWSs (Chapter 2). Since RACMO2/ANT has proven to yield more realistic results for the Antarctic region than ERA-40 (Reijmer *et al.*, 2005), we expected to find differences between $T_{c,final}$ and $T_{c,RACMO}$, but no substantial differences were revealed. If $T_{c,RACMO}$ is a good representation of the real T_c over AWS 9, these findings reject our suggestion that the quality of ERA-40 is the reason for the underestimation of the distillation at low temperatures.

There are some other possible explanations for the underestimation of the depletion, which are more difficult to verify. For instance, isotopic equilibration of surface

snow with atmospheric vapour (Waddington *et al.*, 2002) has not been accounted for in the diffusion model. Furthermore, the contribution of clear-sky precipitation to the total accumulation is unknown, but it is believed to be an important contribution to the total accumulation in the Antarctic interior (Bromwich, 1988). This type of precipitation has not been accounted for in our approach, since no maximum in CWC (in ERA-40) is expected to occur during such precipitation, and hence no trajectories are calculated. On the other hand, as snowfall events at AWS 9 are coupled to more intense cyclones compared to more coastal sites, the isotopic composition of the moisture within these cyclones may deviate more from the mean state as within low-intense cyclones. Together with the fewer number of large events in the Antarctic interior, this may point to problems of the use of climatologically monthly mean ECHAM4 isotope fields as a starting value for the trajectory study for this location. Finally, the influence of diffusive mixing of moisture in the air masses with more depleted ambient moisture has not been taken into account, since the calculated trajectories just follow the air parcels and not necessarily the moisture within them. This can be an important additional source of more depleted moisture.

There is a similarity between modelled and observed d-excess values (Table 5.4 and Figure 5.10), and this offers the possibility to study the forcing behind the d-excess signal. We separated the modelled d-excess results for AWS 6, into two groups of high and low d-excess values, using the local mean value of 1.3 ‰ as separation. Weighted mean trajectories were calculated for both groups. It appears that all relevant parameters (e.g. T, source area) are practically equal for both groups. There was only a difference in height: the trajectories resulting in high d-excess values were advected towards their arrival location at a higher altitude compared to the low d-excess trajectories. This is illustrated in Figure 5.11b, in which the dotted line indicates the mean pressure of the trajectories with a high d-excess value, and the dashed line represents the mean pressure of the trajectories resulting in low d-excess values. The implication of this difference in height can be seen in Figure 5.11a, which shows a contour plot of $d\text{-excess}_{v,ECHAM}$ values, along a section following the meridian over AWS 6. A strong vertical gradient can be recognised. The effect of this vertical gradient on our modelling results is obvious: trajectories starting near the ocean surface start with vapour with a much lower initial d-excess value (from the ECHAM4 fields) than trajectories that originate from a height of several km. For the two groups considered, the difference in d-excess due to the initial value is 3.2 ‰, which is 60 % of the final difference in d-excess (5.3 ‰).

This remaining part of the final difference in d-excess between the two groups of trajectories (40 %) can be attributed to differences in kinetic fractionation along the transport path, especially during the last day of transport. The solid line in Figure 5.11c indicates Δd-excess, and it illustrates that for the two groups considered, the behaviour of d-excess is rather similar along the major part of the transport. The final drop of d-excess during the last day of transport (previously seen in Figure 5.6) is slightly stronger for the trajectories with low d-excess values (dashed line) , which explains the remaining 2.1 ‰ difference in the mean value of d-excess.

This analysis shows that the ECHAM4 fields influence the d-excess modelling results to a large extent. Due to a general lack of measurements of atmospheric d-excess

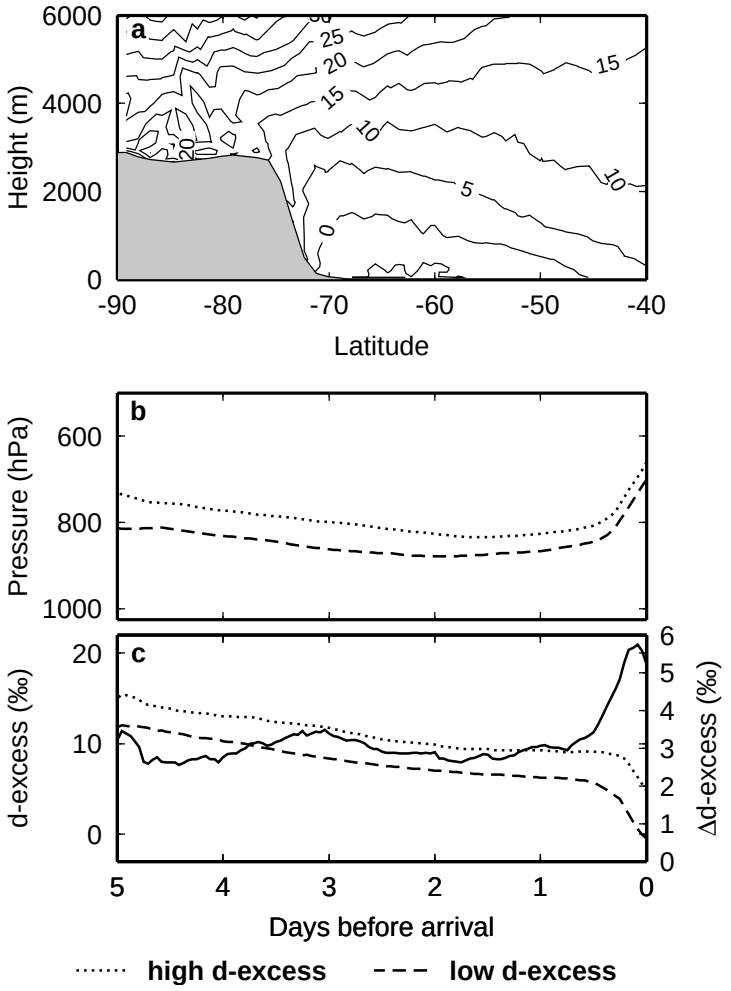

Figure 5.11: *Mean d-excess values of vapour for January in ECHAM4 (a); mean pressure levels (b); and modelled d-excess values of precipitation (c) along trajectories calculated for AWS 6. Dotted lines represent trajectories producing high d-excess values, dashed lines represents trajectories producing low d-excess values. Solid line indicates* Δ*d-excess.*

values, it remains unclear whether GCMs like ECHAM4 produce realistic patterns of atmospheric d-excess. A comparison of different GCM-generated d-excess fields (such as the Stable Water Isotope iNtercomparison Group: SWING, M. Werner, personal communication) seems therefore valuable. Nevertheless, the similarity between modelled and observed d-excess records from this study is an indication that the vertical gradient in the d-excess values of the vapour in ECHAM4 is in line with reality.

The d-excess parameter is often used to extract (paleo-) climatic information of moisture source areas, i.e. RH and sea surface temperature (SST) (e.g. Johnsen *et al.*, 1989; Vimeux *et al.*, 1999; Masson-Delmotte *et al.*, 2003). It is clear that the relative imprint of the initial d-excess value compared to the final d-excess value of the precipitation differs depending on the distillation history. Unfortunately our approach does not provide information about evaporation conditions of the moisture. Consequently, we cannot directly determine to which extent these conditions are preserved along the trajectories. However, our results suggest a prominent influence of the vertical gradient in d-excess over the moisture source region. Possibly, the higher d-excess values on a higher atmospheric level reflect a more distant (tropical?) moisture source, while the low near-surface d-excess values can be attributed to local evaporation. This would be in line with the current interpretation of d-excess in polar ice cores (e.g. Vimeux *et al.*, 1999). However, it is questionable to what extent RH or SST can leave an imprint in the vertical gradient in d-excess over the oceanic source area. Therefore, more insights are needed in the dynamics behind the vertical distribution of the initial d-excess values of the vapour over the ocean.

5.8 Conclusions

Simple isotope distillation models have since long been proved useful in terms of explaining observed spatial gradients (e.g. Jouzel and Merlivat, 1984) and seasonal cycles (e.g. Ciais *et al.*, 1995). In this chapter we went further in applying such a model on individual events.

We used a combination of back-trajectory calculations and isotopic modelling to simulate the isotopic composition of four snow pits in Dronning Maud Land, Antarctica. The trajectories indicate a moisture source area in the southern Atlantic Ocean. The major part of the isotopic fractionation occurs during the last day of transport, when the air masses experience cooling due to the orographic lift over the Antarctic continent. The strength of this final T drop is of primary importance to both the $\delta^{18}O$ and the d-excess value of the final precipitation. However, the seasonal amplitude can only partly be explained by the magnitude of this T drop. Seasonal variations of the isotopic composition of the initial moisture are also important for the final isotopic composition of the snow.

After deposition, diffusion of the δ signal is simulated using a firn diffusion model. These simulations show that the isotope records initially contain sub-seasonal variability, but these variations vanish after some years of firn diffusion.

The resemblance between modelled and observed isotope variations is fairly good, from which we can conclude that the isotopic fractionation is a realistically simulated.

However, for the high Antarctic plateau the isotopic distillation is underestimated. The reasons for this underestimation remain unclear.

The simulation of the behaviour of d-excess indicates that our approach of trajectory calculations in combination with a simple isotope model is able to reproduce mean values and seasonal amplitudes of observed d-excess records in coastal and continental areas. However, an analysis on the controls of the simulated d-excess values shows that the initial height of trajectories plays a crucial role in the final simulated d-excess value. Since the trajectories do not provide information about the origin of this initial moisture, we cannot draw conclusions about the interpretation of the d-excess signal. The next chapter will further address the spatial and temporal patterns of both $\delta^{18}O$ and d-excess in precipitation over the entire Antarctic continent.

Chapter 6

A 22 year simulation of isotopic composition of snowfall over the Antarctic continent

Abstract

The isotopic composition of present-day Antarctic snow is assessed for the period September 1980 to August 2002, using a Rayleigh-type isotope distillation model in combination with backward trajectory calculations with ERA-40 data as meteorological input. Observed spatial isotopic gradients are correctly reproduced, especially in West Antarctica and in the coastal areas. However, isotopic depletion of snow on the East Antarctic plateau is underestimated, a problem that also affects general circulation models equipped with isotope tracers. The spatial isotope-temperature relation varies strongly, which indicates that this widely used relation is not applicable to all sites and periods. Spatial differences in the seasonal amplitude are identified, with maximum values in the Antarctic interior and hardly any seasonal isotope signature in Marie Byrd Land, West Antarctica. The modelled signature of deuterium excess remains largely preserved during the last phase of transport, though the simulated relation of deuterium excess with $\delta^{18}O$ suggests that parameterisations of kinetic isotopic fractionation can be improved. These results can be used to identify general atmospheric patterns in modelled isotopic composition.

Helsen, M.M., R.S.W. van de Wal, M.R. van den Broeke. The isotopic composition of present-day Antarctic snow in a Lagrangian atmospheric simulation. *Submitted to J. Climate.*

6.1 Introduction

Polar ice sheets are valuable archives of paleoclimatic information (North Greenland Ice Core Project members, 2004; EPICA community members, 2004) The main proxy for past temperature (T) is the isotopic concentration of HDO and/or $H_2{}^{18}O$ in the ice (usually expressed as δD and $\delta^{18}O$ in ‰ with respect to the deviation from the Vienna Standard Mean Ocean Water, VSMOW). A significant spatial correlation between the isotopic composition of precipitation (hereafter called δ) and mean annual T over Greenland (Johnsen *et al.*, 1989) and Antarctica (Lorius and Merlivat, 1977; Dahe *et al.*, 1994), forms the empirical basis of the use of water isotopes as a T proxy.

The Antarctic ice sheet is of particular interest, since it contains the longest ice core records on earth (EPICA community members, 2004). Moreover, due to its rather stable polar climate, it is argued that the spatial δ-T relation in central Antarctica can be used as a paleothermometer on a glacial-interglacial time scale (Jouzel *et al.*, 2003). However, on shorter time scales the stability of the Antarctic δ-T relation is questionable, due to a lack of independent T observations or proxies. Furthermore, the spatial δ-T relation can vary from one place to another (e.g. Lorius and Merlivat, 1977; Robin, 1983; Dahe *et al.*, 1994).

The second-order parameter deuterium excess ($d = \delta D - 8\delta^{18}O$, hereafter called d-excess) is determined by non-equilibrium processes. Both in the oceanic source area (Merlivat and Jouzel, 1979) and at low temperatures above the polar ice sheets (Jouzel and Merlivat, 1984) this so-called kinetic fractionation can occur. The d-excess parameter is commonly used as an indicator for (changes in) moisture source regions (e.g. B. Stenni *et al.*, 2001; Masson-Delmotte *et al.*, 2004).

To provide the climatic interpretation of stable water isotopes with a better physical basis, the isotopic composition of atmospheric water has been simulated using simple Rayleigh-type distillation models (e.g. Dansgaard, 1964; Jouzel and Merlivat, 1984; Ciais and Jouzel, 1994), and General Circulation Models (GCMs) equipped with isotope tracers (e.g. Joussaume *et al.*, 1984; Hoffmann *et al.*, 1998; Noone and Simmonds, 2002b). The GCM approach has the advantage of taking into account all relevant processes. However, due to its complexity, it is difficult to isolate different processes. Furthermore, results from GCMs in climate mode cannot directly be compared to specific snowfall events.

Rayleigh-type distillation models are simple to interpret, but badly constrained by meteorological data. To solve this, Helsen *et al.* (2005a) used meteorological data obtained from back-trajectory calculations as an input for a Rayleigh-type distillation model, which enables comparison with individual snowfall events (Chapter 5). There, the mixed cloud isotopic model (MCIM, Ciais and Jouzel, 1994) was used and validated with Antarctic snow pit records.

Here we extend the work of Helsen *et al.* (2005a), to snowfall events over a 22 yr period over the entire Antarctic continent. The modelling approach is explained in section 6.2. The European Centre for Medium-range Weather Forecasts (ECMWF) re-analysis (ERA-40) data set is used as the major meteorological input for the isotope model. Therefore, we first describe some relevant parameters from ERA-40 in the Antarctic region (section 6.3.1), after which results of the 22 yr model run are

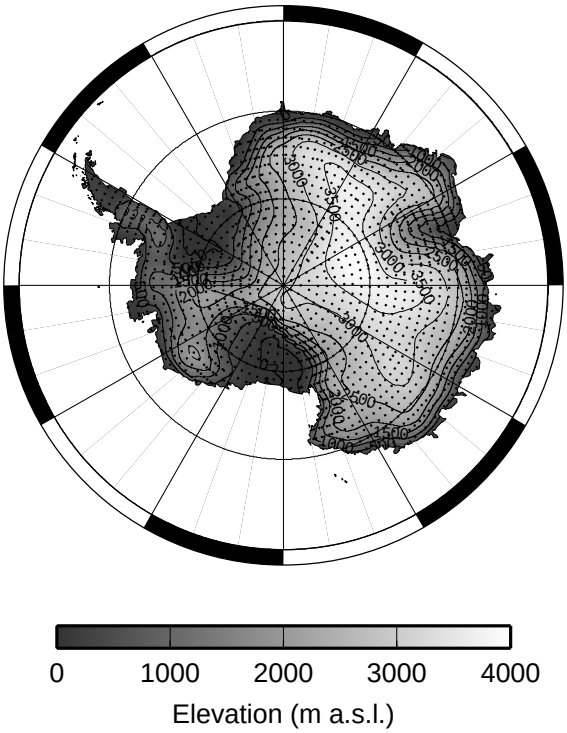

Figure 6.1: *Elevation of the Antarctic continent from ERA-40 (grayscale and contours) and the grid used for this simulation (dots).*

described and discussed for $\delta^{18}O$ (section 6.3.2), and for d-excess (section 6.3.4). In section 6.3.3 spatial δ-T relations are described and the modelled seasonal cycle is discussed in section 6.3.5, followed by a discussion in section 6.4 and conclusions in section 6.5.

6.2 Methods

6.2.1 Trajectory starting points

The ERA-40 data set constitutes the basic meteorological input for this work. The spectral resolution is T159 (corresponding to ∼125 km horizontal spatial resolution) with 60 vertical levels. Here we used gridded data from this archive on a constant 1° resolution in the horizontal plane. This is the required input for the trajectory model, which is described in section 6.2.2.

Based on the resolution of the input data, a network of grid points over Antarctica is defined (Figure 6.1). In latitudinal direction the resolution is 1°, in longitudinal direction the resolution is chosen in such a way that the grid is approximately equidis-

tant (∼111 km). More grid points are added when the coastline is crossed, to ensure a fully covered continent. Furthermore, additional points are added when elevation increases with more than 200 m over 1° in longitudinal direction (e.g. in the Lambert Glacier - Amery Ice Shelf region).

The grayscale in Figure 6.1 indicates Antarctic orography in ERA-40. Obviously, deviations from the real orography will result in errors in the simulated climate. In the Antarctic Peninsula, for instance, model resolution is insufficient to resolve the steep orography (Van Lipzig *et al.*, 2004), and modelling results should be interpreted with care.

6.2.2 Isotopic modelling along trajectories

Daily snowfall totals (0-24 h forecast fields) are retrieved from ERA-40 for the grid described above. Although the data cover the period 1958 to 2002, the quality is questionable before 1980. For example, a strong increase of Antarctic precipitation around 1980 is present in ERA-40 (Bromwich *et al.*, 2004; Van de Berg *et al.*, 2005), probably due to the incorporation of satellite measurements into the re-analysis. Therefore, results presented here cover the 22 yr period of September 1980 to August 2002.

In order to simulate the isotopic composition of the accumulated snow, we use back-trajectory calculations as input for a simple Rayleigh-type isotope distillation model. Chapter 4 and 5 give an extensive description of this approach, which is only briefly addressed here.

For each day of snowfall occurring at a grid point, we calculated a five-days backward trajectory. We used the trajectory model developed by the Royal Netherlands Meteorological Institute (Scheele *et al.*, 1996), which computes the three-dimensional displacement of an air parcel. This model has previously been used to identify Antarctic moisture source areas (Reijmer *et al.*, 2002).

The uncertainty in the calculated trajectories increases backward in time, resulting in a typical uncertainty of ∼1000 km after five days (Stohl *et al.*, 1995). Moreover, the advective pathway of an air parcel is not necessarily equal to the pathway of the moisture. Nevertheless, we consider it the best possible estimate of moisture transport history for individual snowfall events.

Trajectories should ideally be calculated from arrival locations at the exact time and height of snow formation. For the timing of the snowfall events, we used 0-24 h snowfall amounts. If snowfall occurred, we defined the moment of snow formation at 12h GMT. To determine the vertical position of the snow formation, we considered vertical profiles of cloud water content (CWC). The height of maximum CWC was used as the starting level of the back-trajectory calculation.

For the simulation of the isotope distillation process we used a modified version of the Mixed Cloud Isotopic Model (MCIM; originally described by Ciais and Jouzel, 1994). This model describes the isotopic changes in a Lagrangian air parcel, accounting for kinetic isotopic fractionation effects. Furthermore, it allows vapour, liquid and ice to coexist and interact, of particular importance for the simulation of d-excess. Three modifications that Helsen *et al.* (2005a) applied on the MCIM were necessary to enable the coupling of this model to the trajectory data:

Firstly, the initial isotopic composition of the moisture has to be defined. In the classical approach of a Lagrangian isotope distillation model, evaporation from the ocean surface and associated isotopic fractionation is simulated. This approach cannot be used in combination with back-trajectories, since the oceanic origin of the initial moisture in the air parcels is unknown. The fractionation effects of local evaporation do not yield realistic isotopic composition at the air parcels' initial location (Helsen *et al.*, 2004). To by-pass this problem, we use monthly mean three dimensional isotope fields ($\delta^{18}O$ and δD) from a 20 yr climate run of the Hamburg atmospheric climate model ECHAM4 (Roeckner *et al.*, 1996; Hoffmann *et al.*, 1998; Werner and Heimann, 2002), to define the initial isotopic composition. The spectral resolution of ECHAM4 is T106 (1.1°x1.1°) with 19 vertical levels. The use of climatological mean isotope values as initial value for the moisture will introduce additional uncertainty in our modelling results, since isotope values in single storm events show large variability compared to the mean state (Hoffmann *et al.*, 1998), especially in areas with infrequent storm activity. Unfortunately, the use of the ECHAM4 isotope climatology, prohibits a direct interpretation of the influence of source region effects.

Secondly, there is a discrepancy between realistic moisture transport as observed by backward trajectories and the isolated moisture transport as assumed by classical Lagrangian isotope models. In reality, air parcels often show large increases of specific humidity (q) on their way to the polar region. These increases of q are associated with isotopic recharge, i.e. addition of less-depleted water vapour to the air parcel. The MCIM has been adapted at this point, by assuming that any moisture increase exceeding the total available water in the air parcel is provided by ambient water vapour with an isotopic signature determined by the ECHAM4 isotope fields. Using this approach, a strong increase of q will result in near-equilibration with the isotopic value of ECHAM4 at that particular location.

Thirdly, classical Rayleigh-type isotope distillation models assume continuous saturation and rain-out of moisture as a function of T and p, which can be in conflict with observed moisture transport (Chapter 3). Since condensation (and associated isotopic distillation) is not expected to occur during under-saturated conditions, we added a threshold value of relative humidity ($RH_{treshold}$=80 %), in analogy with GCMs (Tiedtke, 1993). Only if $RH > 80$ %, changes in T or p are allowed to induce isotopic distillation. The effect of this threshold is that the modelled isotopic distillation depends entirely on the difference between $T_{RH=80\%}$ and T_{final}, while in the classical approach of Rayleigh-type models, T_{source} was the starting point for distillation, which yielded a slightly stronger distillation.

6.3 Results

6.3.1 Antarctic climate in ERA-40

Mean annual snowfall in Antarctica from ERA-40 are shown in Figure 6.2. ERA-40 reasonably well captures the dry Antarctic interior and the wetter coastal slopes, in particular the high accumulation in the western Antarctic Peninsula and coastal Marie Byrd Land.

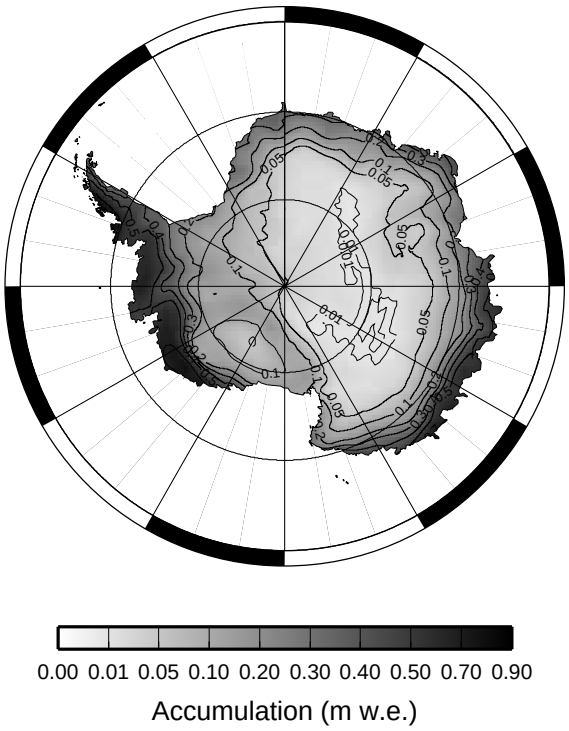

Figure 6.2: *Mean annual snowfall from ERA-40 for the period 1980-2002.*

ERA-40 is too dry on the East Antarctic plateau in comparison with compilations based on observations (Vaughan *et al.*, 1999) and calibrated regional climate models (Van de Berg *et al.*, 2005). Figure 6.2 shows that for the driest locations in this area an annual snowfall of less than 0.01 m w.e. is simulated. Such low values of precipitation are not observed, and are possibly associated with spin-up problems (Genthon, 2002).

Seasonality of precipitation is of major importance for the interpretation of isotope records from ice cores (e.g. Werner *et al.*, 2000). The seasonality in ERA-40 snowfall is shown in Figure 6.3. In the Antarctic interior, seasonal accumulation strongly peaks during the summer season (DJF), while the coastal regions and large ice shelves receive a relatively large amount of snowfall during winter. This is not in agreement with results from regional climate models, which indicate that autumn is the dominant season for inland Antarctic precipitation (Van de Berg *et al.*, 2005; Van Lipzig *et al.*, 2002b). Presumably, the ECMWF model is not able to produce realistic snowfall amounts of inland precipitation during the long Antarctic winter, which causes a considerable seasonality in precipitation. This may be the reason for the underestimation of snowfall amounts in the Antarctic interior. The high contribution of summertime precipitation to the annual mean accumulation has implications for

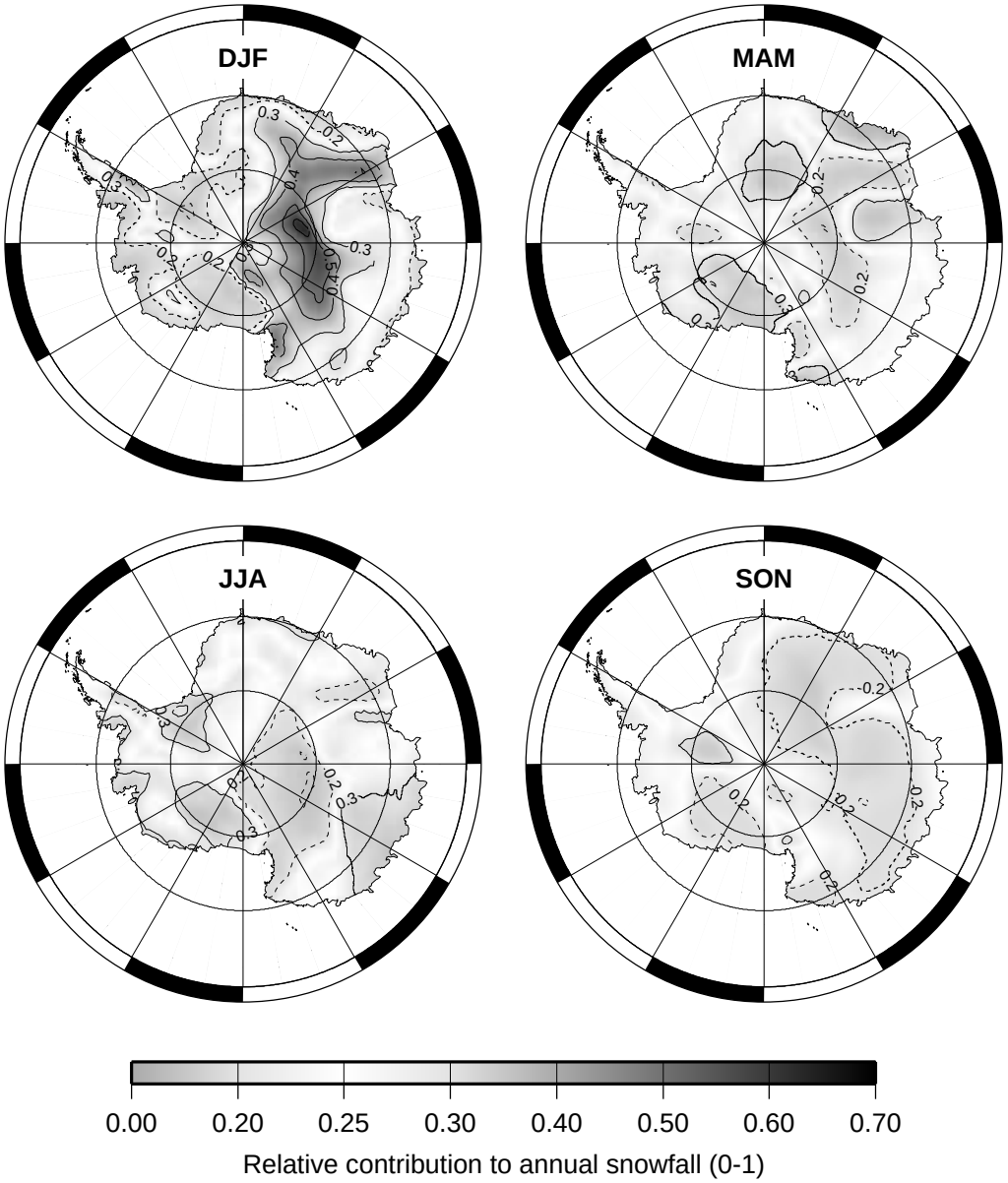

Figure 6.3: *Contribution of seasonal snowfall to annual mean from ERA-40 for the period 1980-2002. When a season contribution equals 0.25, no seasonal bias is introduced. A positive bias (>0.25) is indicated with solid contours, a negative bias (<0.25) has dashed contours.*

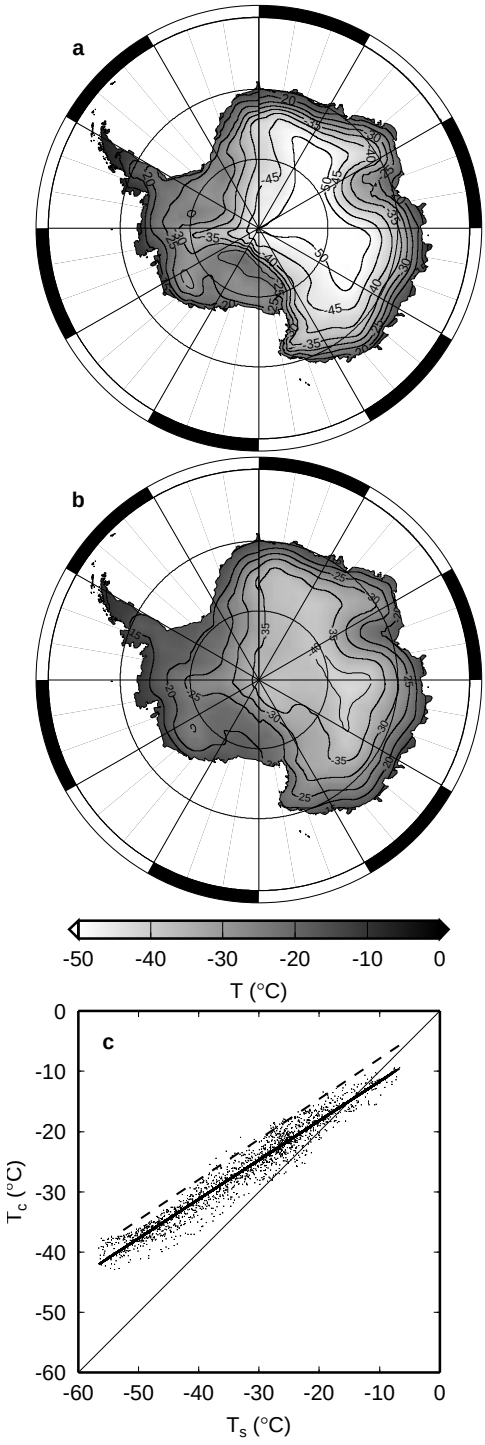

Figure 6.4: *Mean annual T_s (a) and weighted mean values of T_c (b) during snowfall from ERA-40 for the period 1980-2002. Scatter-plot of T_c and T_s (c). The thick solid line is the best fit and the dashed line is the relation between T_s and T_i from Jouzel and Merlivat (1984).*

the mean modelled isotopic composition of inland snow, as outlined below.

According to Genthon (2002), there is warm bias of ∼5°C in ERA-40 temperature averaged over Antarctica, probably related to errors in the surface energy budget. However, he compared 2 m air temperature (T_{2m}) with 10 m firn temperature (T_{deep}), which represents annual mean surface temperature (T_s). The warm bias is less when T_s is used, as will be shown in section 6.3.2. The distribution of T_s in ERA-40 is shown in Figure 6.4a. To calibrate the isotope thermometer, isotopic composition of snow is often correlated to T_{deep} (i.e. T_s). However, values of T_s in Antarctica are strongly influenced by the strength of the temperature inversion in the atmospheric boundary layer (ABL). For the isotopic composition of snow, T_s is thought to be not important. A more relevant parameter is the temperature at which water vapour is condensed to snow (T_c). The condensation process can occur at any height where the water vapour pressure exceeds the saturation vapour pressure. Here we defined T_c as the temperature at the level of maximum CWC (section 6.2.2). Mean annual values of T_c, weighted with accumulation amount and occurrence, are plotted in Figure 6.4b.

The scatter-plot of T_s and T_c in Figure 6.4c points out that T_c is generally higher than T_s, except for the coastal regions. An increase of the inversion strength with decreasing T can be identified the Antarctic interior. Jouzel and Merlivat (1984) compiled a set of observed vertical temperature profiles at several locations in Antarctica, and assumed the inversion temperature (T_i) to be representative for T_c, to infer a relation between T_s and T_c. This relation is plotted as the dashed line in Figure 6.4c. The ERA-40 data indicate that T_c is systematically lower than T_i. T_i and T_c slightly converge towards the Antarctic interior, indicating that the assumption of T_i to represent T_c holds better for the Antarctic interior. In coastal regions, larger errors are introduced when using T_i as an indicator for T_c, as earlier noted by Ekaykin (2003).

To assess the quality of modelled T_c, we compared vertical temperature profiles from ERA-40 with modelled temperature profiles from a regional climate model (Reijmer *et al.*, 2005). This comparison points out that the inversion strength in ERA-40 is somewhat weaker in comparison with the regional climate model; above the ABL, differences hardly exceed 1°C. To conclude, the spatial pattern of T_c in ERA-40 seems to be modelled realistically.

6.3.2 Spatial distribution of $\delta^{18}O$

Figure 6.5 presents mean $\delta^{18}O$ values of Antarctic precipitation as simulated with our Lagrangian isotope model. The main features include greatest depleted values over the Antarctic plateau where the lowest values of T_c occur and strongest isotopic gradients can be found over the steep slopes of East Antarctica, along with the strongest temperature gradients.

Comparing the simulated isotope distribution to compilations such as Zwally *et al.* (1998), shows that the depletion is underestimated by ∼10 ‰ at the highest elevations. Figure 6.6 compares modelled $\delta^{18}O$ with observations along four traverses: (1) the 1990 International Trans-Antarctic Expedition (ITAE), crossing the continent from the Antarctic Peninsula, via South Pole and Vostok, to Mirny in coastal East Antarctica (Dahe *et al.*, 1994), (2) the 1995-1996 East Antarctic traverse from

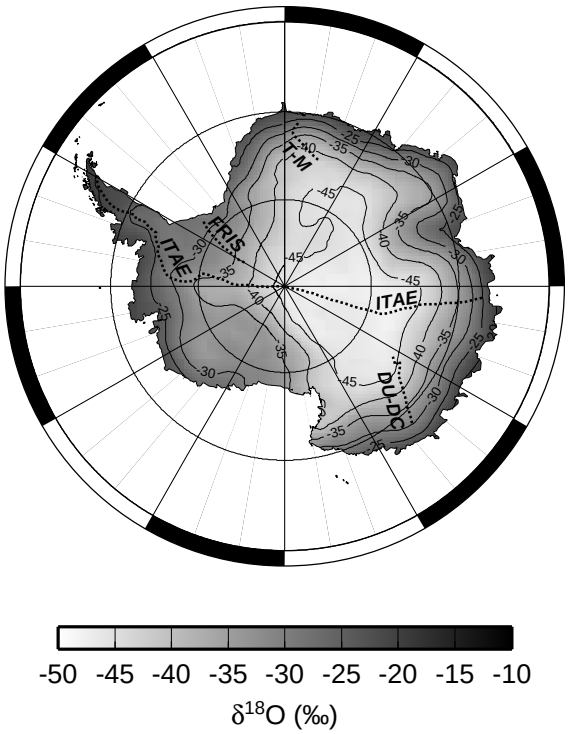

Figure 6.5: *Modelled mean annual $\delta^{18}O$ of snowfall. The dotted lines indicate traverses along comparison with observations are shown in Figure 6.6.*

Dumont d'Urville to Dome C (DU-DC, Delmotte, 1997), (3) the 1995-1996 EPICA pre-site survey in Dronning Maud Land from Troll to Site M (T-M, Van den Broeke *et al.*, 1999; Isaksson *et al.*, 1999) and (4) the 1994-1995 Filchner-V-Campaign crossing the Filchner Ronne Ice Shelf (FRIS) and Foundation Ice Stream (Graf *et al.*, 1994). The locations of the traverses are indicated in Figure 6.5. Observations of mean $\delta^{18}O$ values are generally an average value of multiple samples from the first meter of snow. This implies that these values represent different characteristic time periods, depending on the accumulation of the area. In general, modelled $\delta^{18}O$ closely resembles the observations in areas with relatively high accumulation. Over the dry Antarctic plateau however, isotopic depletion is underestimated. $\delta^{18}O$ is well simulated in the Antarctic Peninsula and over the FRIS, whereas ECHAM4 strongly overestimates $\delta^{18}O$ in these areas.

Figure 6.6b compares observed and modelled T_s for the same traverses. ERA-40 (solid line) slightly overestimates T_s, but differences are smaller than suggested by Genthon (2002) who used T_{2m}, which may differ from T_s by several degrees on the interior plateau. In comparison with ECHAM4, ERA-40 performs better in West Antarctica. Over the ice shelves, there is a major difference between ERA-40 and

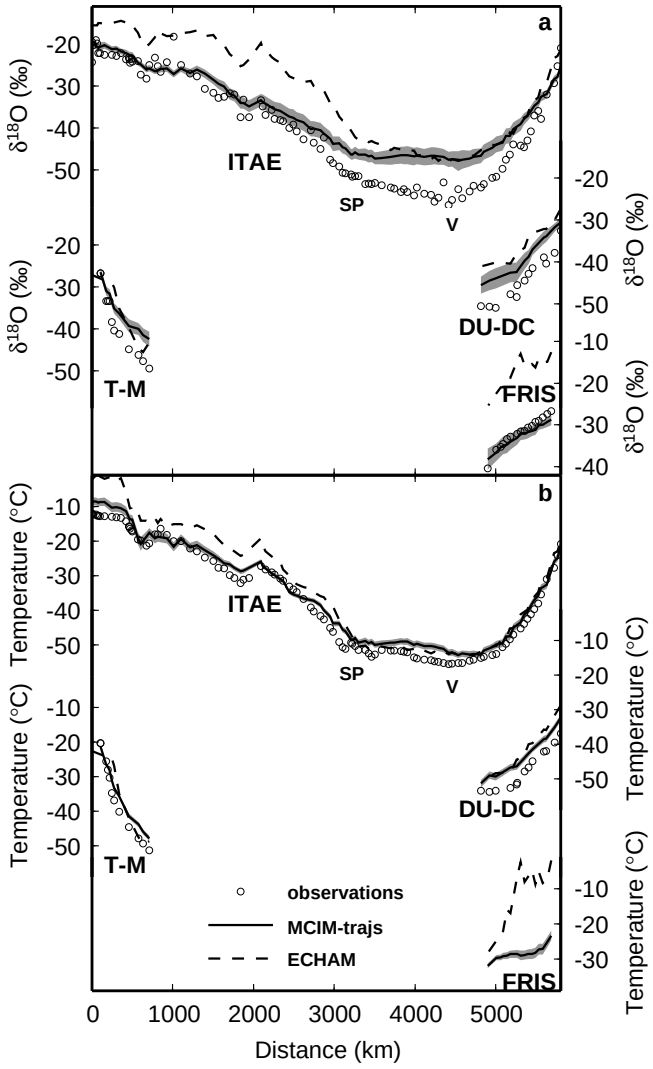

Figure 6.6: *Comparison of modelled (solid lines) and observed (circles) mean annual $\delta^{18}O$ of precipitation (a) and (near-)surface temperature (b) versus distance along the traverses indicated in Figure 6.5. For comparison, mean values from the climate run of ECHAM4 are shown as well (dashed lines). The standard deviation on annual mean values is plotted for our model results (gray). Observed temperatures are mostly 10m firn temperatures, whereas modelled temperatures are T_s from ERA-40. Observations are obtained from Dahe* et al. *(1994) (ITAE), Delmotte (1997) (DU-DC, Isaksson* et al. *(1999) (T-M) and Graf* et al. *(1999) (FRIS). SP and V indicate the locations of South Pole and Vostok, respectively.*

ECHAM4. Although no observed temperatures were available for the traverse over FRIS, nearby measurements of 10 m firn temperature (Graf *et al.*, 1994) indicate that ERA-40 correctly simulates the distribution of T_s, and ECHAM4 overestimates T_s by >15°C. Comparable temperature deviations of ECHAM4 are detected over the Ross Ice Shelf. These large errors in T_s occur because ECHAM erroneously treats ice shelves as sea ice (Van den Broeke, 1997).

The major area where simulated $\delta^{18}O$ deviates from observations is the high Antarctic plateau. A possible explanation for the difference is the artificial seasonality in accumulation in ERA-40. However, this accounts for only part of the difference. If we assume an equal contribution of all seasonal accumulation, the mean modelled $\delta^{18}O$ value for Vostok precipitation would drop from −47.5 ‰ to −48.8 ‰, which is still well above the observed −57.2 ‰. In the area with a maximum summer bias (near Dome A, Figure 6.3), the modelled $\delta^{18}O$ value would decrease from −45.7 ‰ to −48.3 ‰, which is again still much higher than the observed −56 ‰ (Zwally *et al.*, 1998).

Since the temperature distribution of ERA-40 does not deviate strongly from the observed temperatures (Section 6.3.1), there is no reason to assume that the underestimation of the isotopic depletion is caused by a large temperature bias in the trajectory input data for the distillation model. Clearly, there must be another reason for the difference between model results and observations. This point will be addressed in section 6.4.

6.3.3 Spatial δ-T relations

The local spatial relationship between $\delta^{18}O$ and T_s is calculated using all grid points within a 250 km radius (Figure 6.7a). Values are only plotted when the correlation coefficient (r) is larger than 0.7. Figure 6.7a shows that a large spatial variability exists in the spatial slope. Note that the method used here differs from the usual approach that is often based on a single traverse, following a route upward onto the local ice sheet slope. The low $\Delta\delta^{18}O/\Delta T_s$ values (and low r values) in central Antarctica are caused by small changes in isotopic composition, where T_s does show a significant gradient (Figure 6.4 and 6.5). Maximum values of $\Delta\delta^{18}O/\Delta T$ are found over inland Victoria Land and over Vostok, where isotope gradients are high and T_s gradients low. The calculated $\delta^{18}O$-T relation depends on the length of the search radius. Using a search radius of 500 km reduces the variability, but still shows the same general pattern.

The large-scale $\Delta\delta^{18}O/\Delta T$ values can be compared with observations that have been obtained from traverses (Table 6.1). For an objective comparison, values for the modelled spatial relationships in Table 6.1 are calculated using only data along the traverses, which yields somewhat higher values than obtained using a radial symmetric area. Values of simulated $\delta^{18}O - T_s$ gradients are systematically lower than observed, which can be explained by the model's problems in simulating the strongly depleted snow on the Antarctic plateau.

Physically, it is more consistent to compare the spatial isotopic distribution with T_c. Spatial $\Delta\delta^{18}O/\Delta T_c$ values are plotted in Figure 6.7b. The pattern in Figure

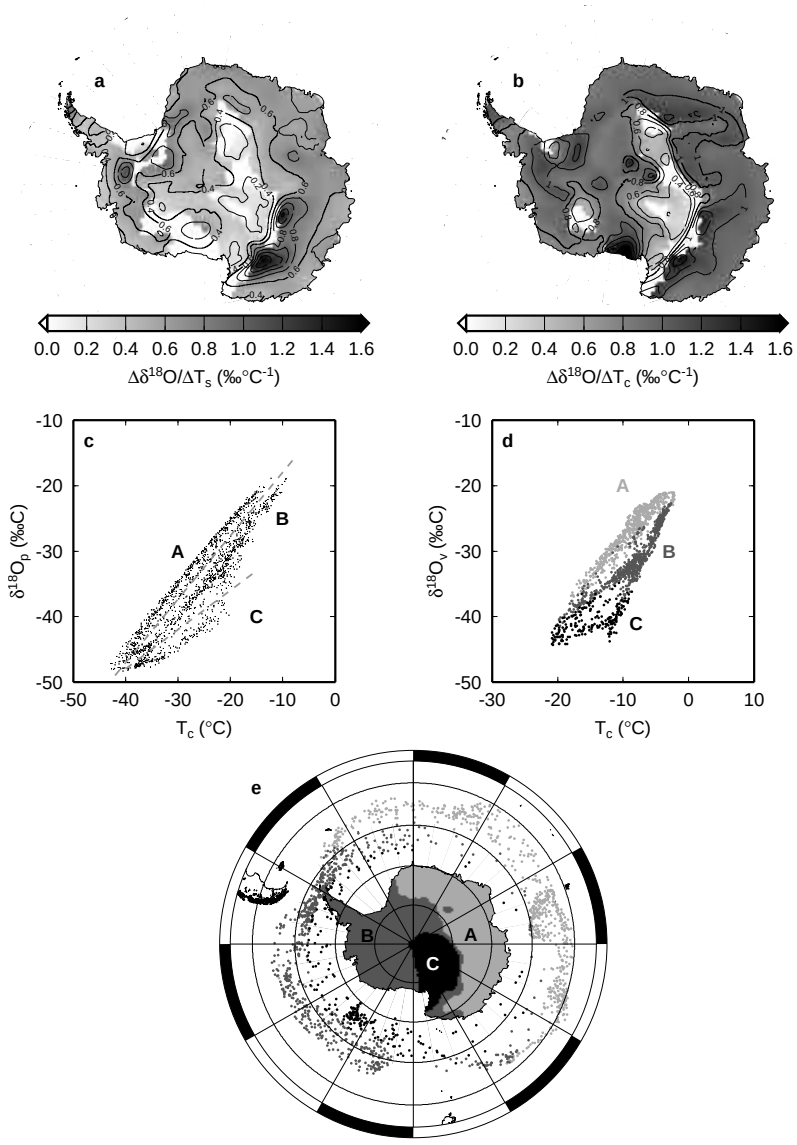

Figure 6.7: *Regional spatial relationships of $\delta^{18}O$ in snow with T_s (a) and with T_c (b). Values are plotted in gray scale when $r > 0.7$. Scatter plot of mean $\delta^{18}O$ as a function of T_c for the entire model domain (c). The dashed lines divide different "distillation lines" into three sectors(A, B and C) which represent different regions, as visible in (e). (d) shows mean $\delta^{18}O$ values of vapour that enters the air parcel as a function of cloud temperature, and reveals the same pattern as (c). The three sectors identified in (c) appear clearly as different Antarctic regions in (e). Dots in (e) represent the mean locations of moisture uptake for each grid point of the model domain, and the colour of the dot refers to the corresponding region (A: light gray, B: dark gray, C: black).*

Table 6.1: *Comparison of modelled and observed spatial isotope - temperature relationships; r values are indicated in parentheses.*

	$\Delta\delta^{18}O/\Delta T_s$ (‰ °C^{-1})		$\Delta\delta^{18}O/\Delta T_c$ (‰ °C^{-1})
	obs	MCIM$_{trajs}$	MCIM$_{trajs}$
East Antarctica		0.63 (0.90)	0.99 (0.90)
South Pole - Mirny[1]	1.03 (0.98)	0.77 (0.98)	1.25 (0.94)
Troll - Site M[2]	0.73 (0.99)	0.59 (0.99)	0.92 (0.9998)
Dumont d'Urville - Dome C[3]	0.96 (0.98)	0.87 (0.99)	1.00 (0.999)
West Antarctica		0.67 (0.93)	0.98 (0.96)
Antarctic Peninsula - South Pole[1]	0.81 (0.98)	0.69 (0.99)	1.06 (0.997)

Observations are taken from [1]Dahe *et al.* (1994), [2]Isaksson *et al.* (1999) and [3]Delmotte (1997).

6.7b is comparable with the spatial relationship with T_s in Figure 6.7a, but overall $\Delta\delta^{18}O/\Delta T_c$ attains higher values. This is caused by smaller spatial gradients in T_c (Figure 6.4). A region with low values of r is found from central East Antarctica toward the coast in Victoria Land.

A scatter plot for all grid points is shown in Figure 6.7c. This plot can be divided into three sectors (A, B and C), indicated by gray dashed lines. Interestingly, these points represent well-defined Antarctic regions (Figure 6.7e). These different "distillation paths" are the result of differences in the isotopic composition of the vapour that enters the trajectories during transport to the arrival site. This becomes evident in Figure 6.7d, showing the mean $\delta^{18}O$ values of the moisture that enters the air parcel along transport, as a function of the temperature during this moisture uptake. At a comparable temperature, air parcels that are heading to sector C take up stronger depleted moisture compared to trajectories heading to sector A. These differences in isotopic composition of the addition vapour are closely associated with the geographical location of the moisture uptake. This can be seen in Figure 6.7e, where each dot represents the average location of moisture uptake for each grid point of our model domain. Evidently, moisture uptake occurs further south for trajectories to region C compared to moisture uptake along trajectories to region B, and moisture uptake for trajectories to region A occurs even more north.

Nevertheless, this mean location of the moisture uptake cannot account for the total difference in isotopic composition as identified in Figure 6.7d. The variation in the latitudinal occurrence of the moisture uptake is important as well, especially since there are large gradients in the isotopic composition over the edge of the Antarctic continent. Hence, when a large part of the moisture uptake occurs at high latitudes, the isotopic signature of moisture in air parcels will be strongly influenced by this depleted moisture. An indication of the relative contribution of this local high-latitude moisture to total moisture along the trajectories is given in Table 6.2, which point out that model results for region C are largely influenced by this local depleted moisture effect. This region can be characterised as a very dry area (Figure 6.2), mainly as a result of a shielding effect of the geometry of the continent, in combination with the

Table 6.2: *Relative contribution of Antarctic (high-latitude) and oceanic moisture uptake along trajectories and its mean isotopic composition. Antarctic moisture uptake is defined as increases in q south of 70° S, oceanic moisture uptake is defined as increases in q north of 70° S.*

	Δq(%)		$\delta^{18}O_v$ (‰)		d-excess$_v$ (‰)	
	Antarctic	oceanic	Antarctic	oceanic	Antarctic	oceanic
region A	2	98	-43.5	-23.0	27.0	9.3
region B	12	88	-46.9	-24.1	31.3	9.6
region C	41	59	-52.9	-26.3	37.4	10.7

steep continent, which prevents depressions to reach this area. Trajectories that bring snowfall to this area generally flow over West Antarctica and take up some moisture over the Ross Ice Shelf, instead of over the ocean. Hence, snowfall that occurs in this area has relatively higher contribution of local (strongly depleted) vapour to the simulated precipitation.

Since ECHAM4 isotope fields are used for the isotopic composition of the added moisture, associated errors can in particular be expected for low accumulation areas with infrequent cyclonic activity, and results for region C will be especially sensitive. However, region C covers the area with low r values in Figure 6.7a and b, and also covers an area in which the simulated and observed $\delta^{18}O$ values deviate strongly (Figure 6.6a). If simulated $\delta^{18}O$ would be more in line with the observations, it would deviate even more from the distillation lines A and B in Figure 6.7c.

6.3.4 Spatial pattern of d-excess

Figure 6.8 shows modelled d-excess of the snowfall. A pattern of increasing d-excess values towards the Antarctic interior is seen, which is in qualitative agreement with observed d-excess patterns over Antarctica (Petit *et al.*, 1991; Dahe *et al.*, 1994).

Figure 6.9a compares modelled d-excess with observations along the traverses of Dahe *et al.* (1994) and Delmotte (1997). In general, d-excess is overestimated. Observed and modelled d-excess values correspond rather well over the Antarctic Peninsula, but modelled d-excess is about 5 ‰ higher than observed over the East Antarctic plateau. ECHAM4 performs better, especially around South Pole, but both simulations overestimate d-excess for the Dumont d'Urville - Dome C traverse. The large inter-annual variability of this parameter is expressed by the high standard deviation in the Antarctic interior.

In Figure 6.9b, d-excess is plotted as a function of $\delta^{18}O$. Both observed and modelled d-excess show an increasing trend with decreasing $\delta^{18}O$ values. However, both in our simulation (MCIM-trajs) and in ECHAM4, the combined d-excess$-\delta^{18}O$ relation is not modelled correctly: d-excess attains too high values with respect to the absolute value of $\delta^{18}O$, in comparison with observations. This points to more general parameterisation problems of kinetic fractionation effects for the water isotopes, which will be further addressed in Section 6.4.

The two branches of our simulation in Figure 6.9b represent different relations for

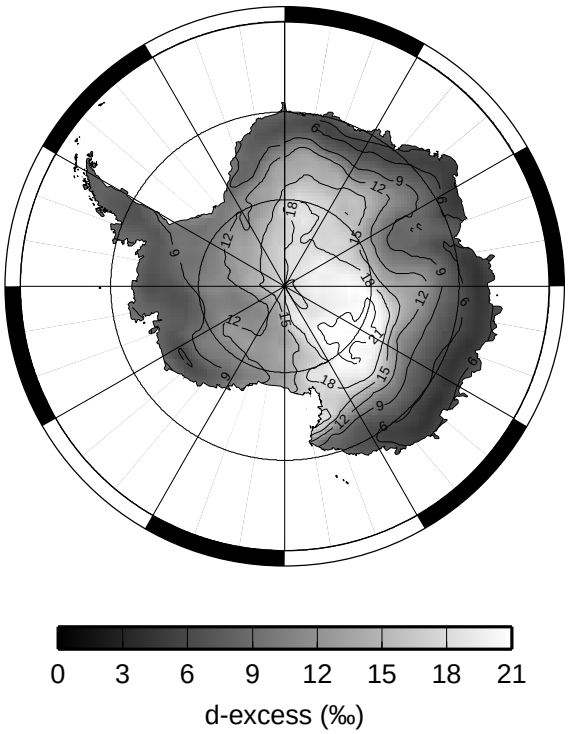

Figure 6.8: *Mean modelled d-excess of snowfall over the period 1980-2002.*

West (upper branch) and East (lower branch) Antarctica. As for $\delta^{18}O$, the reason for this different behaviour can be found in a larger contribution of high-latitude vapour for West Antarctica, which is not only more heavily depleted in $\delta^{18}O$, but also has a much higher d-excess value (Table 6.2).

Figure 6.9c offers more insights in the behaviour of modelled d-excess along its transport path. Plotted in open circles are the observed d-excess values between Dumont d'Urville and Dome C (Delmotte, 1997). The solid circles and crosses are the d-excess values for the nearest grid points as modelled by MCIM-trajs and ECHAM4, respectively. For this particular location, MCIM-trajs produces d-excess values that are closer to the observations, but both models clearly yield too high absolute d-excess values in comparison to their $\delta^{18}O$ value. The gray dotted lines show d-excess as a function of $\delta^{18}O$ along the mean trajectory to each grid point.

Interestingly, the modelled spatial d-excess pattern is not produced by one single air mass transporting moisture from the coast to inland Antarctica. Instead, a unique transport history (and associated d-excess evolution) exists for each location. The final difference in d-excess (between each location along the traverse) is present along the entire modelled transport paths in Figure 6.9, and is largely determined by its initial value. Helsen *et al.* (2005a) showed that the d-excess of this initial moisture

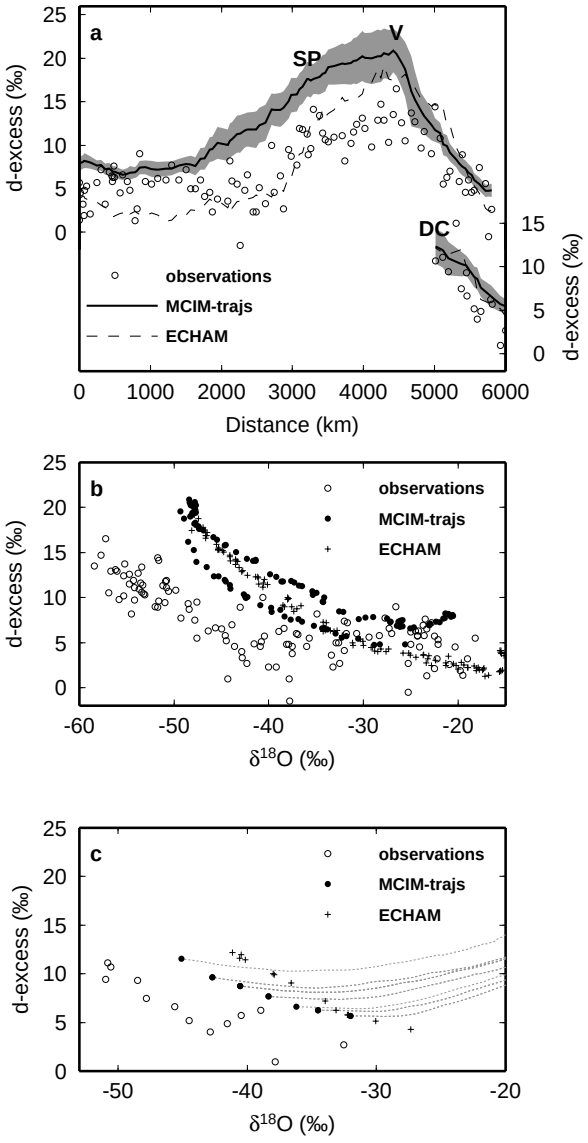

Figure 6.9: *Comparison of modelled and observed mean annual d-excess of precipitation versus distance along the traverse (a) and as a function of $\delta^{18}O$ (b and c). For comparison, mean values from the climate run of ECHAM4 are shown as well. The standard deviation on annual mean values is plotted for our model results in (a) (gray). SP, V and DC indicate the locations of South Pole, Vostok and Dome C, respectively. Observations are obtained from Dahe* et al. *(1994) and Delmotte (1997), see Figure 6.5 for the locations of the traverses). In (c), only data from the Dumont d'Urville - Dome C traverse are plotted, along with the d-excess values along the mean trajectories.*

strongly depends on the height at which vapour enters the air parcel.

These different *d*-excess histories along transport are an intriguing aspect of the simulation, especially for the climatic interpretation of *d*-excess. The dependency of *d*-excess to site and source conditions is often estimated using the assumption that observed spatial *d*-excess patterns can be used to calibrate *d*-excess behaviour along transport (e.g. B. Stenni *et al.*, 2001; Masson-Delmotte *et al.*, 2004). Figure 6.9c demonstrates that this assumption does not hold in our model simulation. However, due to the poor agreement between model results and observations, we cannot draw firm conclusions. Moreover, since the trajectories do not capture the evaporation process over the oceanic source area, this simulation cannot resolve to what extent different temperature and humidity regimes over the oceanic source are preserved in the *d*-excess signal.

6.3.5 The seasonal cycle

When accumulation rate is high enough, a seasonal cycle will be preserved in isotope records. For the Antarctic region, this seasonal cycle has been used as an alternative approach to study the relationship of the isotopic composition with temperature (e.g. Van Ommen and Morgan, 1997; McMorrow *et al.*, 2001; Helsen *et al.*, 2005b). To investigate the magnitude of the seasonal cycle in our simulation, we plotted the difference between minimum and maximum monthly mean values in Figure 6.10a. A distinct pattern of increasing seasonal amplitude with increasing distance to the coast is found. Furthermore, a region with a surprisingly low seasonal amplitude of less than 5 ‰ is found in coastal West Antarctica.

To assess how realistic these results are, we compared the seasonal amplitudes in our model results with a number of sites from which observations are available (Table 6.3). In general, observations and model results both indicate smaller isotopic seasonal amplitudes in coastal areas compared to inland sites. Only in DML, the modelled increasing trend of the seasonal amplitude towards the interior is not recognised in the observations. It should be mentioned that most observations are only based on few (or even just one) years of monitoring. The West Antarctic minimum in seasonal amplitude appears to be real according to the US-ITASE ice core data.

Figure 6.10b shows the relation with the seasonal temperature cycle. Values for $\Delta\delta^{18}O/\Delta T_s$ obtained from seasonal variations are much lower than the spatial relationship (Figure 6.7), which is in agreement with earlier studies (e.g. Van Ommen and Morgan, 1997). However, the modelled values of the seasonal $\delta^{18}O - T$ relation is also consequently lower than observed (Table 6.3). This can be related to the models' problem of producing strongly depleted $\delta^{18}O$ values, which may also be a problem for wintertime snowfall and consequently the seasonal $\delta^{18}O - T$ relation is underestimated.

Figure 6.10 shows the seasonal relationship between $\delta^{18}O$ and T_c. Again, much higher values are obtained compared to the $\delta^{18}O - T_s$ relationship. The difference is caused by the temperature inversion that develops in the Antarctic winter, which causes very low winter values for T_s, but have no influence on T_c.

Figure 6.10 reveals a poor correlation (r <0.7) for large areas in West Antarctica

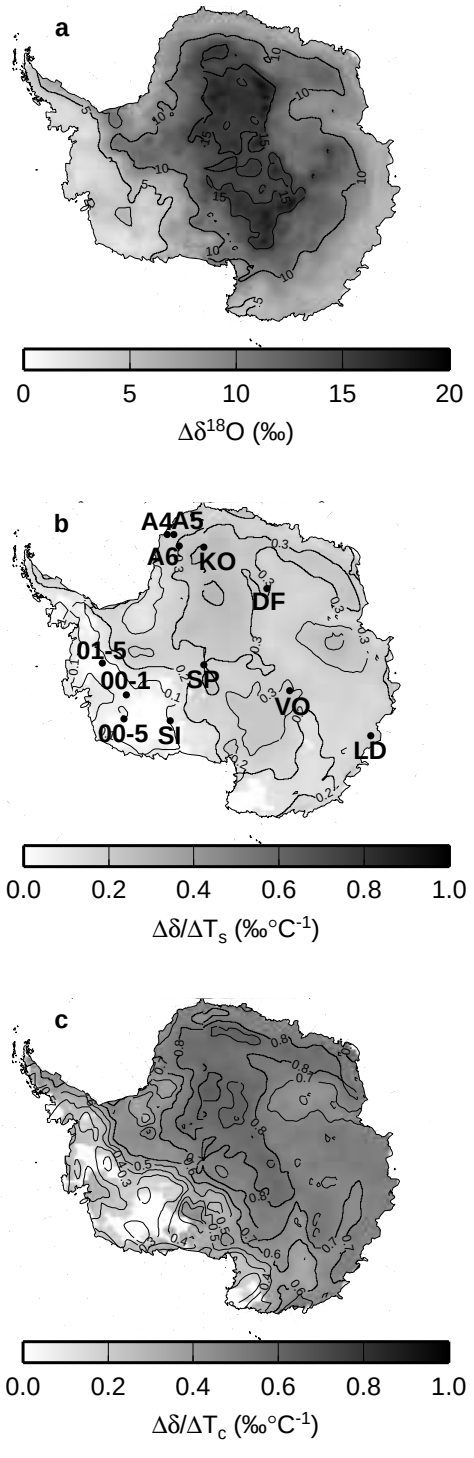

Figure 6.10: *Seasonal difference (summer − winter) of monthly mean $\delta^{18}O$ values (a) and associated seasonal relationships of $\delta^{18}O$ with T_s (b) and T_c (c). Locations of sites in Table 6.3 are indicated with dots. A4=AWS 4, A5=AWS 5, A6=AWS 6, KO=Kohnen, DF=Dome F, LD=Law Dome, VO=Vostok, SP=South Pole, 00-1=US-ITASE 00-1, 00-5=US-ITASE 00-5, 01-5=US-ITASE 01-5, SI=Siple Dome.*

Table 6.3: *Comparison of seasonal isotope - temperature relationships for different Antarctic sites (locations are indicated in Figure 6.10), r values from regression of modelled mean monthly temperature and isotope values are indicated in parentheses.*

	$\Delta\delta^{18}O_{summer-winter}$ (‰)		$\Delta\delta^{18}O/\Delta T_s$ (‰°C^{-1})		$\Delta\delta^{18}O/\Delta T_c$ (‰°C^{-1})	
	obs	MCIM$_{trajs}$	obs	MCIM$_{trajs}$	obs	MCIM$_{trajs}$
AWS 4[a]	14.0	7.6	0.55	0.21 (0.96)	0.57	0.70 (0.91)
AWS 5[a]	7.4	7.6	0.60	0.27 (0.96)	0.83	0.71 (0.90)
AWS 6[a]	11.8	9.7	0.67	0.30 (0.95)	0.77	0.77 (0.94)
Kohnen[a]	9.7	14.8	0.37	0.39 (0.97)	0.49	0.86 (0.98)
Dome F[b]	21.0	17.0	0.47	0.30 (0.89)	1.04*	0.77 (0.97)
Law Dome[c]	6.0	5.9	0.44	0.26 (0.98)	-	0.71 (0.92)
Vostok[d]	13.8	15.6	0.33	0.31 (0.95)	0.97	0.81 (0.97)
South Pole[e]	14.0	14.3	-	0.27 (0.96)	1.40	0.71 (0.91)
US-ITASE 00-1[f]	3.0	4.0	0.13	0.09 (0.80)	-	0.27 (0.85)
US-ITASE 01-5[f]	4.7	3.1	0.21	0.04 (0.36)	-	0.26 (0.61)
	$\Delta\delta D_{summer-winter}$ (‰)		$\Delta\delta D/\Delta T_s$ (‰°C^{-1})		$\Delta\delta D/\Delta T_c$ (‰°C^{-1})	
US-ITASE 00-5[f]	15	45	0.69	0.67 (0.53)	-	2.10 (0.80)
Siple Dome[g]	∼80	55	2.34	0.81 (0.73)	-	2.60 (0.65)

Source of observations and type of seasonal isotope measurements: [a]Helsen *et al.* (2005b): 4 yr snow pits, corrected for diffusion, [b]Motoyama *et al.* (2005): 1 yr freshly fallen snow sampled from container roof, [c]Van Ommen and Morgan (1997): ∼600 yr ice core record, corrected for diffusion, [d]Ekaykin (2003): 1 yr freshly fallen snow sampled in snow traps at 1.5 m height, [e]Aldaz and Deutsch (1967): 1 yr of freshly fallen snow sampled from 0.5 m raised platform, [f]Schneider *et al.* (2004): ice core records, [g]Kreutz *et al.* (1999): 2.5 yr snow pits, not corrected for diffusion.
*T_i is used instead of T_c.

(Marie Byrd Land), mainly because the seasonal amplitude of $\delta^{18}O$ is low for this area. Although the seasonal amplitude of T_c is also small in this area (not shown), this cannot fully explain the total difference in isotopic seasonal amplitude: also the seasonal $\delta^{18}O - T_c$ gradient is much lower in Marie Byrd Land (Figure 6.10c).

Since isotopic depletion of moisture is a function of the temperature difference between source and site (and not just final T_c), seasonal changes in this temperature difference may explain the observed differences. This influence is evaluated for trajectories towards the locations of both maximum and minimum seasonal amplitude. This revealed that trajectories towards Marie Byrd Land experience a similar temperature drop during both winter and summer. On the other hand, wintertime trajectories towards the Antarctic interior originate much more northward than summertime trajectories, and therefore encounter an much larger temperature drop in winter, explaining the large seasonal amplitude.

The seasonal amplitude of *d*-excess is shown in Figure 6.11a. Maximum values of *d*-excess occur in late autumn (May-June), and minimum values occur during early

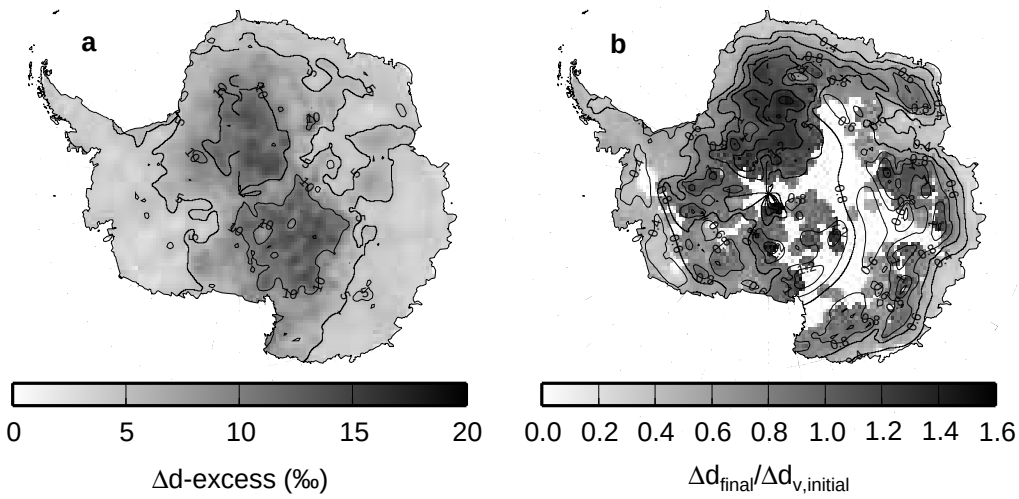

Figure 6.11: *Seasonal of d-excess (a) and relation of d-excess of the final precipitation with d-excess of moisture that enters the air parcel during transport (b). Gray scale is only plotted when $r > 0.7$.*

summer (November-December). Figure 6.9c revealed that concerning the spatial d-excess distribution, the d-excess value of the initial moisture determined to a large extent the final value. Whether this also holds for the seasonal variation is tested by calculating the regression coefficient between the initial d-excess value of moisture five days before arrival and the final value of the precipitation (Figure 6.11b). The seasonal variability of d-excess in a large region ranging from Victoria Lands towards Dome A remains unexplained (too low r values). For the remaining part of the continent, the initial moisture composition largely determines the seasonal signal in d-excess.

6.4 Discussion

The combined approach of backward trajectories and simple isotopic modelling has yielded a unique data set of the isotopic composition of snow in Antarctica. However, the strongly depleted values in inland Antarctica are not correctly reproduced by the model. These problems are also encountered in GCMs equipped with isotope tracers, which highlight the fact that these models do not capture the Antarctic hydrological cycle (and associated isotopic fractionation processes) sufficiently good to explain all observed isotopic variability.

One of the possible causes for the discrepancy may be related to the temperature of condensation, which controls the isotopic composition of snow. In our simulation,

we chose the temperature at the level of maximum condensed moisture (CWC), while in reality condensation occurs over a large vertical range. In GCMs, the condensation process (and its vertical position) is more realistic, but this does not lead to an improved simulation of $\delta^{18}O$, so this is not a likely cause either.

The type of accumulation events can also introduce a bias in the isotopic composition. In Dronning Maud Land, studies with automatic weather stations have revealed that accumulation is dominated by cyclonic precipitation which only occur few times per year (Reijmer and Van den Broeke, 2003; Helsen *et al.*, 2005b). For this type of precipitation, the definition of T_c should be appropriate. On the other hand, clear-sky precipitation is much less intermittent, and evidence exists that this type of precipitation forms a large contribution to the total precipitation on the Antarctic plateau (Bromwich, 1988; Ekaykin, 2003). This type of precipitation is not accounted for in our model approach, since trajectories are only calculated when condensed moisture is detected above the surface. Clear-sky precipitation is likely more depleted than cyclonic precipitation because it is formed at lower T. However, to our knowledge, the most depleted sample of freshly fallen snow ever collected in Antarctica had a value of -75 ‰ and this snowfall occurred as a result of a cyclonic depression that penetrated onto the Antarctic plateau, which was associated with a relatively warm period in winter (Motoyama *et al.*, 2005). This isotopic value is not correctly simulated with our model.

Since our simulation is based on backward trajectory calculations, simulated moisture transport was exclusively advective, and diffusive moisture transport was neglected. Only when moisture increases in trajectories occur, this process was schematically described. Nevertheless, diffusive mixing along transport with (local) depleted moisture may be a key process that can account for the lack of depletion towards the Antarctic interior. However, GCMs do account for this process, but do not produce results more in line with observation, so again, the matter remains unsolved.

Another mechanism not accounted for in our modelling approach, nor in GCMs, is post-depositional isotopic equilibration with atmospheric moisture (Waddington *et al.*, 2002), which is thought to be a significant process in windy, low accumulation sites. This process cannot explain the difference of model results with freshly fallen snow samples, but may have lowered the isotopic composition in firn samples.

Regarding the d-excess parameter, too high values are obtained for the Antarctic interior (Figure 6.9). A solution for this overestimation would be to change the parameterisation of the kinetic fractionation effects, more precisely by increasing the degree of supersaturation of vapour with respect to ice (S_i) as a function of T_c. In a sensitivity experiment using the Goddard Institute for Space Studies (GISS) GCM, Schmidt *et al.* (2005) showed that this leads to a better simulation d-excess. However, increasing S_i also causes a reduction of isotopic distillation, which would result in an even larger difference between observed and modelled $\delta^{18}O$. Hence, the mutual overestimation $\delta^{18}O$ and d-excess in the Antarctic interior points to parameterisation problems of the water isotopes, particularly of kinetic isotope effects. Nevertheless, d-excess does not show large increases during the last phase of transport in our model. The initial imprint of d-excess largely determines our results. Since these initial values are obtained from ECHAM4, this suggests that improvements in parameterisations

of kinetic fractionation effects in ECHAM4 would yield a more realistic d-excess simulation. Indeed, S_i values used in ECHAM4 are systematically lower than in our simulation. It is expected that a slightly higher S_i value would improve the d-excess simulation in ECHAM4.

6.5 Conclusions

Modelling isotope fractionation using both simple distillation models and GCMs equipped with isotope tracers has provided valuable insights in the mechanisms behind observed global isotope variability. In this paper we presented a data set of isotopic composition of Antarctic snow, generated using atmospheric reanalysis data combined with a trajectory model and a simple isotope model. It is demonstrated that this approach is able to reproduce most of the observed spatial gradients, and also qualitatively describes the seasonal cycle. However, isotopic depletion is underestimated for the high Antarctic plateau.

The modelled present-day spatial $\delta^{18}O - T$ relation in Antarctica appears to vary regionally, which is an indication that this widely used relation is not applicable to all sites and periods.

Our results indicate large spatial variability in the amplitude of the seasonal isotope cycle, mostly in agreement with the observed variability. The underlying mechanisms behind these patterns can be attributed to (1) spatial variations in the seasonal amplitude of condensation temperature and (2) strong seasonal fluctuations in the latitudinal extent of the mean transport path.

Modelled d-excess qualitatively follows the observed spatial pattern, but is generally higher than observations in the Antarctic interior. Analysis of the evolution of d-excess along the trajectories indicates that spatial variations in modelled d-excess are not much influenced by the last phase of transport, but are largely determined by their initial values, which are obtained from the ECHAM4 GCM. The mutual behaviour of $\delta^{18}O$ and d-excess suggests that parameterisation of kinetic fractionation effects can be improved.

Future work will try to identify to what extent large-scale atmospheric patterns are preserved in the isotopic composition of present-day Antarctic accumulation.

Bibliography

Aldaz, L. and Deutsch, S. 1967. On a relationship between air temperature and oxygen isotope ratio of snow and firn in the South Pole region. *Earth Planet. Sci. Lett.*, **3**, 267–274.

Arastarain, A. J., Jouzel, J., and Pourchet, M. 1986. Past Antarctic Peninsula climate (1850-1980) deduced from an ice core isotope record. *Clim. Change*, **8**, 69–89.

B. Stenni, V. M.-D., Johnsen, S., Jouzel, J., Longinelli, A., Monnin, E., Röthlisberger, R., and Selmo, E. 2001. An oceanic cold reversal during the last deglaciation. *Science*, **293**, 2074–2077.

Bergeron, T. 1935. On the physics of clouds and precipitation. *Proc. 5th Assembly UGGI Lisbon*, **2**, 156.

Bintanja, R., Van de Wal, R. S. W., and Oerlemans, J. 2005. Modelled atmospheric temperatures and global sea levels over the past million years. *Nature*, **437**, 125–128.

Birks, S. J., Gibson, J. J., Gourcy, L., Aggarwal, P. K., and Edwards, T. W. D. 2002. Maps and animations offer new opportunities for studying the global water cycle. *Eos Trans. AGU Electron Suppl.*, page http://www.agu.org/eos_elec/020082e.html.

Bolzan, J. F. and Pohjola, V. A. 2000. Reconstruction of the undiffused seasonal oxygen isotope signal in central Greenland ice cores. *J. Geophys. Res.*, **105**(C9), 22,095–22,106.

Boyle, E. A. 1997. Cool tropical temperatures shift the global δ^{18}O-T relationship: An explanation for the ice core δ^{18}O - borehole thermometry conflict? *Geophys. Res. Lett.*, **24**(3), 273–276.

Bromwich, D. H. 1988. Snowfall in high southern latitudes. *Rev. Geophys.*, **26**(1), 149–168.

Bromwich, D. H., Guo, Z., Bai, L., and Chen, Q. S. 2004. Modeled Antarctic precipitation. Part I: Spatial and temporal variability. *J. Climate*, **17**(3), 427–447.

Ciais, P. and Jouzel, J. 1994. Deuterium and oxygen 18 in precipitation: Isotopic model, including mixed cloud preocesses. *J. Geophys. Res.*, **99**(D8), 16,793–16,803.

Ciais, P., White, J. W. C., Jouzel, J., and Petit, J. R. 1995. The origin of present-day antarctic precipitation from surface snow deuterium excess data. *J. Geophys. Res.*, **100**(D9), 18,917–18,927.

Connolley, W. M. and Harangozo, S. A. 2001. A comparison of five numerical weather prediction analysis climatologies in southern high latitudes. *J. Climate*, **14**(1), 30–44.

Craig, H. 1961. Isotopic variations in meteoric waters. *Science*, **133**, 1702–1708.

Craig, H. and Gordon, A. 1965. Deuterium and oxygen 18 variations in the ocean and the marine atmosphere. In *Stable Isotopes in Oceanic Studies and Paleotemperatures*, 9–130. Lab. Di Geol. Nucl., Pisa, Italy.

Cuffey, K. M. and Steig, E. J. 1998. Isotopic diffusion on polar firn: implications for interpretation of seasonal climate parameters in ice-core records, with emphasis on central Greenland. *J. Glaciol*, **44**(147), 273–284.

Cuffey, K. M. and Vimeux, F. 2001. Covariation of carbon dioxide and temperature from the Vostok ice core after deuterium-excess correction. *Nature*, **412**, 523–527.

Cuffey, K. M., Alley, R. B., Grootes, P. M., Bolzan, J. M., and Anandakrishnan, S. 1994. Calibration of δ^{18}O isotopic paleothermometer for central Greenland, using borehole temperatures. *J. Glaciol.*, **40**(135), 341–349.

Cuffey, K. M., Clow, G. D., Alley, R. B., Stuiver, M., Waddington, E. D., and Saltus, R. W. 1995. Large Arctic Temperature change at the Wisconsin-Holocene glacial transition. *Science*, **270**, 455–458.

Cullather, R. I., Bromwich, D., and Grumbine, R. W. 1997. Validation of operational numerical analyses in Antarctic latitudes. *J. Geophys. Res.*, **102**(D12), 12,761–13,784.

Dahe, Q., Petit, J. R., Jouzel, J., and Stievenard, M. 1994. Distribution of stable isotopes in surface snow along the route of the 1990 International Trans-Antarctic Expedition. *J. Glaciol*, **40**(134), 107–118.

Dahl-Jensen, D., Morgan, V., and Elcheikh, A. 1999. Monte Carlo inverse modelling of the Law Dome (Antarctica) temperature profile. *Ann. Glaciol*, **29**, 145–150.

Dansgaard, W. 1964. Stable isotopes in precipitation. *Tellus*, **16**, 436–468.

Delaygue, G., Masson, V., Jouzel, J., Koster, R. D., and Healy, R. J. 2000. The origin of Antarctic precipitation: a modelling approach. *Tellus*, **52B**, 19–36.

Delmotte, M. 1997. *Enregistrements climatiques à Law Dome: Variabilité pour les périodes récentes et pour la déglaciation*. Ph.D. thesis, Univ. Joseph Fourier, Grenoble, France.

Delmotte, M., Masson, V., Jouzel, J., and Morgan, V. 2000. A seasonal deuterium excess signal at Law Dome, coastal eastern Antarctica: A southern ocean signature. *J. Geophys. Res*, **105**(D6), 7187–7197.

Ehhalt, D. H., Rohrer, F., and Fried, A. 2005. Vertical profiles of HDO/H_2O in the troposphere. *J. Geophys. Res.*, **110**(D13301), 10.1029/2004JD005569.

Ekaykin, A. A. 2003. *Meteorological regime of central Antarctica and its role in the formation of isotope composition of snow thickness*. Ph.D. thesis, Univ. Joseph Fourier, Grenoble, France.

EPICA community members 2004. Eight glacial cycles from an Antarctic ice core. *Nature*, **429**, 623–628.

Eriksson, E. 1965. Deuterium and oxygen-18 in precipitation and other natural waters: some theoretical considerations. *Tellus*, **17**(4), 498–512.

Findeisen, W. 1938. Die kolloidmeteorologischen Vorgänge bei der Niederschlagsbildung. *Meteorologische Zeitschrift*, **55**, 121.

Fisher, D. A. 1991. Remarks on the deuterium excess in precipitation in cold regions. *Tellus*, **43B**, 401–407.

Fisher, D. A. and Alt, B. T. 1985. A global oxygen isotope model - semi-empirical, zonally averaged. *Ann. Glaciol.*, **7**, 117–124.

Frezzotti, M., Gandolfi, S., and Urbini, S. 2002. Snow megadunes in Antarctica: Sedimentary structure and genesis. *J. Geophys. Res.*, **107**(D18), doi:10.1029/2001JD000673.

Friedman, I., Benson, C., and Cleason, J. 1991. Isotopic changes during snow metamorphism. In H.P. Taylor Jr., R. O'Neill, and I. Kaplan, editors, *Stable Isotope Geochemistry: A Tribute to Samuel Epstein, Special Publication No. 3*, 211–221. The Geochemical Society.

Gat, J. R. 1980. The isotopes of hydrogen and oxygen in precipitation. In P. Fritz and J.Ch.Fontes, editors, *Handbook of Environmental Isotope Geochemistry, Vol 1, The Terrestrial Environment, A*, chapter 1, 21–47. Elsevier.

Gat, J. R., Mook, W. G., and Meijer, H. A. J. 2001. *Environmental isotopes in the hydrological cycle, Principles and applications, Vol 2: Atmospheric water*, **2**. UNESCO, Paris.

Genthon, C. 2002. Climate and surface mass balance of the polar ice sheets in era40/era15. *ECMWF Re-analysis Project Report Series*, **3**, 299–316.

Graf, W., Moser, H., Reinwarth, O., Kipfstuhl, J., , Oerter, H., Minikin, A., and Wagenbach, D. 1994. Snow-accumulation rates and isotopic content (^{2}H, ^{3}H) of near-surface firn from the Filchner-Ronne Ice Shelf, Antarctica. *Ann. Glaciol.*, **20**, 121–128.

Graf, W., Reinwarth, O., Oerter, H., Mayer, C., and Lambrecht, A. 1999. Surface accumulation on Foundation Ice Stream, Antarctica. *Ann. Glaciol.*, **29**, 23–28.

Graf, W., Oerter, H., Reinwarth, O., Stichler, W., Wilhelms, F., Miller, H., and Mulvaney, R. 2002. Stable-isotope records from Dronning Maud Land, Antarctica. *Ann. Glaciol.*, **35**, 195–201.

GRIP Members 1993. Climate instability during the last interglacial period recorded in the GRIP ice core. *Nature*, **364**(6434), 203–207.

Grootes, P. M., Stuiver, M., White, J. W. C., Johnsen, S., and Jouzel, J. 1993. Comparison of oxygen isotope records from the GISP2 and GRIP Greenland ice cores. *Nature*, **366**, 552–554.

Helsen, M. M., Van de Wal, R. S. W., Van den Broeke, M. R., Kerstel, E. R. T., Masson-Delmotte, V., Meijer, H. A. J., Reijmer, C. H., and Scheele, M. P. 2004. Modelling the isotopic composition of snow using backward trajectories: a particular accumulation event in Dronning Maud Land, Antarctica. *Ann. Glaciol.*, **39**, 293–299.

Helsen, M. M., Van de Wal, R. S. W., Van den Broeke, M. R., Masson-Delmotte, V., Meijer, H. A. J., Scheele, M. P., and Werner, M. 2005a. Modeling the isotopic composition of Antarctic snow using backward trajectories: Simulation of snow pit records. *submitted to J. Geophys. Res.*

Helsen, M. M., Van de Wal, R. S. W., Van den Broeke, M. R., Van As, D., Meijer, H. A. J., and Reijmer, C. H. 2005b. Oxygen isotope variability in snow from western Dronning Maud Land, Antarctica and its relation to temperature. *Tellus*, **57B**(5), 423–435.

Hoffmann, G., Werner, M., and Heimann, M. 1998. Water isotope module of the ECHAM atmospheric general circulation model: A study on time scales from days to several years. *J. Geophys. Res.*, **103**(D14), 16,871–16,896.

Hoffmann, G., Jouzel, J., and Masson, V. 2000. Stable water isotopes in atmospheric general circulation models. *Hydrol. Processes*, **14**, 1385–1406.

Holdsworth, G. 2001. Calibration changes in the isotopic thermometer for snow according to different climatic states. *Geophys. Res. Lett.*, **28**(13), 2625–2628.

IAEA 1992. *Statistical treatment of data on environmental isotopes in precipitation*. Vienna, International Atomic Energy Agency (IAEA) Technical Report Series 331.

IPCC 2001. *IPCC Third Assessment Report: Climate Change 2001: The Scientific Basis*. Cambridge University Press, Cambridge.

Isaksson, E., Karlén, W., Gundestrup, N., Mayewski, P., Whitlow, S., and Twickler, M. 1996. A century of accumulation and temperature changes in Dronning Maud Land, Antarctica. *J. Geophys. Res.*, **101**(D3), 7085–7094.

Isaksson, E., Van den Broeke, M. R., Winther, J.-G., Karlöf, L., Pinglot, J. F., and Gundestrup, N. 1999. Accumulation and proxy temperature variability in Dronning Maud Land, Antarctica, determined from shallow firn cores. *Ann. Glaciol.*, **29**, 17–22.

Jakob, C. 1999. Cloud cover in the ECMWF Reanalysis. *J. Climate*, **12**(4), 947–959.

Johnsen, S. J. 1977. Stable isotope homogenization of polar firn and ice. In *Isotopes and Impurities in Snow and Ice*, **publ. 118**, 210–219. International Association of Hydrological Sciences.

Johnsen, S. J., Dansgaard, W., and White, J. W. C. 1989. The origin of Arctic precipitation under present and glacial conditions. *Tellus*, **41B**, 452–468.

Johnsen, S. J., Dahl-Jensen, D., Dansgaard, W., and Gundestrup, N. 1995. Greenland palaeotemperatures derived from GRIP bore hole temperature and ice core isotope profiles. *Tellus*, **47B**, 624–629.

Johnsen, S. J., Clausen, H. B., Cuffey, K. M., Hoffmann, G., Schwander, J., and Creyts, T. 2000. Diffusion of stable isotopes in polar firn and ice: the isotope effect in firn diffusion. In T. Hondoh, editor, *Physics of Ice Core Records*, 121–140. Hokkaido University Press, Sapporo.

Joussaume, J., Sadourny, R., and Jouzel, J. 1984. A general circulation model of water isotope cycles in the atmosphere. *Nature*, **311**, 24–29.

Jouzel, J. and Koster, R. D. 1996. A reconsideration of the initial conditions used for stable water isotope models. *J. Geophys. Res.*, **101**(D17), 22,933–22,938.

Jouzel, J. and Merlivat, L. 1984. Deuterium and oxygen 18 in precipitation: Modeling of the isotopic efects during snow formation. *J. Geophys. Res.*, **89**(D7), 11,749–11,757.

Jouzel, J., Merlivat, L., and Lorius, C. 1982. Deuterium excess in an East Antarctic ice core suggests higher relative humidity at the oceanic surface during the last glacial maximum. *Nature*, **299**, 688–691.

Jouzel, J., Merlivat, L., Petit, J. R., and Lorius, C. 1983. Climatic information over the last century deduced from a detailed isotopic record in the South Pole snow. *J. Geophys. Res.*, **88**(C4), 2693–2703.

Jouzel, J., Russell, G. L., Suozzo, R. J., Koster, R. D., White, J. W. C., and Broecker, W. S. 1987a. Simulations of HDO and $H_2{}^{18}O$ atmospheric cycles using the NASA GISS general circulation model: The seasonal cycle for present-day conditions. *J. Geophys. Res.*, **92**, 14,739–14,760.

Jouzel, J., Lorius, C., Petit, J. R., Genthon, C., Barkov, N. I., Kotlyakov, V. M., and Petrov, V. M. 1987b. Vostok ice core: A continuous isotope temperature record over the last climatic cycle (160,000 years). *Nature*, **329**, 402–408.

Jouzel, J., Alley, R. B., Cuffey, C. M., Dansgaard, W., Grootes, P., Hoffmann, G., Johnsen, S. J., Koster, R. D., Peel, D., Shuman, C. A., Stievenard, M., Stuiver, M., and White, J. 1997. Validity of the temperature reconstruction from water isotopes in ice cores. *J. Geophys. Res.*, **102**(C12), 26,471–26,487.

Jouzel, J., Hoffmann, G., Koster, R. D., and Masson, V. 2000. Water isotopes in precipitation: data/model comparison for present-day and past climates. *Quat. Sci. Rev.*, **19**, 363–379.

Jouzel, J., Vimeux, F., Caillon, N., Delaygue, G., Hoffmann, G., Masson-Delmotte, V., and Parrenin, F. 2003. Magnitude of isotope/temperature scaling for interpretation of central antarctic ice cores. *J. Geophys. Res.*, **108**(D12), doi:10.1029/2002JD002677.

Karlöf, L., Winther, J.-G., Isaksson, E., Kohler, J., Pinglot, J. F., Wilhelms, F., Hansson, M., Holmlund, P., Nyman, M., Pettersson, R., Stenberg, M., Thomassen, M. P. A., Van der Veen, C., and Van de Wal, R. S. W. 2000. A 1500 year record of accumulation at Amundsenisen western Dronning Maud Land, Antarctica, derived drom electrical and radioactive measurements on a 120 m ice core. *J. Geophys. Res.*, **105**(D10), 12,471–12,483.

Kavanaugh, J. L. and Cuffey, K. M. 2003. Space and time variation of δ^{18}O and δD in Antarctic precipitation revised. *Global Biogeochem. Cycles*, **17**(1), doi:10.1029/2002GB001910.

King, J. C. and Turner, J. 1997. *Antarctic Meteorology and Climatology*. Cambridge University Press, Cambridge.

King, J. C., Andersen, P. S., Vaughan, D. G., Mann, G. W., Mobbs, S. D., and Vosper, S. B. 2004. Wind-borne redistribution of snow across an Antarctic ice rise. *J. Geophys. Res.*, **109**, 10.1029/2003JD004361.

Kottmeier, C. and Fay, B. 1998. Trajectories in the antarctic lower troposphere. *J. Geophys. Res.*, **103**(D9), 10,947–10,959.

Kreutz, K. J., Mayewski, P. A., Twickler, M. S., Whitlow, S. I., White, J. W. C., Shuman, C. A., Raymond, C. F., Conway, H., and McConnell, J. R. 1999. Seasonal variations of glaciochemical, isotopic and stratigraphic properties in siple dome (antarctica) surface snow. *Ann. Glaciol.*, **29**, 38–44.

Landais, A., Barnola, J. M., Masson-Delmotte, V., Jouzel, J., Chappellaz, J., Caillon, N., Huber, C., and Johnsen, S. J. 2004. A continuous record of temperature evolution over a sequence of Dansgaard-Oeschger events during Marine Isotopic Stage 4 (76 to 62 kyr BP). *Geophys. Res. Lett.*, **31**, 10.1029/2004GL021193.

Lisiecki, L. E. and Raymo, M. E. 2005. A Piocene-Pleistocene stack of 57 globally distributed benthic $\delta^{18}O$ records. *Paleoceanography*, **20**, doi:10.1029/2004PA001071.

Liu, H., Jezek, K., Li, B., and Zhao, Z. 2001. *Radarsat Antarctic Mapping Project digital elevation model version 2*. Boulder, CO: National Snow and Ice Data Center. Digital media.

Loewe, F. 1936. The greenland ice cap as seen by a meteorologist. *Quart. J. Roy. Meteorol. Soc.*, **62**, 359–377.

Lorius, F. and Merlivat, L. 1977. Distribution of mean surface stable isotope values in East Antarctica: observed changes with depth in the coastal area. In *Isotopes and Impurities in Snow and Ice*, **publ. 118**, 127–137. International Association of Hydrological Sciences.

Majoube, M. 1971a. Fractionnement en oxygene 18 et en deuterium entre la glace et la vapeur d'eau. *J. Chim. Phys.*, **68**, 625–636.

Majoube, M. 1971b. Fractionnement en oxygene 18 et en deuterium entre l'eau et sa vapeur. *J. Chim. Phys.*, **10**, 1423–1436.

Massom, R. A., Pook, M. J., Comiso, J. C., Adams, N., Turner, J., Lachlan-Cope, T., and Gibson, T. T. 2004. Precipitation over the interior East Antarctic ice sheet related to midlatitude blocking-high activity. *J. Climate*, **17**, 1914–1928.

Masson-Delmotte, V., Delmotte, M., Morgan, V., Etheridge, D., Ommen, T. V., Tartarin, S., and Hoffmann, G. 2003. Recent southern Indian Ocean climate variability inferred from a Law Dome ice core: new insights for the interpretation of coastal Antarctic isotopic records. *Clim. Dynamics*, **21**(2), 153–166.

Masson-Delmotte, V., Stenni, B., and Jouzel, J. 2004. Common millennial-scale variability of Antarctic and Southern Ocean temperatures during the past 5000 years reconstructed from the EPICA Dome C ice core. *The Holocene*, **14**(2), 145–151.

Mathieu, R., Pollard, D., Cole, J. E., White, J. W. C., Webb, R. S., and Thompson, S. L. 2002. Simulation of stable water isotope variations by the GENESIS GCM for modern conditions. *J. Geophys. Res.*, **107**(D4), doi:10.1029/2002JD900255.

McMorrow, A. J., Curran, M. A. J., Van Ommen, T. D., Morgan, V. I., Pook, M. A. J., and Allison, I. 2001. Intercomparison of firn core and meteorological data. *Antarct. Sci.*, **13**(3), 329–337.

Merlivat, L. and Jouzel, J. 1979. Global climatic interpretation of the deuterium-oxygen 18 relationship for precipitation. *J. Geophys. Res.*, **84**(C8), 5029–5033.

Merlivat, L. and Nief, G. 1967. Fractionnement isotopique lors des changements d'état solide-vapeur et liquide-vapeur de l'eau à des températures inférieures à 0°c. *Tellus*, **19**, 122–127.

Motoyama, H., Hirasawa, N., Satow, K., and Watanabe, O. 2005. Seasonal variations in oxygen isotope ratios of daily collected precipitation and wind drift samples and in the final snow cover at Dome Fuji Station, Antarctica. *J. Geophys. Res.*, **110**(D11106), doi:10.1029/2004JD004953.

Neumann, T. A. and Waddington, E. D. 2004. Effects of firn ventilation on isotopic exchange. *J. Glaciol.*, **50**(169), 183–194.

Noone, D. and Simmonds, I. 2002a. Annular variations in moisture transport mechanisms and the abundance of δ^{18}O in Antarctic snow. *J. Geophys. Res.*, **107**(D24), doi:1029/2002JD002262.

Noone, D. and Simmonds, I. 2002b. Associations between δ^{18}O of water and climate parameters in a simulation of atmospheric circulation for 1979-95. *J. Climate*, **15**(22), 3150–3169.

Noone, D., Turner, J., and Mulvaney, R. 1999. Atmospheric signals and characteristics of accumulation on Dronning Maud Land, Antarctica. *J. Geophys. Res.*, **104**(D16), 19,191–19,211.

North Greenland Ice Core Project members 2004. High-resolution record of Northern Hemisphere climate extending into the last interglacial period. *Nature*, **431**, 147–151.

Oerter, H., Graf, W., Wilhelms, F., Minikin, A., and Miller, H. 1999. Accumulation studies on Amundsenisen, Dronning Maud Land, Antarctica, by means of tritium, dielectric profiling and stable-isotope measurements: first results from the 1995-96 and 1996-97 field seasons. *Ann. Glaciol.*, **29**, 1–9.

Peel, D. A., Mulvaney, R., and Davison, B. R. 1988. Stable-isotope / air-temperature relationships in ice cores from Dolleman Island and the Palmer Land plateau, Antarctic Peninsula. *Ann. Glaciol.*, **10**, 130–136.

Petit, J. R., White, J. W. C., Young, N. W., Jouzel, J., and Korotkevich, Y. 1991. Deuterium excess in recent Antarctic snow. *J. Geophys. Res.*, **96**(D3), 5113–5122.

Petit, J. R., Jouzel, J., Raynaud, D., Barkov, N. I., Barnola, J.-M., Basile, I., Bender, M., Chappellaz, J., Davis, M., Delaygue, G., Delmotte, M., Kotlyakov, V. M., Legrand, M., Lipenkov, V. Y., Lorius, C., Pépin, L., Ritz, C., Saltzman, E., and Stievenard, M. 1999. Climate and atmospheric history of the past 420,000 years from the Vostok ice core, Antarctica. *Nature*, **399**, 429–436.

Physick, W. L. 1981. Winter depression tracks and climatological jet streams in the southern hemisphere during the FGGE year. *Quart. J. Roy. Met. Soc.*, **107**, 883–898.

Radok, U., Streten, N., and Weller, G. E. 1975. Atmosphere and ice. *Oceanus*, **18**, 16–27.

Reijmer, C. H. and Oerlemans, J. 2002. Temporal and spatial variability of the surface energy balance in Dronning Maud Land, East Antarctica. *J. Geophys. Res.*, **107**(D24), doi:10.1029/2000JD000110.

Reijmer, C. H. and Van den Broeke, M. R. 2001. Moisture source of precipitation in Western Dronning Maud Land, Antarctica. *Antarct. Sci.*, **13**(2), 210–220.

Reijmer, C. H. and Van den Broeke, M. R. 2003. Temporal and spatial variability of the surface mass balance in Dronning Maud Land, Antarctica, as derived from automatic weather stations. *J. Glaciol.*, **49**(167), 512–520.

Reijmer, C. H., Van den Broeke, M. R., and Scheele, M. P. 2002. Air parcel trajectories and snowfall related to five deep drilling locations in Antarctica based om tje ERA-15 dataset. *J. Climate*, **15**, 1957–1968.

Reijmer, C. H., Van Meijgaard, E., and Van den Broeke, M. R. 2005. Evaluation of temperature and wind over Antarctica in a Regional Atmospheric Climate Model using one year of automatic weather station data and upper air observations. *J. Geophys. Res.*, **110**(D4), doi:10.1029/2004JD005234.

Richardson, C., Aarholt, E., Hamran, S.-E., Holmlund, P., and Esaksson, E. 1997. Spatial distribution of snow in western Dronning Maud Land, East Antarctica, mapped by a ground-based snow radar. *J. Geophys. Res.*, **102**(B9), 20,343–20,353.

Robin, G. 1983. The climatic record from ice cores. In G. Robin, editor, *The climatic record in polar ice sheets*, 180–195. Cambridge University Press, Cambridge.

Roeckner, E., Arpe, K., Bengtsson, L., Christoph, M., Claussen, M., Dmenil, L., Esch, M., Giorgetta, M., Schlese, U., and Schulzweida, U. 1996. *The atmospheric general circulation model ECHAM-4: model description and simulation of present-day climate*. MPI-Report 218. Max-Planck-Institute for Meteorology, Hamburg.

Scheele, M. P., Siegmund, P. C., and Van Velthoven, P. F. J. 1996. Sensitivity of trajectories to data resolution and its dependence on the starting point: in or outside a tropopause fold. *Meteorol.Appl.*, **3**, 267–273.

Schmidt, G. A., Hoffmann, G., Shindell, D. T., and Hu, Y. 2005. Modeling atmospheric stable water isotopes and the potential for constraining cloud processes and stratosphere-troposphere water exchange. *J. Geophys. Res.*, **110**(D21314), doi:10.1029/2005JD005790.

Schneider, D. P., Steig, E. J., and Van Ommen, T. 2004. Interpretation of high resolution ice core stable isotopic records from Antarctica: towards interannual climate reconstruction. *Ann. Glaciol.*

Shackleton, N. J. 2000. The 100,000-year ice-age cycle identified and found to lag temperature, carbon dioxide and orbital eccentricity. *Science*, **289**, 1897–1902.

Shuman, C. A., Alley, R. B., Anandakrishnan, S., White, J. W. C., Grootes, P. M., and Stearns, C. R. 1995. Temperature and accumulation at the Greenland Summit: comparison of high-resolution isotope profiles and satellite passive microwave brightness temperature trends. *J. Geophys. Res.*, **100**(D5), 9165–9177.

Siegenthaler, U., Stocker, T. F., Monnin, E., Lüthi, D., Schwander, J., Stauffer, B., Raynaud, D., Barnola, J.-M., Fischer, H., Masson-Delmotte, V., and Jouzel, J. 2005. Stable carbon cycle-climate relationship during the late Pleistocene. *Science*, **310**, 1313–1317.

Sinclair, M. R. 1981. Record-high temperatures in the Antarctic − a synoptic case study. *Mon. Wea. Rev.*, **109**, 2234–2242.

Spahni, R., Chappellaz, J., Stocker, T. F., Loulergue, L., Hausammann, G., Kawamura, K., Flückiger, J., Schwander, J., Raynaud, D., Masson-Delmotte, V., and Jouzel, J. 2005. Atmospheric methane and nitrous oxide of the late Pleistocene from Antarctic ice cores. *Science*, **310**, 1317–1321.

Stohl, A., Wotawa, G., Seibert, P., and Kromp-Kolb, H. 1995. Interpolation errors in wind fields as a function of spatial and temporal resolution and their impact of different types of kinematic trajectories. *J. Appl. Meteorol.*, **34**(10), 2149–2165.

Tiedtke, M. 1993. Representation of clouds in large-scale models. *Mon. Wea. Rev.*, **121**(11), 3040–3061.

Turner, J., Connolley, W. M., Leonard, S., Marshall, G. J., and Vaughan, D. G. 1999. Spatial and temporal variability of net snow accumulation over the Antarctic from ECMWF re-analysis project data. *Int. J. Climatol.*, **19**(7), 697–724.

Van de Berg, W. J., Van den Broeke, M. R., Reijmer, C. H., and van Meijgaard, E. 2005. Characteristics of the Antarctic surface mass balance (1958-2002) using a Regional Antmospheric Climate Model. *Ann. Glaciol.*, **41**.

Van den Broeke, M., Reijmer, C., and Van de Wal, R. 2004. Surface radiation balance in Antarctica as measured with automatic weather stations. *J. Geophys. Res.*, **109**, doi:10.1029/2003JD004394.

Van den Broeke, M. R. 1997. Spatial and temporal variation of sublimation on Antarctica: Results of a high-resolution general circulation model. *J. Geophys. Res.*, **102**(D25), 29,765–29,777.

Van den Broeke, M. R. and Van Lipzig, N. P. M. 2003. Factors controlling the near-surface wind field in Antarctica. *Mon. Wea. Rev.*, **131**(4), 733–743.

Van den Broeke, M. R., Winther, J.-G., Isaksson, E., Pinglot, J. F., Karlöf, L., Eiken, T., and Conrads, L. 1999. Climate variables along a traverse line in Dronning Maud Land, East Antarctica. *J. Glaciol.*, **45**(150), 295–302.

Van den Broeke, M. R., Van Lipzig, N. P. M., and Van Meijgaard, E. 2002. Momentum budget of the east Antarctic atmospheric boundary layer: results of a regional climate model. *J. Atmos. Sci.*, **59**(21), 3117–3129.

Van den Broeke, M. R., Van As, D., Reijmer, C. H., and Van de Wal, R. S. W. 2005. Seasonal cycles of Antarctic surface energy balance using automatic weather stations. *Annals of Glaciology*, **41**(in press).

Van Lipzig, N. P. M., Van Meijgaard, E., and Oerlemans, J. 2002a. The effect of temporal variations in the surface mass balance and temperature-inversion strength on the interpretation of ice-core signals. *J. Glaciol.*, **48**(163), 611–621.

Van Lipzig, N. P. M., Van Meijgaard, E., and Oerlemans., J. 2002b. The spatial and temporal variability of the surface mass balance of antarctica: Results from a regional atmospheric climate model. *Int. J. Climatol.*, **22**, 1197–1217.

Van Lipzig, N. P. M., King, J. C., Lachlan-Cope, T. A., and Van den Broeke, M. R. 2004. Precipitation, sublimation, and snow drift in the antarctic peninsula region from a regional atmospheric model. *J. Geophys. Res.*, **109**(D24106), doi:10.1029/2004JD004701.

Van Ommen, T. D. and Morgan, V. 1997. Calibrating the ice core paleothermometer using seasonality. *J. Geophys. Res.*, **102**(D8), 9351–9357.

Vaughan, D. G., Bamber, J. L., Giovinetto, M., and Cooper, J. R. A. P. R. 1999. Reassessment of net surface mass balance in Antarctica. *J. Climate*, **12**, 933–946.

Vimeux, F., Masson, V., Jouzel, J., and Stievenard, M. 1999. Glacial-interglacial changes in ocean surface conditions in the Southern Hemisphere. *Nature*, **398**, 410–413.

Vuille, M., Bradley, R. S., Werner, M., Healy, R., and Keimig, F. 2003. Modelling δ^{18}O in precipitation over the tropical Americas: 1. Interannual variability and climatic controls. *J. Geophys. Res.*, **108**(D6), doi:10.1029/2001JD002038.

Waddington, E. D., Steig, E. J., and Neumann, T. A. 2002. Using characteristic times to assess whether stable isotopes in polar snow can be reversibly deposited. *Ann. Glaciol.*, **35**, 118–124.

Werner, M. and Heimann, M. 2002. Modeling interannual variability of water isotopes in Greenland and Antarctica. *J. Geophys. Res.*, **107**(D1), doi:10.1029/2001JD900253.

Werner, M., Mikolajewicz, U., Heimann, M., and Hoffmann, G. 2000. Borehole versus isotope temperatures on Greenland: Seasonality does matter. *Geophys. Res.Lett.*, **27**(5), 723–726.

Werner, M., Heimann, M., and Hoffmann, G. 2001. Isotopic composition and origin of polar precipitation in present an glacial climate simulations. *Tellus*, **53B**, 53–71.

Whillans, I. M. and Grootes, P. M. 1985. Isotopic diffusion on cold snow and firn. *J. Geophys. Res.*, **90**(D2), 3910–3918.

Zwally, H. J., Giovinetto, M., Craven, M., Morgan, V., and Goodwin, I. 1998. Areal distribution of the oxygen-isotope ratio in antarctica: comparison of results based on field and remotely sensed data. *Ann. Glaciol.*, **27**, 583–590.

Summary

The interpretation of stable isotopes in Antarctic snow is the subject of this thesis. Isotope ratios of oxygen ($\delta^{18}O$) and/or deuterium (δD) are widely used as proxies for atmospheric temperature, on a variety of time scales. A significant spatial correlation between mean annual surface temperature (T_s) and the average isotopic composition of snow (δ) is commonly used as argument to use δ values as a paleothermometer. However, previous research has shown that this spatial $\delta - T_s$ relation is also influenced by other processes, and is not always constant over time. This obscures the interpretation of isotope records, and points out that isotope records from ice cores should not be quantitatively translated to temperature changes without calibration, using independent temperature records. The goal of this thesis is to improve the interpretation of stable isotope records in Antarctic snow by addressing the influence of present-day meteorological conditions on the isotopic composition of Antarctic precipitation. Therefore, the focus is on short time scales (days to several years), where sufficient meteorological data are avalable. The spatial scale of this study varies from local sites to the entire Antarctic continent.

In the austral summer of 2001-02, snow samples from snow pits in Dronning Maud Land (DML) were taken for stable isotope analyses, from locations where automatic weather stations (AWSs) monitored local meteorology. This enabled the comparison with temperature and accumulation records over the period 1998-2002 (Chapter 2). The AWS data reveal highly intermittent accumulation patterns, which result sometimes in the exclusion of entire seasons in the isotope records. A comparison of the isotope records with near-surface temperature and condensation temperature points out that on a time scale of days to several years, isotopic variability cannot be interpreted with confidence as local temperature changes. Furthermore, the AWS data show that snowfall in this area is associated with much higher temperatures than average conditions, which results in a warm bias (5-10 °C) in the isotope records. However, the warm bias is not constant from year to year. The measured isotope records reveal that wintertime snowfall has much lower $\delta^{18}O$ values than expected from local temperature during snowfall. Clearly, the isotopic record is not just determined by local conditions, but it is a more complex regional signal, influenced by conditions along transport paths and moisture source regions.

In order to study the influence of moisture transport paths, an isotope distillation model (MCIM) is combined with backward trajectory calculations, to describe isotopic fractionation during transport. In a first attempt to do so, one particularly large accumulation event has been studied (Chapter 3). This heavy snowstorm occurred

in summer 2002 and brought a considerable amount of fresh snow, which could easily be sampled, a few days after the storm calmed. Backward trajectory calculations for this event have revealed that air masses bringing moisture to the sampling site were not saturated along most of the transport paths. This is in contrast with assumptions in isotope distillation models. Moreover, results from the isotope distillation model point out that the temperature drop that occurred during the final stage of transport is not large enough to explain the total observed isotopic distillation. Only with a spatially dependent isotope field that serves as a starting value for the δ value of the water vapour (instead of calculating the initial isotopic composition from local evaporative conditions), the observed isotopic distillation towards the precipitation site can be reproduced.

Hence, for a successful continuation of the aimed approach, a reconsideration of the initial isotopic composition of the moisture at the start of the trajectories was crucial (Chapter 4). In order to do so, the isotope distillation model is adapted such that the initial isotopic composition is determined using monthly mean three-dimensional isotope fields from a general circulation model (ECHAM4). These isotope values are also used for the isotopic composition of any additional moisture that enters the air parcel along transport, which allows the description of isotopic recharge. Furthermore, a realistic threshold value of the relative humidity is used as an indicator for condensation and associated isotopic fractionation. The latter is necessary to prevent unrealistic isotopic fractionation in undersaturated air.

In Chapter 5, this modified MCIM is combined with backward trajectory calculations for all snowfall events that occurred at the locations of the AWSs during 1998-2002, i.e. the same period as evaluated in Chapter 2. Atmospheric data from the European Centre for Medium-range Weather Forecast Reanalysis data set (ERA-40) serve as meteorological input for the trajectory calculations. This simulation points out that most of the isotopic depletion occurs during the last day of transport, confirming the conclusions that were drawn earlier based on only a single snowfall event. The strength of the final temperature drop is of primary importance to both $\delta^{18}O$ and deuterium-excess (d-excess $= \delta D - 8\delta^{18}O$) of the final precipitation, but cannot fully explain the total seasonal isotopic amplitude. Seasonal variations in the initial isotopic composition of the moisture are also important for the final simulated seasonal isotopic amplitude, which highlights the regional character of isotope records in snow and complicates the interpretation of isotope records as temperature proxy. To validate the model, results are compared with the measured isotope records over the same period. For a sound comparison, post-depositional diffusion is also taken into account by modelling isotopic diffusion in firn after deposition of the snow. The simulated isotope records are mostly in good agreement with the observed seasonal variability in the snow, although at low temperatures the total distillation is underestimated, especially on the high Antarctic plateau.

Simulated d-excess compares surprisingly good with the observations, but is strongly influenced by the height at which the initial moisture enters the air parcel. This is due to the strong vertical gradient in d-excess in the ECHAM4 isotope fields, used for the initial state. If this gradient also exists in reality, this may obscure the widely-used interpretation of d-excess as an indicator for moisture source conditions, since it is

not clear to what extent conditions at the oceanic surface can leave an imprint in the vertical gradient in d-excess over the oceanic source area. Nevertheless, model formulations of kinetic fractionation effects (which determine the d-excess value) can be improved, since d-excess is overestimated at low temperatures. With the current parameterisations of kinetic fractionation, and with initial isotopic composition from the ECHAM4 fields, it is not possible that both $\delta^{18}O$ and d-excess can be simultaneously modelled correctly.

Finally, the combined approach of backward trajectories and isotopic modelling is applied on snowfall over the entire Antarctic continent, for the period from September 1980 to August 2002, using ERA-40 as meteorological input (Chapter 6). This 22 yr simulation has produced a realistic isotope distribution, with comparable spatial isotopic gradients as observed. However, isotopic depletion of snow on the East Antarctic plateau is underestimated, just like on a regional scale in DML as presented in Chapter 5.

The simulated present-day spatial $\delta - T$ relationship varies strongly, indicating that one simple relation is not applicable to all sites and time periods. Furthermore, spatial differences in the seasonal isotopic amplitude are identified, with large amplitudes in the Antarctic interior, an hardly any seasonal isotope signal in Marie Byrd Land, West Antarctica. These differences can be attributed to (1) larger seasonal amplitudes in (local) condensation temperature in the Antarctic interior, and (2) trajectories towards the Antarctic interior have a more northerly origin in winter, and therefore experience a larger temperature gradient over which distillation occurs.

The underestimation of isotopic depletion of snowfall in the Antarctic interior stresses the fact that our approach does not capture the Antarctic hydrological cycle sufficiently good to explain all observed isotopic variability. Two processes seem to be candidates to explain the deficiency. Firstly, the approach followed in this thesis focusses on advective moisture transport. Diffusive mixing of moisture is only schematically accounted for. However, mixing of strongly depleted (Antarctic) vapour with moisture that is advected over Antarctica may explain the additional depletion that is necessary to reproduce the observations better. On the other hand, clear sky precipitation (formation of fine ice crystals as a result of radiative cooling in or just above the cold atmospheric boundary layer) is another process that is not captured in our approach. In the Antarctic interior, this type of precipitation probably contributes significantly to the local mass balance. It is likely that a realistic simulation of isotopic depletion associated with this process can explain the current shortage of distillation.

To conclude, the efforts in isotopic modelling as presented in this thesis emphasise the complexity of isotopic changes in the hydrological cycle, in contrast to the sometimes too easily taken assumption that the isotopic composition of polar precipitation is linearly and solely related to temperature.

Samenvatting

Voor het wereldwijde klimaatonderzoek zijn ijskernen van polaire ijskappen van groot belang. Klimaatfluctuaties van de afgelopen honderdduizend(en) jaren zijn namelijk zeer gedetailleerd opgeslagen in deze kilometers dikke ijskappen, door neerslag die in de loop der tijd is omgevormd tot ijs. Door diepe kernen te boren uit deze ijskappen en deze vervolgens laagje voor laagje te analyseren, wordt uit de samenstelling van het ijs informatie verkregen over de veranderingen in het klimaat.

De basis van deze methode is het onderzoek naar variaties in de isotopensamenstelling van het ijs. Isotopen zijn deeltjes van hetzelfde chemisch element, met een verschillende massa. Sneeuw bestaat uit watermoleculen, die op hun beurt weer zijn opgebouwd uit deeltjes die een verschillend gewicht kunnen hebben, waardoor er zware en lichte watermoleculen bestaan. Aangezien water is opgebouwd uit zuurstof (O) en waterstof (H), bestaan er twee verschillende soorten isotopen die gemeten kunnen worden: de verhouding tussen zwaar en licht zuurstof ($\delta^{18}O$) en die tussen zwaar en licht waterstof (δD, zwaar waterstof heet deuterium, D). De verhouding tussen dit zware en lichte water varieert in sneeuw, en blijkt mede te worden beïnvloed door temperatuur. Zo wordt er in warme gebieden 'zware' neerslag gevonden (veel zware isotopen), terwijl in poolgebieden juist zeer 'lichte' neerslag valt (weinig zware isotopen). Op basis van deze waarneming worden deze isotoopverhoudingen in ijskernen gebruikt als indicator voor temperatuur.

Een significante ruimtelijke correlatie tussen de jaargemiddelde temperatuur en de gemiddelde isotoopwaarde van sneeuw wordt vaak als ijking voor de relatie tussen isotopen en temperatuur gebruikt. Echter, deze ruimtelijke relatie wordt ook beïnvloed door andere processen, en het is zeer waarschijnlijk dat deze relatie niet zomaar te gebruiken is om alle isotoopvariaties in de tijd om te zetten naar temperatuurvariaties. Dit bemoeilijkt de interpretatie van isotoopsignalen, en daarom mogen isotoopwaarden uit ijskernen niet direct als temperaturen worden gekwantificeerd, zonder gedegen kalibratie met onafhankelijke informatie over temperatuur.

Om de fysische grondslag achter isotoopvariaties beter te begrijpen, is een groot deel van dit proefschrift gewijd aan simulaties van veranderingen in isotoopverhoudingen in atmosferisch vocht. Het proces dat hierbij gemodelleerd wordt, kan als volgt worden omschreven: Tijdens atmosferisch transport van de oceaan naar bijvoorbeeld een ijskap koelt lucht af, en regent er steeds meer vocht uit. De waterdamp in deze lucht krijgt gaandeweg een steeds lagere concentratie zware isotopen, aangezien zware watermoleculen eerder condenseren dan lichte watermoleculen. Dit proces wordt isotopenfractionering genoemd. Hoe meer de lucht afkoelt, hoe minder zware isotopen er

zullen overblijven in het vocht, waardoor de zware isotopen allengs uit de lucht worden gedestilleerd. Omdat de hoeveelheid vocht die lucht kan vasthouden sterk afhangt van temperatuur, wordt de uiteindelijke verhouding van zware en lichte isotopen in sneeuw beïnvloed door de temperatuur waarop sneeuw wordt gevormd. Echter, er zijn ook andere factoren van belang, waaronder condities in het brongebied, tussentijdse verdamping, menging met andere luchtmassas, en eerdere condensatiecycli.

Het doel van dit proefschrift is om de interpretatie van stabiele isotopen in Antarctische sneeuw te verbeteren, door de invloed van meteorologische omstandigheden op de isotoopverhoudingen in Antarctische neerslag te bestuderen. Er is getracht om waargenomen verschillen in Antarctische isotoopwaarden op een gedetailleerde manier te verklaren met relevante meteorologische gegevens. De nadruk ligt op korte tijdschalen (dagen tot enkele jaren), aangezien over deze periode veel meteorologische gegevens beschikbaar zijn. De ruimtelijke schaal die deze studie bestrijkt varieert van een individuele locatie tot het gehele Antarctische continent.

Vanaf 1998 is de lokale meteorologie op verschillende plaatsen in Dronning Maud Land (DML), Antarctica gemeten met behulp van automatische weerstations. In de zuidelijke zomer van 2001-02 zijn op vier van deze locaties sneeuwmonsters verzameld, om ze vervolgens te analyseren op zowel $\delta^{18}O$ als op δD. Dit maakt een vergelijking met de lokale temperatuur en accumulatie van sneeuw mogelijk over de periode 1998-2002 (hoofdstuk 2). De data van de weerstations laten een sterk onregelmatig accumulatiepatroon zien, waar sneeuwbuien worden afgewisseld door lange perioden van droogte. Dit resulteert soms in het ontbreken van hele seizoenen in het isotoopsignaal. Een vergelijking van isotoopvariaties in de sneeuw met atmosferische temperatuur wijst erop dat op een tijdschaal van dagen tot enkele jaren, isotoopsignalen geen betrouwbare informatie bevatten over lokale veranderingen in temperatuur. Verder laten de data van de weerstations zien dat sneeuwval in dit gebied samen gaat met veel hogere temperaturen dan gemiddeld, waardoor er in het isotoopsignaal een warme afwijking zit (5-10 °C). Deze afwijking is echter niet constant van jaar tot jaar, wat de interpretatie van jaargemiddelde isotoopwaarden bemoeilijkt. De gemeten isotoopwaarden hebben een veel lagere $\delta^{18}O$ waarde in de winter dan zou mogen worden verwacht op basis van uitsluitend de lokale temperatuur tijdens sneeuwval. Dit wijst er duidelijk op, dat het isotoopsignaal niet alleen wordt bepaald door lokale condities, maar dat het een veel complexer, regionaal signaal is, dat beïnvloed wordt door omstandigheden langs atmosferische transportpaden en condities in het brongebied van het vocht.

Om de invloed van condities langs atmosferische transportpaden (trajectoriën) te bestuderen, is een isotoopdestillatie model gecombineerd met een trajectoriënmodel. Dit trajectoriënmodel berekent het driedimensionale atmosferische pad van een luchtpakketje voorafgaand aan het tijdstip van sneeuwen, op basis van een globale meteorologische dataset van het Europees centrum voor weersverwachtingen (ECMWF). Door middel van deze combinatie van modellen kan de isotopenfractionering tijdens transport beschreven worden. In hoofdstuk 3 is een eerste poging gedaan om dit doel te bereiken, door een bijzonder hevige sneeuwstorm te bestuderen. Deze zware sneeuwstorm vond plaats in de zomer van 2002, en bracht een aanzienlijke hoeveelheid

verse sneeuw in DML. Deze sneeuw was enkele dagen nadat de storm ging liggen gemakkelijk te bemonsteren. Trajectoriën voor deze storm laten zien dat de luchtmassa's die vocht naar het gebied brachten niet verzadigd waren gedurende het grootste deel van het transportpad. Dit is niet in overeenstemming met aannames in isotoopdestillatie-modellen. Bovendien wijzen berekeningen van isotoopdestillatie erop dat de temperatuurdaling tijdens de laatste fase van transport niet toereikend is om de totale waargenomen destillatie te verklaren. Slechts met een ruimtelijk variërend isotoopveld wat als beginwaarde dient voor de waterdamp (in plaats van een berekening van de initiële waarden uit lokale verdampingsomstandigheden), kan de waargenomen isotoopwaarde worden gereproduceerd.

Om de gecombineerde aanpak van isotoopmodellering langs trajectoriën te laten slagen, was een heroverweging van de manier waarop de isotoopwaarden van het vocht aan het begin van de trajectoriën werden bepaald van groot belang (hoofdstuk 4). Daarom is het destillatiemodel zodanig aangepast dat de initiële waarde wordt bepaald uit maandgemiddelde isotoopvelden van een algemeen circulatiemodel (ECHAM4). Deze isotoopvelden worden ook gebruikt voor de waarde van eventueel extra vocht dat een luchtpakketje opneemt tijdens transport. Verder wordt in het aangepaste model een drempelwaarde van de relatieve vochtigheid gebruikt als indicator voor het optreden van condensatie, en de hiermee samengaande isotopenfractionering. Deze drempelwaarde is nodig om onrealistische fractionering te voorkomen in onverzadigde lucht.

Dit aangepaste destillatiemodel is in hoofdstuk 5 gecombineerd met de trajectoriën voor alle sneeuwval die plaats vond op de locaties van de weerstations in de periode 1998-2002, die ook beschreven staat in hoofdstuk 2. Atmosferische data uit heranalyse van het ECMWF zijn gebruikt als meteorologische input voor het trajectoriënmodel. Deze simulatie laat zien dat de meeste isotopenfractionering plaats vindt tijdens de laatste dag van het transport. Dit bevestigt de conclusies die in hoofdstuk 3 getrokken waren op basis van een enkele sneeuwbui. De grootte van de temperatuurdaling die plaatsvindt tijdens deze laatste fase van transport is van primair belang voor de isotopenfractionering. Echter, deze daling in temperatuur kan niet de totale seizoensvariatie in isotoopverhoudingen verklaren: seizoensvariaties in de initiële isotoopverhoudingen (aan het begin van de trajectoriën) zijn ook belangrijk voor de uiteindelijk gemodelleerde seizoensamplitude. Dit benadrukt de regionale invloed op isotoopwaarden van sneeuw, en bemoeilijkt de interpretatie van isotoopsignalen in termen van temperatuurverschillen. Om het model te valideren zijn de resultaten vergeleken met de gemeten isotoopprofielen over dezelfde periode. Om een gedegen vergelijking mogelijk te maken, moest ook rekening gehouden worden met de invloed van diffusie van isotopen in de sneeuw. Daarom is een diffusiemodel toegepast op de gesimuleerde isotoopprofielen. De gesimuleerde isotoopprofielen zijn over het algemeen in overeenstemming met de waargenomen seizoensvariatie in de sneeuw, hoewel de totale destillatie door het model wordt onderschat. Dit probleem manifesteert zich met name op het Antarctische plateau.

Een tweede-orde parameter uit metingen van stabiele isotopen in ijskernen is deuterium-excess (d-excess $= \delta D - 8\delta^{18}O$). Fluctuaties in deze parameter kunnen ontstaan als gevolg van isotopenfractionering waarbij geen evenwicht is tussen de iso-

toopverhoudingen in de damp en in het condenserende water/ijs. Dit wordt kinetische fractionering genoemd. Er wordt aangenomen dat d-excess voornamelijk gevoelig is voor omstandigheden tijdens verdamping van oceaanwater, en ook voor omstandigheden tijdens hele lage temperaturen, dus tijdens de vorming van sneeuw. Door deze eigenschap wordt d-excess gebruikt als indicator van (veranderingen in) omstandigheden in het brongebied van het vocht.

Ondanks de onderschatting van de totale fractionering, vallen de gesimuleerde waarden van d-excess verrassend goed samen met de waarnemingen, en blijken vooral te worden beïnvloed door de hoogte waarop (initieel) vocht door het luchtdeeltje wordt opgenomen (hoofdstuk 5). Deze sterke afhankelijkheid van de hoogte wordt veroorzaakt door een sterke verticale gradiënt in de isotoopvelden van ECHAM4, die gebruikt worden voor de definiëring van de initiële isotoopwaarde. Als deze gradiënt ook in werkelijkheid bestaat, en als zodanig een belangrijke rol speelt in de bepaling van d-excess van het vocht dat naar Antarctica wordt getransporteerd, dan vertroebelt dit de algemeen gebruikelijke interpretatie van d-excess als indicator voor condities in het brongebied. Het is namelijk niet duidelijk in hoeverre condities in het brongebied (zoals temperatuur van het zeewater en relatieve vochtigheid over de oceaan) nog worden gereflecteerd in die verticale gradiënt in d-excess, enkele kilometers boven het zeeoppervlak. Desalniettemin wijzen de resultaten erop dat de modelformuleringen die de kinetische fractionering beschrijven kunnen worden verbeterd, aangezien d-excess wordt overschat bij lage temperaturen. Met de huidige parameterisatie van kinetische fractionering (in combinatie met initiële isotoopvelden van ECHAM4) is het niet mogelijk om zowel $\delta^{18}O$ als d-excess correct te simuleren, waardoor het (nog) onduidelijk is hoe deze parameter werkelijk moet worden geïnterpreteerd.

Uiteindelijk is de gecombineerde aanpak van isotoopmodellering langs trajectoriën toegepast op sneeuwval voor het gehele Antarctische continent, voor de periode van september 1980 tot augustus 2002 (hoofdstuk 6). Deze simulatie heeft een waardevol overzicht opgeleverd van de variatie van de gemiddelde huidige isotoopverhoudingen over het gehele continent. Uit vergelijkingen van deze simulatie met beschikbare waarnemingen blijkt dat de ruimtelijke gradiënten overeenkomen, maar dat de absolute grootte van de fractionering voor sneeuwval op het Oost-Antarctisch plateau is onderschat in de simulatie, hetgeen vergelijkbaar is met de resultaten van de regionale studie in hoofdstuk 5.

De ruimtelijke relatie van $\delta^{18}O$ met temperatuur varieert sterk over Antarctica in het huidige klimaat. Dit wijst erop dat één simpele relatie niet toepasbaar is voor de interpretatie van isotoopsignalen voor alle locaties en perioden. Bovendien zijn er ruimtelijke verschillen in de gemodelleerde seizoensamplitude van het isotoopsignaal vastgesteld, met grote amplitudes in het binnenland van Antarctica en nauwelijks enig seizoenssignaal in Marie Byrd Land, West-Antarctica. Deze verschillen kunnen worden toegeschreven aan (1) grotere seizoensvariatie in lokale (condensatie-) temperatuur in het binnenland van Antarctica, en (2) het feit dat het vocht dat in de winter als sneeuw in het binnenland van Antarctica valt een meer noordelijk brongebied heeft, waardoor het een veel grotere temperatuursdaling ondergaat waarover isotoopdestillatie plaatsvindt.

De onderschatting van de totale isotopenfractionering van sneeuw op het Antarc-

tisch plateau benadrukt het feit dat onze methode de hydrologische kringloop niet toereikend genoeg beschrijft om alle waargenomen isotoopvariaties te verklaren. Twee processen zijn hier waarschijnlijk de oorzaak van. Ten eerste beschrijft de methode die gevolgd wordt in dit proefschrift enkel het advectieve deel van het vochttransport; diffuse menging van vocht wordt slechts schematisch meegenomen zodra daar aanleiding voor te vinden was in de trajectoriën. Echter, menging van sterk gedestilleerd vocht boven Antarctica met vocht dat advectief wordt aangevoerd zou de extra isotopische verarming van het aangevoerde vocht kunnen verklaren, waardoor waarnemingen beter kunnen worden gereproduceerd.

Ten tweede is het proces *clear sky precipitation* niet meegenomen in onze methode. Tijdens dit proces worden zeer fijne ijskristallen gevormd door stralingsafkoeling in, of net boven de atmosferische grenslaag. Boven het Antarctisch plateau draagt dit proces waarschijnlijk aanzienlijk bij aan de lokale hoeveelheid neerslag die slechts enkele centimeters per jaar is. Het is aannemelijk dat het huidige tekort aan destillatie kan worden verklaard door een realistische simulatie van de isotoopdestillatie die samenhangt met dit proces.

Er kan worden geconcludeerd dat de hier beschreven pogingen tot isotoopmodellering benadrukken hoe complex de variabiliteit in isotoopverhoudingen in de hydrologische kringloop kan zijn. Dit staat in schril contrast met de aanname dat isotoopsignalen in polaire neerslag lineair, en alleen gerelateerd zijn aan lokale temperatuur; een aanname die soms te gemakkelijk gemaakt wordt.

Scientific publications

J.C. Boelhouwers, F.C.W. Craemers, M.M. Helsen. 2001. Geomorphic evolution of debris fans in the Du Toit's Kloof. *South African Geographical Journal*, **83** (3), 263-273.

Helsen, M.M., P.J.M. Koop, H. van Steijn. 2002. Magnitude-frequency relationship for debris flows on the fan of the Chalance torrent, Valgaudemar (French Alps). *Earth Surface Processes and Landforms*, **27** (12), 1299-1307.

Helsen, M.M., R.S.W. van de Wal, M.R. van den Broeke, E.R.Th. Kerstel, V. Masson-Delmotte, H.A.J. Meijer, C.H. Reijmer, M.P. Scheele. 2004. Modelling the isotopic composition of snow using backward trajectories: a particular precipitation event in Dronning Maud Land, Antarctica. *Annals of Glaciology*, **39**, 293-299.

Helsen, M.M., R.S.W. van de Wal, M.R. van den Broeke, D. van As, H.A.J. Meijer, C.H. Reijmer. 2004. Oxygen isotope variability in snow from western Dronning Maud Land, Antarctica and its relation to temperature. *Tellus*, **57B** (5), 423-435.

Van As, D., M.R. van den Broeke, M.M. Helsen. Structure and dynamics of the summertime atmospheric boundary layer over the Antarctic plateau I: Measurements and model validation. 2005. *Journal of Geophysical Research*, in press.

Helsen, M.M., R.S.W. van de Wal, M.R. van den Broeke, V. Masson-Delmotte, M.P. Scheele, M. Werner. 2005. Modeling the isotopic composition of Antarctic snow: Simulation of snow pit records. *Journal of Geophysical Research*, under review.

Helsen, M.M., R.S.W. van de Wal, M.R. van den Broeke. 2005. Journal of Climate *Journal of Climate*, submitted.

Curriculum Vitae

Michiel Helsen is geboren op 30 april 1977 te Enschede. Hij is opgegroeid in Oldenzaal, waar hij in 1995 zijn VWO diploma behaalde aan het Twents Carmellyceum. Vervolgens bracht de interesse in aardrijkskunde (en de nieuwgierigheid naar het leven in een grote stad) hem naar Utrecht, alwaar hij Fysische Geografie studeerde. In de laatste fase van zijn studie hield hij zich vooral bezig met de invloed van het klimaat op de ontwikkeling van berghellingen: Dit was het onderwerp van een stage bij Jan Boelhouwers aan de University of the Western Cape, Zuid-Afrika, alsook het afstudeeronderzoek in de Franse Alpen, onder begeleiding van Henk van Steijn. Ondertussen was hij in contact gekomen met Roderik van de Wal door een bijvak te doen aan het Instituut voor Marien en Atmosferisch onderzoek Utrecht (IMAU) met als onderwerp de energiebalans van Groenland. Na in 2001 te zijn afgestudeerd wist Roderik hem te verleiden tot een promotieonderzoek op het IMAU, waarvoor hij kort daarna samen met Dan Zwartz aan een Antarctische expeditie naar Dronning Maud Land kon deelnemen. Het resultaat van dit promotieonderzoek heeft u hier voor u, en zal hij op 8 februari 2006 verdedigen. De komende drie jaar blijft Michiel als post-doc verbonden aan het IMAU en zal zijn Antarctisch onderzoek voortzetten.

Dank je!

Begin 2000 liep ik voor het eerst de kamer binnen van Roderik van de Wal. Destijds wilde ik als afsluiting van mijn studie wat modelleerervaring opdoen door onder zijn begeleiding te werken aan een project over de Groenlandse ijskap. Toen had ik uiteraard niet kunnen denken dat deze ontmoeting 6 jaar later uit zou monden in dit proefschrift. Roderik, jou wil ik hiervoor als eerste bedanken. Niet alleen voor de kans die je me geboden hebt om dit onderzoek op me te nemen, maar zeker ook voor de manier waarop je me de afgelopen jaren hebt bijgestaan, -gestuurd, -geschoold en gemotiveerd. Ik ben er dan ook heel gelukkig mee dat onze samenwerking de komende paar jaar nog verlengd wordt.

Zeker zo belangrijk was ons gezamenlijke "isotopenoverleg", waarbij Michiel van den Broeke aanschoof. De enthousiaste manier waarop Michiel mijn resultaten wist te interpreteren leidde zonder uitzondering bij mij tot veel meer inzichten, en kon ik vol goede moed weer verder gaan. Daarnaast ben ik jullie misschien nog wel de meeste dank verschuldigd voor de ultieme kans die jullie me boden om aan het begin van mijn promotietijd mee te gaan op een Antarctische expeditie. Fantastisch. Roderik en Michiel, ik weet zeker dat ik het heel goed getroffen heb mijn jullie als begeleiders, bedankt!

Hoewel de begeleiding bij Roderik en Michiel in prima handen was, wil ik ook mijn promotor Hans Oerlemans bedanken, die ondanks zijn vele verplichtingen altijd klaar stond om me van adviezen te voorzien. Dit geldt overigens ook voor Richard, Wouter en de rest van de IJs en Klimaatgroep op het IMAU, vooral ook alle AIO's die geduldig al mijn onbegrijpelijke isotoopverhalen aanhoorden op het (on)regelmatig terugkerende HOERA-overleg.

The stay in Antarctica has been an overwhelming experience for me. I would like to thank all members of SWEDARP en FINNARP of the 2001-02 season for this. Dan Zwartz was tijdens deze expeditie mijn steun en toeverlaat, en we hebben een prachtige tijd gehad. Vooral tijdens de heftige sneeuwstormen die we samen in een klein tentje moesten doorstaan waren onvergetelijk. Dan, bedankt voor de fantastische tijd!

Een vaak gehoorde wijsheid over promoveren is wel dat je er alleen voorstaat, dat het een eenzame klus is. De oplettende lezer heeft uit de voetnoten van de verschillende hoofdstukken kunnen concluderen dat dit voor mij wellicht slechts ten dele gold: Wat een hoeveelheid co-auteurs! Inderdaad, een indicatie dat ik flink heb weten te profiteren van andermans data en expertise. Bij deze bedank ik iedereen voor hun bijdrage, met name Harro Meijer voor alle analyses aan sneeuwmonsters die op het

CIO zijn uitgevoerd, en zeker ook voor de al je tips op isotopengebied. Furthermore, I'm very grateful to Valérie Masson-Delmotte for her assistance regarding the isotope modelling, and Martin Werner for supplying the ECHAM isotope data, thanks. Carleen Reijmer en de IMAU-technici waren verantwoordelijk voor de beschikbaarheid van de waardevolle Antarctische weerstationdata, en Rinus Scheele heeft me goed wegwijs gemaakt in de wereld van de trajectoriën.

Buiten alle werk om waren er gelukkig veel mensen in mijn omgeving waarmee ik het over andere zaken kon hebben dan isotopen: Esther, Francesco, Franny, Jaap, Maarten, Maartje, Olav, Nick, Nico, Hiddo, Judith, badmintonners, Geert, Ries, Piet, voetbalpoulers, Faezeh, Amici di Pierluigi, Elise, Arjáán, Hylke, Kim, Pim, Tom, Tamara, Remke, Remko, Han, Lon, Ton, Anna, Ronald, Hanneke, Annerieke, Lé, POP, Werchtermensjes, Marianne, Marieke, Carina, Harm, Kirsten, Susanne, Mischa, Lisette, Eeske, 'tussen-de-happen-door'-spelers, Jessie, Hester, Petra, Astrid, Kitty, Ruud, Bouke, Laura, Ylva, ik wil jullie allemaal bedanken voor jullie vriendschap, biertjes, zin en onzin, liefde, aanwezigheid en gezelligheid. En nu maar hopen dat ik niemand vergeten ben...

Dirk en Peter, onvolprezen paranimfen en dikke vriendjes, ik kan me (gelukkig) maar moeilijk indenken hoe de afgelopen jaren zouden zijn geweest zonder jullie. Een speciale alinea vol lof naar jullie: superbedankt voor alle steun, vriendschap en betrokkenheid die jullie aan de dag weten te leggen, in goede en slechte tijden.

Als laatste wil ik mijn familie bedanken voor hun steun en vertouwen in mij. Armand, René en Marianne (jij grote voorbeeldzus), hartstikke bedankt voor al jullie interesse, medeleven en steun. Pap en mam, dankzij jullie eindeloze aanmoedigingen leek een promotie soms nog wel een grotere prestatie dan dat het eigenlijk was. Bedankt voor alles!